PhD Degree in Molecular Medicine

(curriculum in Molecular Oncology)

European School of Molecular Medicine (SEMM)

University of Milan and University of Naples "Federico II'

Settore disciplinare: Bio/11

Functional dissection of *ST18* in liver cancer

Micol Ravà

IEO, Milan

Matricola n. R09389

Supervisor: Dr. Bruno Amati

IEO, IIT, Milan

Added Supervisor: Dr. Stefano Campaner

IIT, Milan

LIST OF ABBREVIATIONS

ABC= ATP binding cassette

AFP= Alfa-Fetoprotein

ALB= Albumin

ALT= Alanine aminotransferase

CCM= Cerebral cavernous malformation

CK= Cytokeratin

DEG= Differentially expressed gene

Doxy= Doxycycline

E= Embryonic day

EGF= Epidermal growth factor

EMT= Epithelial to mesenchymal transition

EndMT= Endothelial to mesenchymal transition

ES= Enriched score

EV= Empty vector

FDA= Food and Drug Administration

FFPE= Formalin-fixed paraffin-embedded

GFP= Green fluorescent protein

GSEA= Gene Set Enrichment Analysis

GT= Glutamyltranspeptidase

H&E= Hematoxylin and eosin

HBV= Viral hepatitis B

HCC= Hepatocellular carcinoma

HCV= Viral hepatitis C

HGF= Hepatocyte growth factor

IFN= Interferon

IHC= Immunohistochemistry

IL= Inteurleukin

IPA= Ingenuity pathway analyzer

KD= Knockdown

Ko= Knockout

L1= Long interspersed element 1

log2FC= log2 Fold Change

LPS= Lipopolysaccharide

Mdr= Multidrug resistance

MEF2= Myocyte enhancer factor 2

MOI= Multiplicity of infection

MSigDB= Molecular Signature Database

Myt= Myelin transcription factor

N/C= Nucleus to Cytoplasm ratios

NFkB= Nuclear factor kappa-light-chain-enhancer of activated B cells

NZF = Neural zinc finger

OHT= 4-hyydroxy-tamoxifen

PC= Phosphatidylcholine

PFIC= Progressive familial intrahepatic cholestasis

PS= Phosphatidylserine

RPKM= Reads Per Kilobase per Million

shP53= shRNA targeting p53

shRNA= Short hairpin RNA

ST18= Suppression of tumorigenicity 18

STAT= Signal transducer and activator of transcription

TGF= Tumor growth factor

TNF= Tumor necrosis factor

VCAM= Vascular adhesion molecule

VEGF= Vascular endothelial growth factor

FIGURE INDEX

TABLE INDEX

ABSTRACT

The molecular mechanisms and pathways responsible for the progression of hepatocellular carcinoma (HCC) remain to be fully characterized. Among the genetic lesions associated with HCC progression, Shukla et al. (2013) identified insertions of the L1 transposon proximal to the gene encoding the zinc-finger DNA-binding protein *ST18* (suppression of tumorigenicity 18) and suggested that this actually functions as an oncogene in HCC. However, functional evidence for a cancer-promoting activity of *ST18* and insight into its mode of action are missing. Here, I pursued the functional characterization of *ST18* in a mouse model of HCC based on *ex vivo* transformation and subcutaneous transplantation of embryonic hepatoblasts. *ST18* was undetectable in either normal liver or cultured hepatoblasts, but was induced in the subcutaneous tumors. *ST18* was also expressed in either chronically or acutely inflamed mouse livers (as assessed in *Mdr2-/-* or LPS-treated mice) as well as in human Progressive Familial Intrahepatic Cholestasis 2 (PFIC2: a condition associated with chronic inflammation), suggesting its induction by inflammatory stimuli. The knockdown of *ST18* delayed tumor formation or, if induced in already formed tumors, led to rapid hemorrhage, pervasive morphological changes in the tumor cells reminiscent of an epithelial-to-mesenchymal transition (EMT) and eventually tumor regression. RNA profiling revealed that *ST18* silencing caused expression of EMT-associated genes, among others. Previous studies have linked inflammation to the induction of EMT in other epithelia: we hypothesize that the concomitant activation of *ST18* constitutes a safeguard against EMT, inactivation of this control mechanism causing the dramatic phenotypic switch observed in our model. These data warrant further evaluation of the mode of action of *ST18* and of its potential value as a therapeutic target in HCC.

1 INTRODUCTION

1.1 Pathogenesis and treatment of Hepatocellular carcinoma (HCC)

Hepatocellular carcinoma (HCC) is the most common primary form of liver cancer, followed by cholangiocarcinoma. With more than 750,000 new cases diagnosed every year, HCC represents the sixth most frequent cancer worldwide (Jemal et al., 2011) and the third most frequent cause of cancer-related death (Parkin et al., 2001), preceded only by lung and stomach cancer (Llovet and Bruix, 2003) and HCC occurs predominantly in men and in elderly individuals. The etiological agents, including infection by viral hepatitis B (HBV) and C (HCV), alcohol abuse and aflatoxin exposure, are relatively well understood (Gomaa et al., 2008). Additionally, metabolic disorders such as obesity and diabetes are also considered risk factors (Gomaa et al., 2008). The incidence of HCC is increasing due to the increasing frequency of HCV infection, while vaccination campaigns and antiviral treatment have diminished the occurrence of HBV-related HCC in the Western countries. Southeast Asia and sub-Saharan Africa, where HBV infection is endemic, show the highest rates of HCC (El-Serag, 2011). Liver cirrhosis and/or advanced fibrosis constitute the major clinical risk factors for the development of HCC present in 80% of cases (Severi et al., 2010). In particular, cirrhosis that origins from chronic liver injury provides a mutagenic and mitogenic environment that favors hepatocyte transformation leading to the HCC development. HCC is most frequently diagnosed at advanced stages, when limited therapeutic options are available. Moreover, it is a chemoresistant cancer, thus the only treatments existing so far are surgical resection or liver transplantation (Llovet and Bruix, 2003). Surgical intervention is effective for the treatment of patients with localized disease. However, over 80% of all patient present multifocal HCC, which limits the usefulness of this treatment. The phase 3 SHARP (Sorafenib HCC

Assessment Randomized Protocol) trial showed that Sorafenib, improved survival of patient with advanced HCC (Llovet et al., 2008). Sorafenib is a multikinase inhibitor that blocks the MAPK pathway and causes apoptosis in cancer cells as well as decreases angiogenesis, cell migration and proliferation (Llovet et al., 2008). In 2007 the U.S. Food and Drug Administration (FDA) has approved the use of Sorafenib in patients with inoperable hepatocellular carcinoma, albeit treatment is often followed by the development of resistance. Recently, a combination of Sorafenib and Mapk14 blockade emerged as a promising approach to increase therapeutic efficiency in human HCC (Rudalska et al., 2014)

1.2 Histological aspects of HCC

Recently the classification of HCC has shifted from a morphology-based approach to a functional clinical classification (such as the Barcelona-Clinic Liver Cancer staging system) centered on the stage of the disease related to treatment strategies (Roncalli et al., 2010). In this chapter we will describe the histological patterns and the molecular markers used to diagnose and characterize HCC.

HCC can be detected rapidly in sections stained with hematoxylin and eosin (H&E), and can be classified into three major histological patterns important for diagnostic purpose, albeit with little evidence that these morphological features have any biological and clinical significance. The classical histological patterns are: trabecular, pseudoglandular and solid (Fig. 1.1). The trabecular pattern is the most common in well- and moderately differentiated HCCs. In this pattern, tumoral hepatocytes recapitulate normal liver cell plate of variable thickness that are separated by prominent sinusoidal endothelial cells. Pseudoglandular or acinar patterns are referred to as “pseudoglands” or “pseudoacini” because the gland-like structures are not true

glands but abnormal bile canaliculi formed between tumour cells. The solid pattern is basically a trabecular pattern but the sinusoid-like blood spaces are compressed into a compact mass, giving the tumour a solid appearance. The solid pattern is common in poorly differentiated tumours (Paradis, 2013).

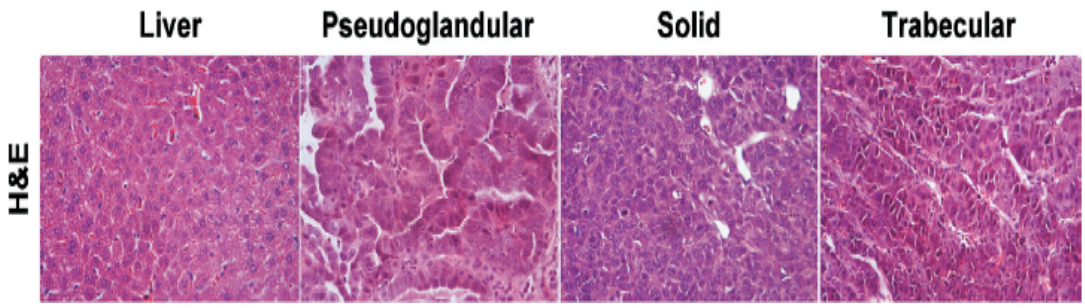

Figure 1.1: Histopathological subtypes of HCC. The three major architectural patterns in HCC are pseudoglandular, solid, trabecular. (Zender et al., 2005).

The histopathology of murine liver cancer recapitulates that of human HCC. Zender et al. (2005) have shown that HCC arising from genetic manipulation of hepatoblasts were classified mostly as solid or solid/trabecular growth pattern and a small proportion resembled human pseudoglandular HCC.

Clearly, morphologic criteria are not sufficient to well define HCC and the advent of the immunohistochemistry application has improved the diagnosis. A large variety of immunological markers of HCC have been described, including a number of highly specific markers such as albumin (ALB), fibrinogen, 1-anti-trypsin and alfa-fetoprotein (AFP) (Paradis, 2013). An increased level of AFP strongly suggests HCC, although not all cases of HCC are associated with AFP elevation, which may also be found in other liver diseases. In case of poorly differentiated tumors, the available markers are inadequate and additional markers would be useful. Finally, at the cellular level, HCC displays phenotypic traits of progenitor cells, retaining stem cell marker such as cytokeratin (CK) 19 that is expressed also in biliary epithelium

(Roncalli et al., 2010). Importantly, expression of CK19 in HCC is correlated with enhanced aggressiveness and poor prognosis. New immunological markers will allow a better characterization of the tumor and will provide useful information for the treatment of HCC patient.

1.3 Genetic alterations in HCC

Hepatocarcinogenesis is a multistep process in which multiple cancer-related genes are mutated. The molecular mechanisms and oncogenic pathways that are deregulated and/or mutated in HCC have not been completely elucidated, but are known to include changes in tumor suppressor genes, oncogenes, reactivation of developmental pathways and growth factors. Although many genetic alterations are present in HCC, the frequency of each individual gene modification is relatively low. Here, we will briefly discuss the major signaling pathways implicated in HCC such as p53, Wnt signalling, TGFβ, Myc. Finally, we will discuss new endogenous L1-mediated insertional mutagenesis as a potential source of mutation in HCC.

p53 was dubbed as "the guardian of the genome" referring to its capacity to respond to cellular stress and DNA damage by inducing cell cycle arrest, hence permitting DNA repair, or apoptosis (Vousden and Lane, 2007). Based on its role in conserving genetic stability and preventing genome mutation, it is understandable why p53 is the most frequently altered gene during human carcinogenesis. However, compared to other solid tumors, mutations in p53 are relative rare in HCC and vary in different geographic areas, reflecting differences etiological agents. In sub-Saharan Africa and China, where aflatoxin B1 exposure is responsible for a high incidence of HCC, p53 was frequently mutated (~50%), while p53 mutation is rare in HCC not induced by aflatoxin (Shiraha et al., 2013). A point mutation at the third position of codon 249 resulting in a G:C to T:A transversion was shown to occur also in non-tumoral livers

and reflected the exposure to aflatoxin B1 in a dose dependent manner (Bressac et al., 1991), indicating that this alteration is an early mutational event in hepatocarcinogenesis.

Other major risk factors for developing HCC are viral hepatitis B and C, each associated with different p53 mutation profiles and frequencies: in HBV-related HCC, p53 mutation (45%) was significantly higher than that in HCV-related HCC (13%) (Teramoto et al., 1994). The p53 abnormality in HBV-related HCC is due to the viral HBX protein, encoded by HBV genome. The HBX protein binds to the C terminus of p53 in the cytoplasm, resulting in the blockage of p53 entry into the nucleus and inhibition of several critical p53-mediated cellular processes, including sequence-specific DNA binding, transcriptional activation and apoptosis (Wang et al., 1994). The blockage of p53-mediated apoptosis, in particular, provides a selective advantage to preneoplastic hepatocytes (Arbuthnot et al., 2000).

The Wnt/β-catenin pathway is another key regulator of tumor development and differentiation and has been shown to have an essential role in HCC. In particular, cytoplasm accumulation of β-catenin was shown to occur in 62% off all HCC, and to correlate with poor prognosis and tumor recurrence (Wong et al., 2001).

The transforming growth factor beta (TGF-β) pathway has an important role in cell growth, differentiation and apoptosis. In the liver, TGF-β limits hepatocyte regeneration after injury by inhibiting DNA synthesis and inducing apoptosis (Oberhammer et al., 1992). TGF-β has been also described as tumor promoter by inducing epithelial to mesenchymal transition (EMT) that renders tumor cells more invasive (Giannelli et al., 2014). TGF-β has been reported frequently overexpressed in HCC, which correlated with increased tumor angiogenesis and poor prognosis (Teufel et al., 2007). A switch of TGF-β action during liver carcinogenesis from a tumor

suppressing effect to a tumor promoting function has been proposed. Especially, it has been shown that TGFβ induced apoptosis and EMT are mutually exclusive in physiological context, however in some conditions, TGFβ can induce apoptosis in a fraction of cells and simultaneously induce EMT in other cells meaning that hepatoblasts can respond differentially to the same factor (Song, 2007).

The role of known oncogenes in liver tumor formation and progression has been widely studied, and in particular that of c-Myc. The association of c-Myc with liver carcinogenesis was first identified through the observation of high expression of c-Myc in chronic liver disease and in HCC, by frequent c-*Myc* amplification in liver cancer tissue commonly seen in young patients with poor prognosis (Chan et al., 2004). The overexpression of c-Myc in the liver of transgenic mice induced liver tumorigenesis and its inactivation was sufficient to induce tumor regression (Shachaf et al., 2004).

L1 retrotransposon (long interspersed element 1) are autonomous mobile genetic elements and a source of endogenous mutagenesis in humans (Burns and Boeke, 2012). Retrotransposons transpose DNA sequences through an RNA intermediate by a copy and paste mechanism (Hancks and Kazazian, 2012). L1 elements are present at more than 500000 copies in the human genome, but the majority are inactivated due to point mutations, rearrangement or truncation and just 80-100 elements are transposition-competent, and active in any individual (Brouha et al., 2003). L1 insertions can alter gene structure and function and have been associated with hereditable and spontaneous retrotransposition events in different diseases (Faulkner, 2011). Despite this capacity, until very recently, just few L1 insertions have been found in human tumors, and their possible causative role remained to be demonstrated. The first successful mapping of somatic L1 insertion was achieved in

colorectal tumors, where a single L1 insertion integrated within the APC gene was sufficient to drive oncogenesis (Miki et al., 1992). Recently, Shukla et al. (2013) have mapped L1 integration sites in a cohort of HCC patient using retrotransposon capture sequencing (RC-seq) and identified 12 *de novo* tumor specific L1 insertions. One of these somatic L1 insertions was shown to activate *ST18* (Suppressor of Tumorigenicity 18), pointing to *ST18* as a putative oncogene in liver cancer (Shukla et al., 2013).

1.4 ST18

The *ST18* gene (Suppressor of Tumorigenicity 18) encodes a zinc-finger DNA-binding protein, with six C_2HC-type fingers arranged in two main clusters, each of which binding DNA (Yang et al., 2008) (Jandrig et al., 2004). *ST18* shows similarity to members of the *NZF/MyT1* family of transcription factors (Yee and Yu, 1998), a nonclassical zinc finger family that plays an important role in the development of the central nervous system (Lee and Michel, 2014). Three proteins are part of this family: neural zinc finger factor-1 (NZF-1), myelin transcription factor-1 (Myt1) and ST18 (NZF-3 or MYT3). *ST18* is constitutively expressed in the brain, it has been reported to be upregulated during neuronal differentiation, and its overexpression in neuronal progenitor cells caused spontaneous differentiation (Kameyama et al., 2011).

Despite the potential importance of *ST18,* little is known about its role and mechanisms of action in cancer, with contradictory reports on its pro- or anti-tumoral activities. *ST18* was first described as tumor suppressor in breast cancer because of the strong correlation between hypermethylation of its promoter and loss of expression in tumor cells (Jandrig et al., 2004). *ST18* is expressed at low levels in normal breast tissue, but is significantly down-regulated in primary breast tumors and in breast cancer cell lines (Jandrig et al., 2004). Ectopic *ST18* expression in breast

cancer cells inhibits xenograft tumor formation and colony formation in soft agar, suggesting that *ST18* behaves as a suppressor of tumor growth (Jandrig et al., 2004). Based on mRNA profiling and silencing with small interfering RNAs (siRNAs), it has been proposed that *ST18* regulates pro-apoptotic and pro-inflammatory gene expression in human fibroblasts (Yang et al., 2008): accordingly, siRNA-mediated knockdown of *ST18* reduced TNF-α induced apoptosis and pro-inflammatory gene expression, whereas its overexpression significantly increased apoptosis and expression of TNF-α, inteurleukin (IL)-1α and IL-6 (Yang et al., 2008). These data, along with a recent paper on the pro-apoptotic action of *ST18* in pancreatic β-cell (Henry et al., 2014), are consistent with a role in tumor suppression. Importantly, ectopic expression of the protein may cause artificial toxicity to the cells, and genetic proof that *ST18* loss or reduction actively contributes to tumor progression - hence formal proof for a tumor suppressor activity of this protein - is missing so far.

ST18 was significantly overexpressed in pediatric acute myeloid leukemia compared with healthy bone marrow, whilst its expression decreased to normal levels in patients with complete remission, pointing to *ST18* as an oncogene with a diagnostic potential of becoming a new marker in leukemia (Steinbach et al., 2006). As mentioned above, in a recent paper by Shukla et al. (2013), L1-mediated insertional mutagenesis was shown to occur at the *ST18* locus in human HCC, pointing to *ST18* as a candidate oncogene in HCC (Shukla et al., 2013). The authors corroborated further the oncogenic function of *ST18* showing that ectopic *ST18* translation and transcription was seen in tumoral but not in control liver and frequent amplification of *ST18* was observed in HCC nodules from Mdr2-/- mice (see below). However, a functional validation of *ST18* as an oncogene in liver carcinogenesis is still missing. Following up from the report by Shukla and co-authors (2013), we have therefore embarked

upon the investigation of the role of *ST18* during liver tumorigenesis and maintenance.

1.5 Generation of genetically defined liver carcinoma

Zender et al. (2005) developed a new mouse model of liver cancer based on *ex vivo* genetic manipulation of liver progenitor cells (hepatoblasts) followed by the transplantation of these cells into wild-type recipients. Practically, the authors isolated E-cadherin positive liver progenitors cells by indirect labeling, infected them with a combination of oncogenes (Myc or RAS) or short hairpin RNAs (shRNAs) directed against the tumor suppressor p53 (shp53) and finally transplanted these cells into immuno-compromised mice. Tumors arose rapidly and recapitulated the histopathology of human HCC, whilst immunohistochemistry confirmed their association with the liver lineage.

Interestingly, depending from the embryonic day of hepatocyte purification, transduced hepatoblasts acquired different phenotypes. Embryonic hepatoblasts harvested from p53 deficient mouse fetal livers at embryonic day (E) 14.5 and transduced with a retrovirus encoding c-Myc (or H-Ras^{v12}) rapidly acquired an immortal phenotype and generated spontaneous tumors when injected subcutaneously. On the contrary, when the same cells are harvested at a later stage (E18.5), c-Myc immortalizes, but does not transform them (Zender et al., 2005). Hence, these E18.5 p53$^{-/-}$/c-Myc hepatoblasts provide a sensitized background to test whether overexpression of potential oncogenes or knockdown of putative tumor suppressors triggers tumorigenesis. As expected, H-Ras^{v12} could transform these immortalized hepatoblasts (Table 1.1).

Embryonic day	Genetics modifications			Phenotype
14.5	p53-/- (or shp53)	c-Myc		Transformed
14.5	p53-/- (or shp53)	H-Rasv12		Transformed
18.5	p53-/- (or shp53)	c-Myc		Immortalized
18.5	p53-/- (or shp53)	H-Rasv12		Transformed
18.5	p53-/- (or shp53)	c-Myc	H-Rasv12	Transformed

Table 1.1: Schematic of hepatoblast immortalization and transformation capacities.
Hepatoblasts harvested from mouse fetal livers at different embryonic days and transduced with shp53 and/or c-Myc and/or H-Ras^{v12} rapidly acquire immortal or transform phenotypes, as indicated.

To identify genes required for the proliferation or survival of cancer cells, several groups have performed genetic screens and related functional validation in this mouse models and in human HCC cell lines (Zender et al., 2006) (Huang et al., 2014; Wuestefeld et al., 2013; Zender et al., 2008).

1.6 Inflammation

Inflammation is an immediate response of the immune system to infection and physical injury, aimed at restoring tissue homeostasis. Inflammation can be classified as acute or chronic, with the two forms being distinguished by their duration and the type of infiltrating inflammatory cells. Acute inflammation is an immediate protective response characterized by increased blood flow and leukocyte infiltration of the injured tissue, to remove the stimulus and repair the affected site. Chronic inflammation is a prolonged process acting as a favorable pre-neoplastic setting due to persistent aggressive stimuli that lead to more damage than healing.

Chronic inflammation and cancer have been linked for the first time by Rudolf Virchow in 1863, based on the presence of leukocytes within neoplastic tissue (Balkwill and Mantovani, 2001). This association has received growing support in recent years, as data revealing that inflammation is itself an important factor leading to cancer progression have accumulated (Hanahan and Weinberg, 2011). The relationship between inflammation and cancer consists of two pathways: an extrinsic pathway driven by inflammation or infection *per se* that increased cancer risk and an intrinsic pathway driven by genetic alteration that cause inflammation, and both can drive to neoplasia (Mantovani et al., 2008). The proof of the involvement of inflammation in cancer formation is starting to have implications for prevention and treatment. In particular, anti-inflammatory drugs have been reported to prevent or delay tumor progression in colon cancer (Wang and DuBois, 2013). Up to 15% of human cancers are associated with inflammation, while more than 90% of HCC cases originating from an inflammatory context as detailed above (Bishayee, 2014). Regardless the etiology (HBV,HCV, alcohol…), liver injury initiates in a background of inflammation that sequentially progresses through repeated cycles of apoptosis and regeneration, leading to epigenetic changes in the hepatocytes that finally culminate in neoplastic alterations (Cairo and Buendia, 2012). In particular, the neoplastic lesion in liver consecutively progresses from fibrosis to cirrhosis and finally culminates in HCC. Liver cirrhosis, which is linked to the development of the vast majority of cases of HCC, is characterized by a strong inflammatory response and the presence of senescent cells (Ramakrishna et al., 2013).

Many molecules compose the inflammatory microenvironment involved in tumor initiation and progression. Specifically, cytokines such as interleukin (IL) 1β, IL6, interferon (IFN) γ or tumor necrosis factor (TNF) α, participate in chronic hepatic

inflammation. IL1β promotes tumorigenesis through increased angiogenesis and is a potent mediator of metastasis, which altered the interaction between tumor and endothelial cells by upregulating vascular adhesion molecule-1 (VCAM-1) and vascular endothelial growth factor (VEGF) (Sansone and Bromberg, 2011). IL6 signaling leads to increased production of inflammatory cytokines through the activation of transcription factors such as NFkB (nuclear factor kappa-light-chain-enhancer of activated B cells) and STAT3 (signal transducer and activator of transcription-3). Using Mdr2 knockout mice, a model of chronic inflammation that develops cholangitis, chronic liver inflammation and finally HCC (see below), it has been shown that the TNF-NFkB axis has a pro-carcinogenic effect on the liver: inhibiting the NF-kB circuitry by treatment with anti-TNF-α prevented inflammation and inhibited tumor progression (Pikarsky et al., 2004). STAT3 was also reported as a crucial link between inflammation an HCC progression (He and Karin, 2011). Interestingly, STAT3 is activated in human HCC but not in the surrounding normal hepatocytes and has been shown to increase the capacity of tumors to suppress the immune response (He and Karin, 2011; Kortylewski et al., 2005). Whatever the etiology, activation of NF-kB and STAT3 have been shown to be frequent and early events that contribute to the acquisition of a transformed phenotype during hepatocarcinogenesis (Liu et al., 2002).

Although the existence of a link between liver inflammation and tumorigenesis is certain, little is known on the cellular pathways and the role of epigenetic changes involved in the inflammatory cascade in HCC. In an attempt to study the effects of acute inflammation *in vivo*, a model based on the inflammatory potential of lipopolysaccharide (LPS) was devised. LPS is a component of the cell wall of gram-negative bacteria that causes polyclonal activation of B cells and stimulates

accumulation of macrophages and induces release of many inflammatory cytokines such as IL1b, TNF-a, TGFb and IL-6, leading to acute inflammatory response (Zhong et al., 2006). To study chronic liver inflammation many mouse models have been used, including the Mdr2-/- mice, the outline of which we will given later on.

Finally, in this work we will describe experiments aimed at the validation of the role of our gene of interest based on either acute and chronic inflammation model.

1.7 Progressive familial intrahepatic cholestasis (PFIC)

Progressive familial intrahepatic cholestasis (PFIC) is a rare autosomal recessive disorder that manifests itself in the neonatal period, characterized by a cholestasis of hepatocellular origin that progresses to fatal liver failure during childhood. PFIC is a rare disease with an estimated incidence that varies between 1 every 50.000 and 100.000 births, with no geographical or gender preference (Davit-Spraul et al., 2009). PFIC comes in three types of autosomal recessive disease: PFIC1, PFIC2 and PFIC3, respectively mutated in the hepatocyte membrane transporter genes ATP8B1, ABCB11 and ABCB4 (Fig.1.2). ABCB11, a bile salt export pump, and ABCB4, a phosphatidylcholine (PC) floppase, are both members of the ATP binding cassette (ABC) family and transport the two major components of bile, bile salt and PC, through the membrane using ATP hydrolysis to pump against a substrate concentration gradient. ATP8B1 also known as FIC1, encodes for a P-type ATPase, and appear to flip a membrane phospholipid, phosphatidylserine (PS), in the opposite direction (Davit-Spraul et al., 2009; Nicolaou et al., 2012). An effective transport system is required for the removal of cholesterol, which is insoluble in water, bile acids and phospholipids (Kubitz et al., 2012). Alteration of bile acid excretion from hepatocytes into bile ducts due to an increase in hepatic and serum levels of bile salts, leads to chronic liver damage and to the early onset of hepatocellular carcinoma.

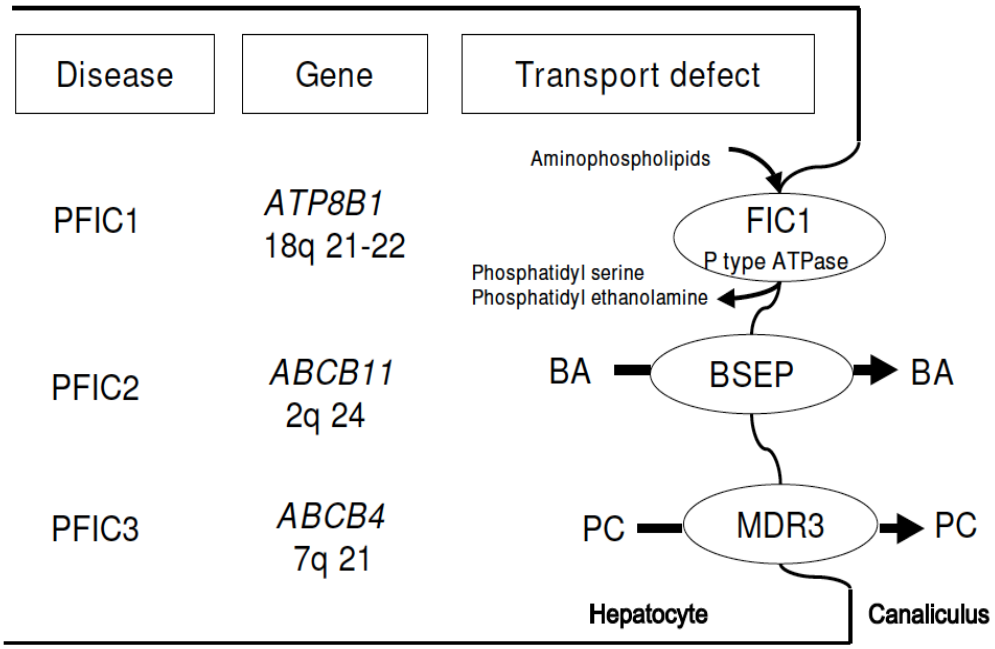

Figure 1.2: Progressive Familial Intrahepatic Cholestasis scheme. The three different types of autosomal recessive disease: PFIC1, PFIC2 and PFIC3 are mutated in the hepatocytes membrane transporter genes ATP8B1, ABCB11 and ABCB4, respectively, leading to different transport defect. BA: bile acid, PC: phosphatidylcholine (Davit-Spraul et al., 2009)

The common outcome of all PFIC types is cirrhosis and severe liver failure within the second decade of life. Patients with PFIC1, due to ATP8B1 deficiency, generally have canalicular cholestasis, and compared to PFIC2-3 the liver biopsies reveal mild liver damage, with a preserved lobular architecture and absence of giant cells (Clayton et al., 1969). PFIC1 is also known as Byler disease, electron microscopy revealing the so-called "Byler bile", granular bile accumulated in the hepatocytes. The serum levels of hepatic enzymes routinely screened as markers of hepatic damage, gamma-glutamyltranspeptidase (γ-GT) and alanine aminotransferase (ALT), are only mildly elevated in PFIC1 patients. The ATP8B1 gene is expressed in various tissues including liver, pancreas, cochlear hair cells and intestine: hence, unlike PFIC2 and 3, PFIC1 shows several extrahepatic symptoms such as pancreatitis, hearing loss and chronic diarrhea (Davit-Spraul et al., 2009).

PFIC2 patients have mutations in the ABCB11 gene, which encodes for a bile salt export pump, the principal conveyor of bile acids from the hepatocyte cytoplasm into the bile canaliculus. Mutations in this protein are responsible for the decreased bile salt secretion that leads to reduced bile flow and accumulation of bile salts inside the hepatocytes. As a consequence, patients have very low biliary bile salts but abnormally high serum bile salts. The levels of γGT and cholesterol in PFIC2 patients are normal but they have elevated serum ALT activity (Nicolaou et al., 2012). PFIC2 is the most severe form of PFIC and is the only form of PFIC that has been reported to degenerate into hepatocellular carcinoma or cholangiocarcinoma. Histologically, pre-tumoral PFIC2 livers are characterized by giant cell hepatitis, bile duct proliferation and portal fibrosis (Chan and Vandeberg, 2012).

The third type of PFIC, called PFIC3, is caused by genetic mutation in the ABCB4 gene, encoding a phospholipid floppase involved in biliary PC secretion. The ABCB4 gene, also called multidrug resistance-3 (MDR3) is the ortholog of the gene abrogated in Mdr2-/- mice and will be described later on. PFIC3 is characterized by increased γGT levels (Kubitz et al., 2012) and total absence of biliary PC. Liver histology reveals bile duct proliferation, portal fibrosis and biliary cirrhosis at advanced stage but no liver tumors have been related to PFIC3 (Chan and Vandeberg, 2012).

1.8 Mouse models of PFIC

As previously mentioned, PFIC2 is the only PFIC associated with liver cancer, with a tumorigenic process that follows a progression from dysplasia, through adenoma to HCC. Undoubtedly, the generation of a mouse model that mimics this spontaneous hepatocarcinogenesis would be really advantageous for the study of involved genes. Unfortunately, ABCB11 knockout mice display a less severe phenotype and do not

develop HCC (Lam et al., 2005). In these mice the total output of bile salts is unaffected due the compensatory role of another ABC transporter, ABCB1A otherwise unaffected in PFIC2 patients (Lam et al., 2005). Instead, Mdr2-/- mice (FVB.129P2-^{Abcb4tm1Bor}) represent a model of chronic inflammation and spontaneous hepatocarcinogenesis that shares a very close etiologic background with PFIC2, even though Mdr2 is the ortholog of the human MDR3 gene, mutated in PFIC3, which in humans is not associated with a progression to HCC.

The Mdr2 P-glycoprotein is present in the bile canalicular membrane of hepatocytes suggesting a role in biliary excretion (Smit et al., 1993): this protein is a transporter that functions as a flippase, translocating PC phospholipids from the inner to the outer leaflet of the hepatocytes canalicular membrane (Smit et al., 1993). In the absence of PC translocation activity, as in Mdr2-/- mice, there is no lipid secretion, persistent biliary epithelium damage induced by high concentrations of monomeric bile salts, and a consequent inflammatory response, followed by HCC (Fickert et al., 2004; Mauad et al., 1994). In Mdr2-/- mice tissues other than the liver have not shown any abnormalities. The liver looked anatomically normal until the second week after birth, when structural differences became clear in hepatocytes, with an increased number of acidophilic bodies, nuclear polymorphism and abnormally high proliferative activity and mitotic figures (Smit et al., 1993). Changes were not limited to the hepatocytes, but also the bile ducts were affected. The bile ducts showed persistent biliary epithelium damage, due to regurgitation of bile acid into portal interstitium and consequent inflammation and slight fibrosis (Smit et al., 1993). Mdr2-/- mice develop liver tumors following chronic inflammation in the early stage (8 weeks) characterized by extensive portal inflammation with mixed inflammatory infiltrates, rich in CD3+ cells, bile duct hyperplasia and hepatomegaly (Pikarsky et al., 2004).

From 4 months of age mdr2-/- mice start to develop preneoplastic lesions in the liver, and start to be affected by severe architectural and cytological liver dysplasia. Between 12 and 16 months of age, Mdr2-/- livers show multiple adenomatous lesions that progress to carcinoma (Katzenellenbogen et al., 2007) (Fig 1.3).

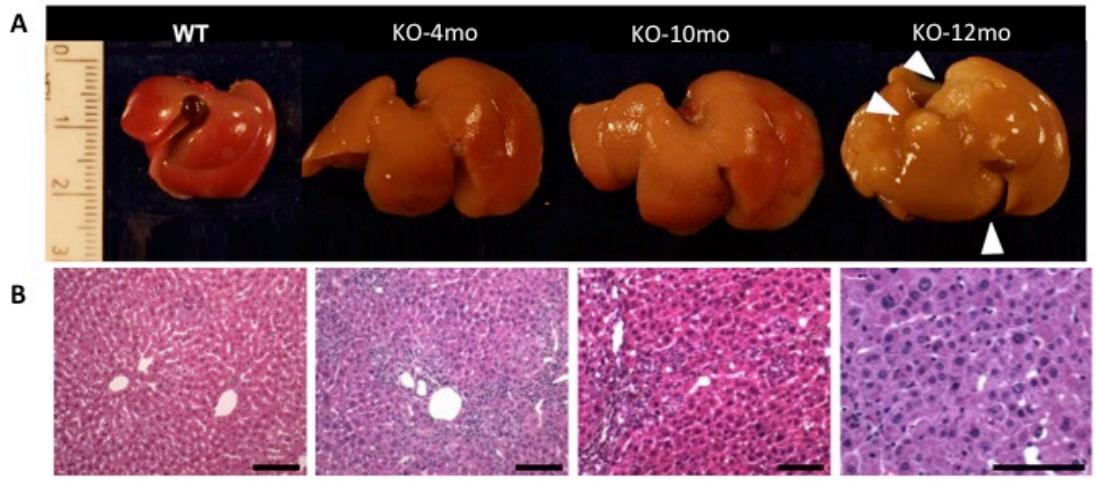

Figure 1.3: Dynamic changes in Mdr2-/- livers. Panel a. Livers of WT and KO mice at 4/10/12 months. Mdr2-/- mice develop hepatocellular carcinoma (indicated by arrowheads) after chronic hepatitis at shorter time points (4-10 month). Panel b. H&E stained sections from livers from WT and KO mice. At 4 months, inflammation is prominent, at 10 months there is severe architectural and cytologic dysplasia and HCC develops after 12 months .Modified from (Pikarsky et al., 2004).

We will take advantage of this well characterized model of inflammation-associated HCC using immunohistochemical analyses to study the induction of our candidate gene, ST18, by chronic liver inflammation.

1.10 Aim of the project

The molecular mechanisms and pathways responsible for the progression of hepatocellular carcinoma (HCC) remain to be fully characterized. Among the genetic lesions associated with HCC progression, Shukla et al. identified insertions of the L1 transposon proximal to the *ST18* (suppression of tumorigenicity 18) locus and suggested that *ST18* actually functions as an oncogene in HCC (Shukla et al., 2013). Despite the potential importance of *ST18* little is known about its role and mechanisms of action in cancer, with contradictory reports on its pro- or anti-tumoral activities. *ST18* was depicted as tumor suppressor in breast cancer (Jandrig et al., 2004) and as an oncogene in acute myeloid leukemia (Steinbach et al., 2006), but functional validation is missing in either case, precluding definitive understanding of the contribution of *ST18* to tumor progression. The aim of this project was to functionally validate the oncogenic function of *ST18* in HCC and, having done so, to characterize it at the molecular level. To this end, we have taken advantage of an ex-vivo model of liver carcinoma described previously by Zender et al. (2005). This approach is based on genetic manipulation of liver progenitor cells purified from mouse embryos and their seeding into recipient mice, resulting in the development of subcutaneous tumors that resemble human HCC.

2 MATERIALS AND METHODS

2.1 Isolation, culture and retroviral infection of liver progenitor cells.

We derived hepatoblasts from different strains of mice: C57/JHsd mice (Harlan laboratories), TRP53/C57 mice (Jackson laboratories), RERT2 (from Barbacid group, CNIO) following this protocol.

Liver cell suspensions from fetal livers of E 14.5-18.5 mice were diced and treated with Dispase (Gibco) 1000U/ml for one hour at 37C°. The livers were dispersed into single cells by pipetting and filtrated trough a nylon mesh filter (pore size,100um). The cellular pellet was washed with hypotonic lysis buffer (150 mM NH_4Cl 10 mM $KHCO_3$ 100 μM EDTA) for 3 min at 4°C, than centrifuge and put in ice.

Purification of E-cadherin positive hepatoblasts was performed using the MACS® magnetic cell sorting system (Miltenyi) through indirect labeling with the rat anti-mouse E-cadherin (ECCD-1) antibody (Calbiochem). Because E-cadherin is exclusively expressed on the cell membrane of hepatoblasts, we could obtain a highly pure population from the initial liver suspension.

Before loading onto MACS MS size column liver cell suspension were incubated with the antibody complex for 45 minutes at 4C°. Previously 4μg of ECCD-1 were incubated with 20μl of immunomagnetic beads at room temperature for one hour.

Cells eluted were plated in laminin-coated plate (Sigma) in DMEM (Lonza) 10% FBS NA supplemented with HGF (40ng/ml Peprotech), EGF(20 ng/ml Peprotech) and Dexamethasone (10-6M sigma).

After 48h cultured hepatoblasts were transduced with a combination of retrovirus co-expressing c-myc, inactivated p53 (sh-p53), oncogenic RAS ($H\text{-}Ras^{V12}$).

Others plasmid used for hepatoblasts transduction were: MSCV-ST18-FLAG-IRES-GFP, MSCV-LSL-ST18-FLAG, MLP-shST18, TtRMPVIR shST18.

Briefly, retrovirus were produced in Phoenix packaging cells and collected in hepatocyte growth medium. Supernatant was passed through a 0.45 μm filter and supplemented with polybrene (2μg/ml). The infection procedure was repeated three times every 4 hours, then we add fresh medium supplemented with HGF (40ng/ml Peprotech), EGF (20 ng/ml Peprotech) and Dexamethasone (10-6M sigma).

To activate the MSCV-LSL-ST18-FLAG we added 500nM 4-Hidroxytamoxifen (4-OHT) (H7904 Sigma) in the medium of s and we checked for Cre recombination after 72 hours by pcr using the following primers Fw: CCCTTGAACCTCCTCGTTCGACC Rv: TTATCTTCAACCTCGGCATCC. As control, we added 50μg/ml of TAT-Cre (home made) in Optimem (Life technologies) for 2 hours, and then we add the normal hepatoblast medium.

2.2 Generation of subcutaneus tumors.

$3x10^5$ genetically modified hepatoblasts in 0.3ml of PBS were injected subcutaneously in CD1-NUDE-HO (Charles River). Animals were monitored for signs of disease and tumor size was measured using a caliper.

2.3 Doxycycline treatment

CD1- nude mice injected with the conditional vector (TtRMPVIR shST18) to silence ST18 were treated with Doxycycline to activate the knock down of ST18. Mice were fed with 625mg/kg Doxycycline containing food (Mucedola). In some experiment we had also administrate the first hit of 200mg/ML Doxycycline (Sigma) in 300ul of water by oral gavage.

2.4 LPS treatment

C57/JHsd mice were injected intraperitoneally with 100 µg of lipopolysaccharide (LPS) and sacrificed after 24h of treatment. Liver portion were dissected from pathological analysis.

2.5 Pathological and immunohistochemistry analysis

Tumors or liver portions assigned to histological assessment were fixed in 4% formaldehyde overnight. The next day the sample was washed in 70% ethanol and submitted for paraffin embedding. 5 um sections were stained with hematoxilin/eosin, and submitted for inspection to a mouse pathologist (Enrico Radaelli, VIB Center for the Biology of Disease, KU Leuven Center for Human Genetics, Belgium, and Camilla Recordati, Fondazione Filarete, Milan Italy).

Human samples in the study were obtained from FFPE material from 4 children diagnosed with PFIC2-related HCC or chirrosis. All specimens were obtained at native-liver hepatectomy during transplantation at Ospedali Civici di Bergamo (Italy).FFPE material from Mdr2-/- mice were obtained from Natoli laboratory (IEO, Milan, Italy).

Immunohistochemistry analysis was performing following this protocol. Briefly, 5 um sections were de-waxed and re-hydrated through an ethanol scale, heated in EDTA o,25mM ph9 (Dako #S2368)or citra solution (BioGenex #HK086-9K) in a water bath at 99°C for 30 minutes for antigen de-masking and left to cool down for 20 min. Washed once in water and after 5 minutes of treatment with 3% H2O2 for quenching of endogenous peroxidases, slides were incubated with the primary antibody (Table 2.1) in a blocking solution (2% BSA, 2% goat serum, 0.02% Tween20, in TBS 1x) for 3h RT. After primary incubation, slides were washed twice with TBS 1x, and

incubate with the secondary antibody (DAKO Cytomation Envision System Labelled Polymer-HRP) for 45 minutes. After washed twice with TBS 1x were developed with peroxidase substrate solution with DAB (DAKO) for 2-10 minutes. Slides were finally counterstained with hematoxylin, de-hydrated through alcoholic scale and mounted with Eukitt.

Primary Ab	**Species**	**Dilution**	**Unmasking**	**Code/Company**
polyclonal anti-Albumin	Chicken	1:400	Citrate	#106582 Abcam
polyclonal anti-α-fetoprotein	Rabbit	1:800	-------	#0008 Dako
Monoclonal cytokeratin 19	Mouse	1:100	Citrate	#901-242-012811 Biocare medical
polyclonal anti ST-18	Rabbit	1:200	Citrate	#86563 Abcam
Monoclonal Ki-67	Mouse	1:500	Citrate	#M7249 Dako
Cleaved Caspase-3	Rabbit	1:200	Citrate	#9661 Cell Signaling
Polyclonal Ve-Cadherin	Goat	1:200	EDTA	#6458 Santa Cruz

Table 2.1: Primary antibodies used for immunohistochemistry

2.6 RNA extraction and analysis

Frozen tissue samples were homogenized with a dounce homogenizer or with GentleMACS Dissociator (Miltenyi Biotec), depending on the tissue volume, prior to column extraction. DNA from formalin-fixed, paraffin-embedded (FFPE) samples was purified with the AllPrep DNA/RNA FFPE kit (Qiagen). RNA was extracted in Trizol (Invitrogen) using the RNeasy Mini Kit (Qiagen) according to the manufacturer's instructions. 0.5 ug of total RNA was used for cDNA synthesis (using the ImProm-II Reverse Transcriptase, Promega), and 1 µl of the obtained cDNA was generally used as template for qPCR expression analyses. Quantification was performed on Nanodrop, and quality was assessed on Bioanalyzer (Agilent).

1 µl cDNA from each reaction was used for qRT-PCR using the mouse ST18 primers (F' GAAAACGGCACATTGGACTT;R' GGTGAGGAAGTTGGGGGTAT).

qRT-PCR (SYBR-green) analysis was performed on an Applied Biosystems 7500 Real-time PCR system. Values were normalized to *RPPO (F'* TTCATTGTGGGAGCAGAC; R' CAGCAGTTTCTCCAGAGC).

For RNAseq, RNA quality was assessed using the BioAnalyser 2100. For each sample, 5µg of total RNA were depleted of ribosomal RNA with the Ribo-Zero^{TM} rRNA Removal Kit from Epicentre®. Ribosomal RNA removal was checked using the BioAnalyser 2100. RNAseq libraries were prepared with the Illumina TruSeq RNA sample preparation kit v2 following the manufacturer's protocol. Briefly, RNA was fragmented and cDNA was synthesized, end-repaired and 3'-end-adenylated. Following adapter ligation, libraries were amplified by PCR for 15 cycles. Libraries with distinct TruSeq adapter index were multiplexed (3 libraries per lane) on a HiSeq 2000 and sequenced for 50 bases in the paired-end mode. Deseq2 was used to analyze

RNAseq data. RNA seq duplicates were eliminated using rmdup function from the suite samtools (http://samtools.sourceforge.net/). Genes were hierarchically clustered with the R function hclust. Functional annotation was performed using the Gene Ontology categories of the bioinformatics tool Gene Set Enrichment Analysis (GSEA) based on Molecular Signatures Database (MSigDB). QIAGEN'S Ingenuity Pathway Analysis (IPA) was, also, used to interpreted the biological meaning.

2.7 Immunoblotting

Tumor tissue or cell pellets were lysed with 20mM HEPES at pH 7.5, 300mM NaCl, 5mM EDTA, 10%Glycerol, 1% Triton X-100 supplemented with protease inhibitors (Mini, Roche) using a tissue homogenizer. Equal amounts of protein (50µg) were separated on 10% SDS-polyacrylamide gels and transferred to PVDF membranes. The blots were probed with antibodies against: anti-FLAG (1:8000 Sigma), anti-GFP (1:1000 home-made), Vinculin (1:10000 Sigma) anti ST18 (1:1000 Abcam).

2.8 Flow cytometry

Hepatoblasts GFP tagged were not fixed and directly monitored by flow cytometry. Single cell suspension was resuspended in PBS. Cells were analyzed using a FACSCalibur (Becton-Dickinson; Mountain View, CA) flow cytometer. GFP-expressing cells were detected using the FL1 channel (absorption spectra 530/30 nm). Before doing FACS analysis from tumors, to verify the presence of Venus, tumors were diced and treated with dispase (Gibco) 1000U/ml for one hour at 37C° and dispersed into single cells by pipetting and filtrated trough a nylon mesh filter. All FACS data were analyzed by using FlowJo software (TreeStart).

2.9 Colony forming assay

In vitro, transformation assay was performed by placing a cell suspension into a semi-solid medium, such as methylcellulose, MethoCult™ SF M3236, followed by incubation at 37°C for periods ranging from a few days to several weeks. In detail 5.000 hepatoblasts resuspended in 250uL of hepatocytes growth medium were added to 1250uL of Methylcellulose stock (9 mL of MethoCult, P/S 100 uL, Glutammine 100 uL, (10%)FBS NA 1mL). The suspension was placed in a 6-well plate untreated and incubated at 37°C. Colonies are visible after 7-15 days.

3 RESULTS

3.1 Generation of hepatocellular-like carcinomas from transplanted liver progenitor cells

To pursue the functional validation of genes involved in the initiation, progression or maintenance of HCC we initially set up an appropriate experimental system to model HCC in mice: this was based on previously published work (Zender et al., 2005), and consisted in the purification of liver progenitor cells from mouse embryos, genetic manipulation of the cells *ex vivo,* followed by their transplantation into recipient mice (Figure 3.1). Hepatoblasts were isolated from the fetal liver taken from C57BL/6 embryos on embryonic day (E) 14.5-18.5 by immuno-affinity purification on magnetic beads with an antibody against E-cadherin, a marker of liver hepatoblasts (Nitou et al., 2002). Purified cells were cultured on laminin-coated plates for 48hrs in a chemically defined medium supplemented with hepatocyte growth factor (HGF), epidermal growth factor (EGF) and dexametasone. Following *in vitro* expansion, hepatoblasts were transduced with different combinations of retroviruses expressing c-*myc*, an shRNA targeting p53, or oncogenic Ras (H-Ras^{V12}), each of which affects signaling pathways altered in human liver cancer. As expected, p53-deficient E14.5 hepatoblasts transduced with a retrovirus encoding c-myc rapidly acquire an immortal phenotype in culture and become transformed, as shown by their ability to generate tumors when injected subcutaneously. Moreover, when the same cells are harvested and manipulated at a later stage (E18.5), c-myc immortalizes, but does not transform them (Zender et al., 2005). Genetically modified cells were injected subcutaneously into immunocompromised CD-1 nude mice. Animals were monitored for signs of disease and tumor size was measured using a caliper. After 14 days from the injection, tumors were harvested and processed for histological analysis.

An experienced mouse-pathologist examined several tumor sections stained with hematoxylin and eosin (H&E) and confirmed their liver origin. Tumors were classified as pseudoglandular, mixed pseudoglandular tubular, or mixed solid trabecular each resembling a typical growth pattern of human HCC (Zender et al., 2005)(Fig. 3.2). In addition, tumors were stained with liver-specific markers: albumin (differentiated liver cells), α-fetoprotein (fetal-specific glycoprotein, expressed in tumors), cytokeratin 19 (marker of biliary differentiation) conforming their identity as liver tumor (Fig. 3.3). Thus, as observed by Zender et al (2005), tumors arising from *ex vivo* manipulated liver progenitor cells exhibited features of human HCC, providing a valid experimental system to investigate the role of oncogenic and tumor suppressive events in this tumor model.

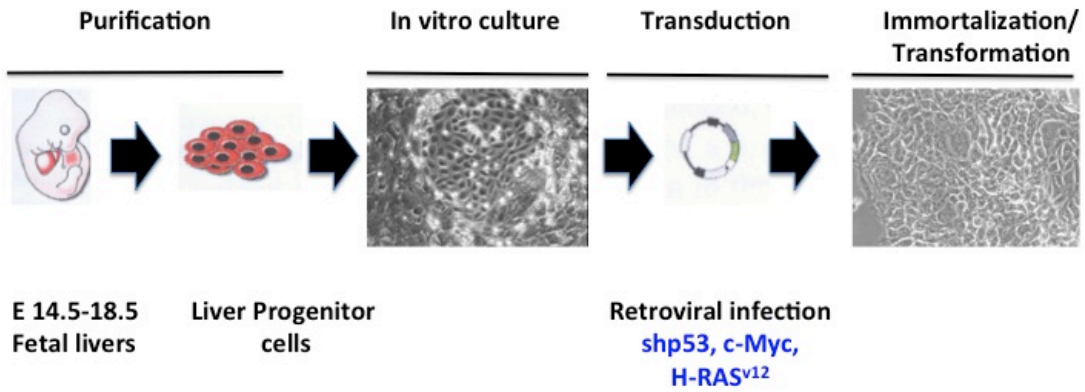

Figure 3.1: **Schematic representation of the general strategy**. E-Cadherin-positive fetal liver hepatoblasts were purified using an immunomagnetic bead based procedure and cultured on laminin-coated plates for two days. Cells were retrovirally transduced with c-myc, H-Ras^{V12} and/or an shRNA directed against the tumor suppressor gene p53. Upon clonal expansion, cells were injected subcutaneously into recipient mice or used for *in vitro* experiments.

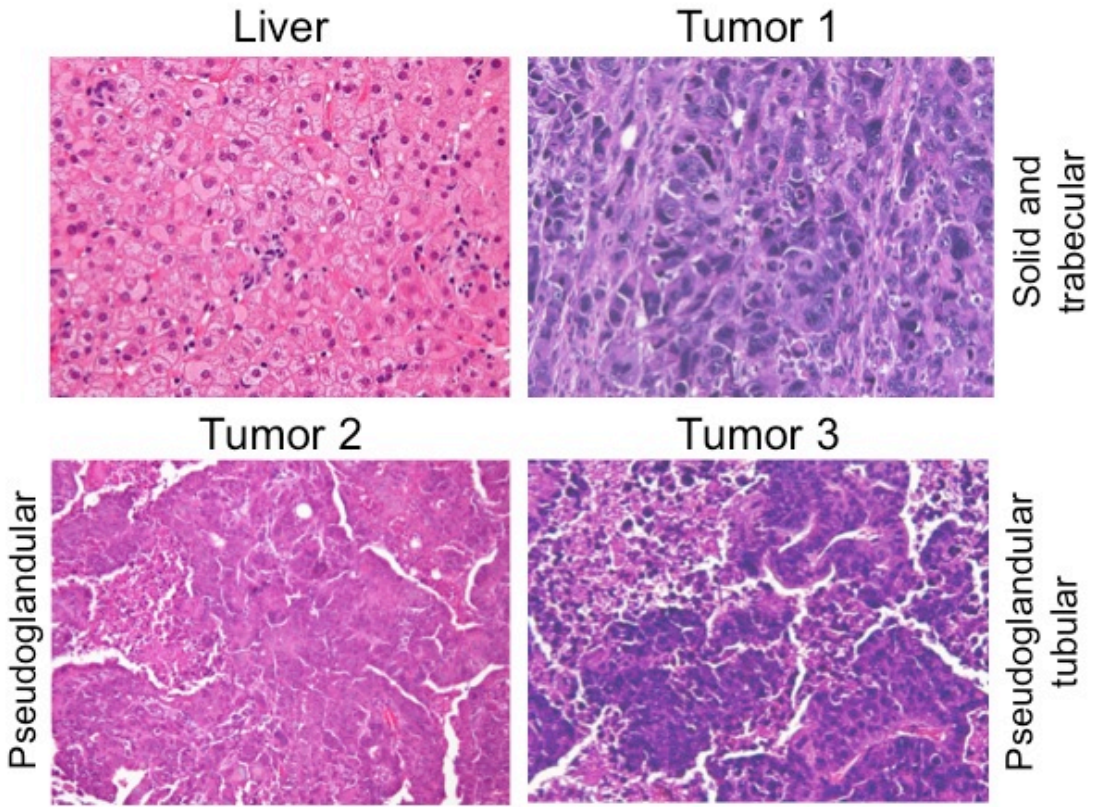

Figure 3.2: **H&E of subcutaneous tumors reveal histopathological subtypes of human HCC.** Histopathological analysis of tumors derived from E14.5 E-Cadherin^{+} liver progenitor cells transduced with different combinations of H-Ras^{V12}, Myc and shp53. Subcutaneous tumors closely resembled different histological subtypes of human HCC, as indicated beside each panel. Magnification is 20x.

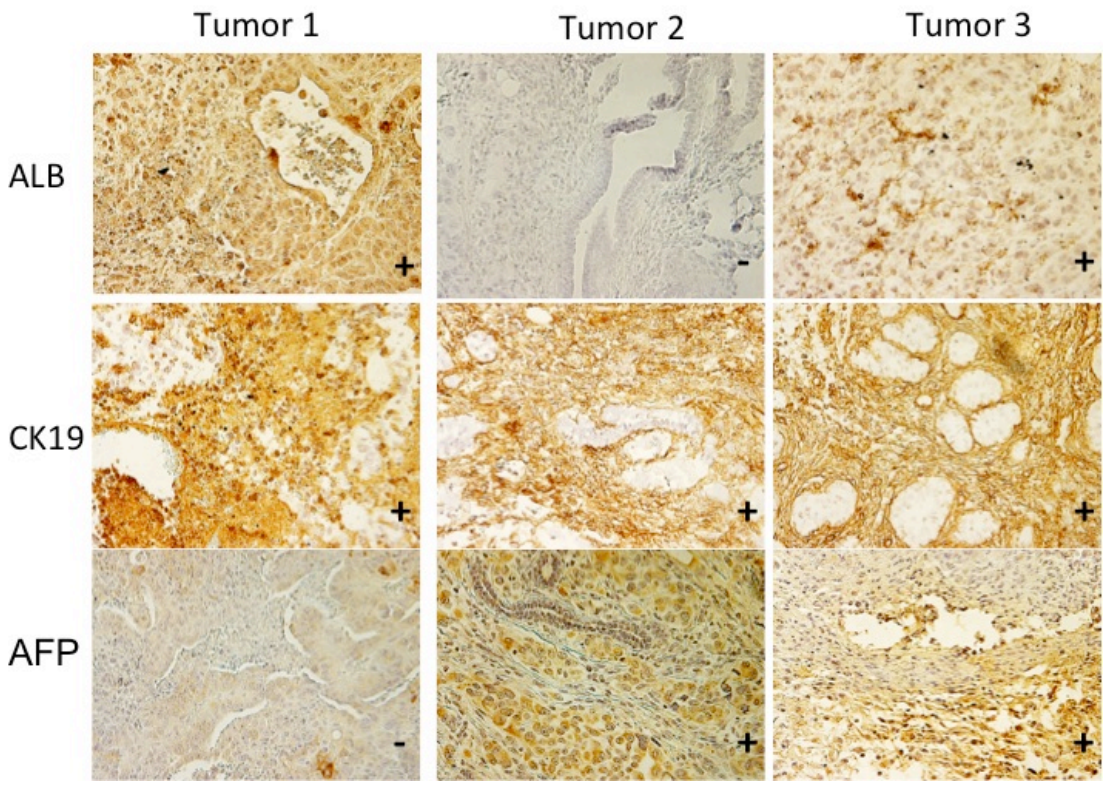

Figure 3.3: **Immunohistochemical staining of subcutaneous HCC-like tumors**. Tumors were stained for albumin (ALB) and α-fetoprotein (AFP), markers of embryonic liver progenitors and HCC, and cytokeratin 19 (CK-19), a marker of bi-potential liver progenitors. All tumors examined were positive for at least one of these markers confirming their liver origin. Magnification is 20x.

3.2 ST18 is poorly expressed in cell lines but highly expressed in tumor samples

ST18 is poorly expressed in liver (Jandrig et al. 2004), but a recent profiling of L1 retro-transposition events in human HCC has led to the proposal that its up-regulation may be a tumor-promoting event (Shukla et al., 2013). We thus sought to determine whether *ST18* is expressed in our mouse tumor model. We used quantitative RT-PCR to measure mRNA expression levels of *ST18* in *in vitro* cultured liver progenitors cells as well as matched tumor samples derived from subcutaneous injection of the same cell population. Genetically modified hepatoblasts, whether immortalized or transformed, poorly expressed *ST18* (Fig. 3.4-A). Instead, subcutaneous tumors

derived from the same transformed cells displayed higher *ST18* mRNA levels (Fig. 3.4-B). We confirmed these results by immunohistochemistry on tumor sections using an antibody against the ST18 protein. Indeed, normal liver tissue showed little or no ST18 signal while tumors stained positive for ST18 (Fig. 3.5). Moreover, as expected for a zinc finger DNA binding protein, we observed a predominantly nuclear staining in tumors (Jandrig et al. 2004).

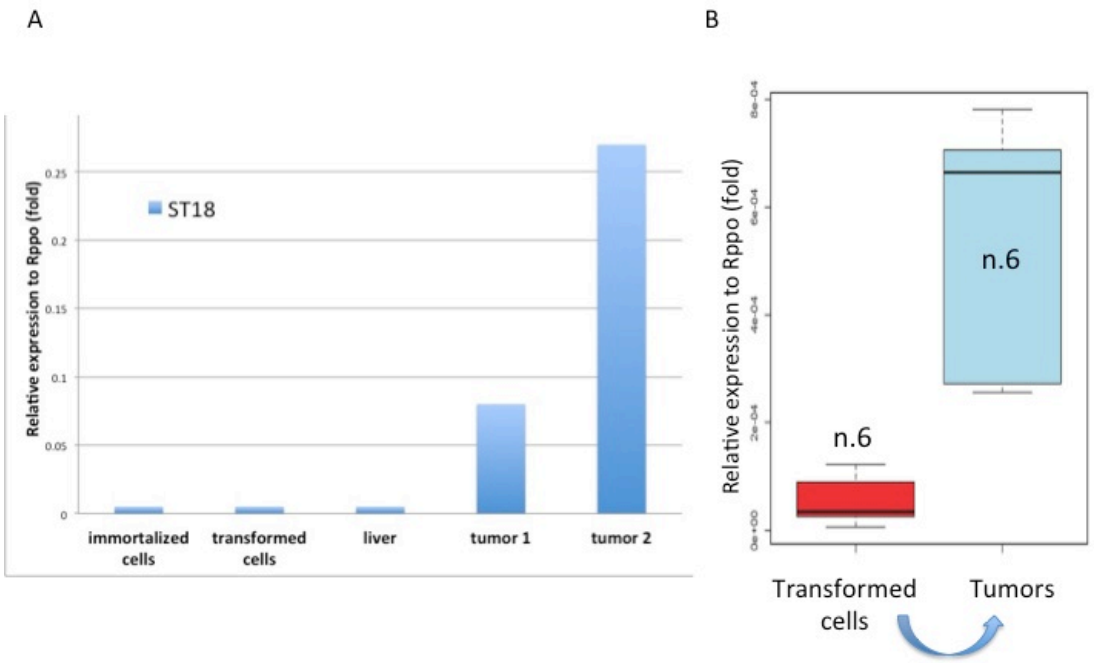

Figure 3.4: mRNA expression analysis of *ST18* in cultured cells and tumor tissue. Panel A: Quantitative real-time RT-PCR analysis of *ST18* expression in immortalized hepatoblasts (E18.5 shp53/c-Myc), in transformed hepatoblasts (E14.5 shp53/c-Myc), in liver and in two different tumors arising after subcutaneous seeding of transformed cells in CD-1 nude mice. Panel B: Quantification of *ST18* expressing levels in six different cell lines derived from various combinations of H-Ras^{V12}, c-Myc and shp53, and their corresponding tumors. Despite heterogeneity of expression amongst the tumors, the *ST18* levels were significantly higher in tumors compared to cultured transformed cells.

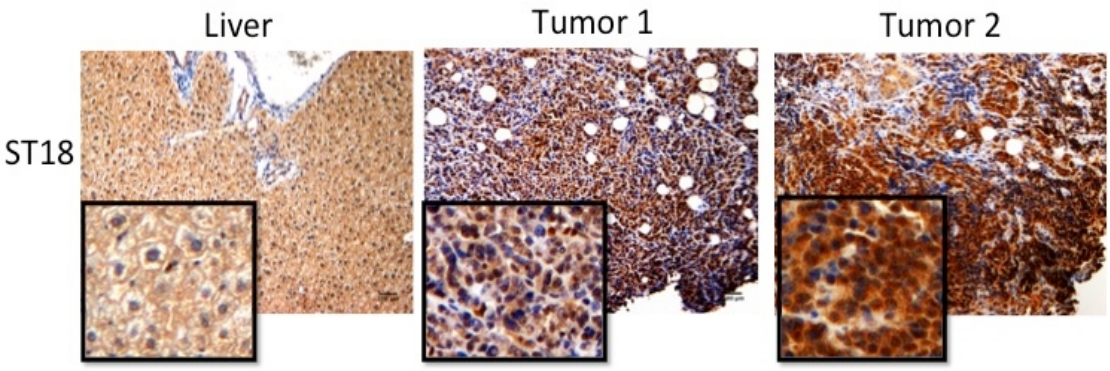

Figure 3.5: Immunohistochemistry for ST18 in tumors and liver tissue. Normal adult liver and two different subcutaneous tumors were stained using antibodies against ST18 revealing positivity in tumors compare to normal liver. Insets (40x magnification) denote the high nuclear positivity in tumors and low signal in normal liver tissue. Big panels are shown at magnification of x10.

3.3 ST18 is induced by inflammatory stimuli

The data presented above showed that ST18 expression increases both at the mRNA and protein level in tumors, while it is almost undetectable in normal liver tissue. ST18 may also regulate pro-inflammatory gene expression in fibroblast (Yang et al., 2008), pointing to a direct role in the inflammatory response.

To address a possible link between ST18 expression and inflammation, we induced an acute inflammatory response in C57BL/6 mice by intra-peritoneal injection of bacterial lipopolysaccharide (LPS) (Zhong et al., 2006)and we sacrificed the mice 24 hours after injection. Formalin-fixed paraffin-embedded (FFPE) liver sections from control and LPS treated mice were stained with hematoxylin/eosin (Fig. 3.6, upper panel). As expected (reviewed in (Nesseler et al., 2012), LPS administration causes severe hepatic dysfunction and liver damage. Additionally, as shown in Fig 3.6, ST18 expression was induced upon LPS treatment, especially nearby blood vessels and bile ducts. We conclude that ST18 expression is augmented upon acute liver inflammation.

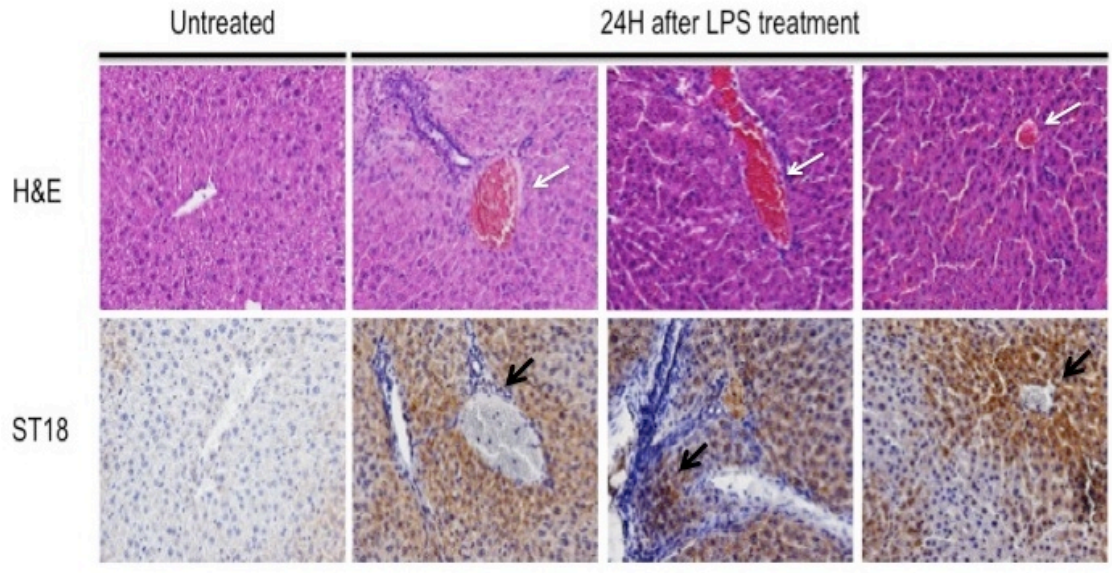

Figure 3.6: **LPS treatment induces ST18 expression in liver**. First row: Hematoxylin and eosin staining shows severe hepatic dysfunction and infiltration (white arrows) in mouse livers 24 hours post treatment with LPS compared to untreated liver. Second row: IHC performed on the same livers samples using an antibody against ST18. LPS treated livers showed high positivity for ST18 in the vicinity of blood vessels and bile ducts as shown by black arrows, instead in untreated liver the expression of ST18 is very low. (10x magnification)

Next, we investigated whether upregulation of ST18 also occurs in chronically inflamed livers. It has been shown that the *ST18* locus is frequently amplified in HCC nodules from the *Mdr2*$^{-/-}$ mouse model of inflammation-driven HCC (Shukla et al 2013). These mice lack the P-glycoprotein of the bile canaliculi membrane of hepatocytes, and as a consequence lack lipid secretion, show persistent damage of the biliary epithelium - induced by high concentration of monomeric bile salts - and a chronic inflammatory response (Fickert et al., 2004; Mauad et al., 1994). Mdr2-/- mice have an age-dependent progressive deregulation of genes that lead to development of pre-neoplastic lesions and liver dysplasia within the first 10 months of age followed by the development of HCC (Katzenellenbogen et al., 2007).

We decided to verify the expression of ST18 protein in FFPE liver sections from pretumoral Mdr2-/- mice. Sections of inflamed, pre-neoplastic livers obtained from Mdr2-/- mice at the age 4-10 months were stained with an antibody against ST18. Liver from control mice showed a weak staining while Mdr2-/- livers were positive for ST18 (Figure 3.7). We thus confirmed that ST18 expression correlates with chronic liver inflammation in the Mdr2-/- mouse model.

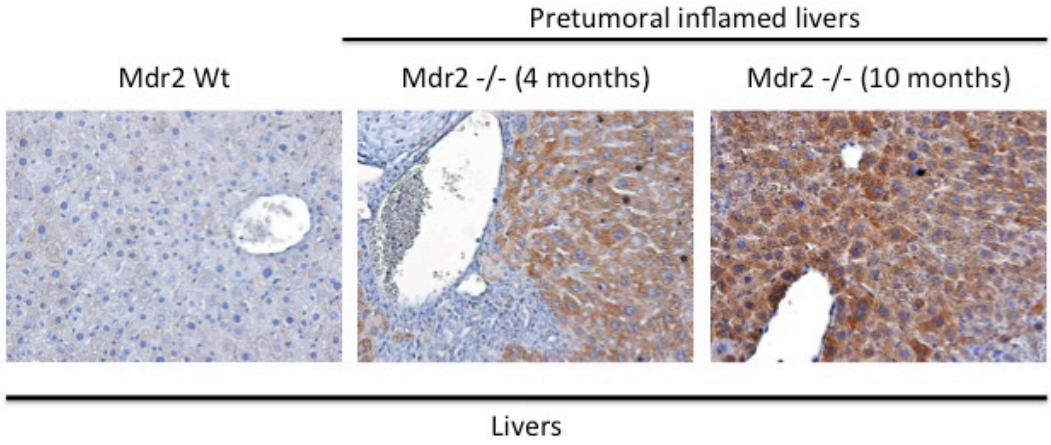

Figure 3.7: **Pretumoral inflamed livers from Mdr2 -/- mice express ST18.** IHC with anti-ST18 in Mdr2 wt liver and in two different Mdr2-/- livers showing that pretumoral inflamed Mdr2-/- livers were highly positive for ST18 compared to the low expression in normal liver tissue.

Despite minor differences between murine and human disease, HCC lesions developed by Mdr2-/- mice share a very close tumorigenic process with those observed in a chronic inflammatory setting in pediatric patients with progressive familial intrahepatic cholestasis 2 (PFIC2). As detailed in the Introduction (see section 1.7), these patients have a mutation in the *ABCB11* gene, which encodes a membrane transporter required for the export of bile salts from hepatocytes, leading to chronic inflammation and to HCC (Knisely et al., 2006). In order to investigate whether ST18 might also be up-regulated in individuals with PFIC2 mutations, we performed immunohistochemical analysis using an antibody against ST18 on FFPE

sections from liver biopsies from these patients as well as from livers affected by cirrhosis, to distinguish between neoplastic cells and cirrhotic surrounding tissue. Normal liver tissue and cirrhotic tissue showed low ST18 expression, while PFIC2 livers were strongly positive for ST18 (Fig 3.8). Hence, deficiency of the membrane transporter genes *Mdr2* and *ABCB11* led to analogous effects in mice and humans, respectively, with chronic inflammation and induction of ST18 expression.

We therefore hypothesized that expression of ST18 in tumors might be the result of an upregulation of inflammatory pathways during tumor development.

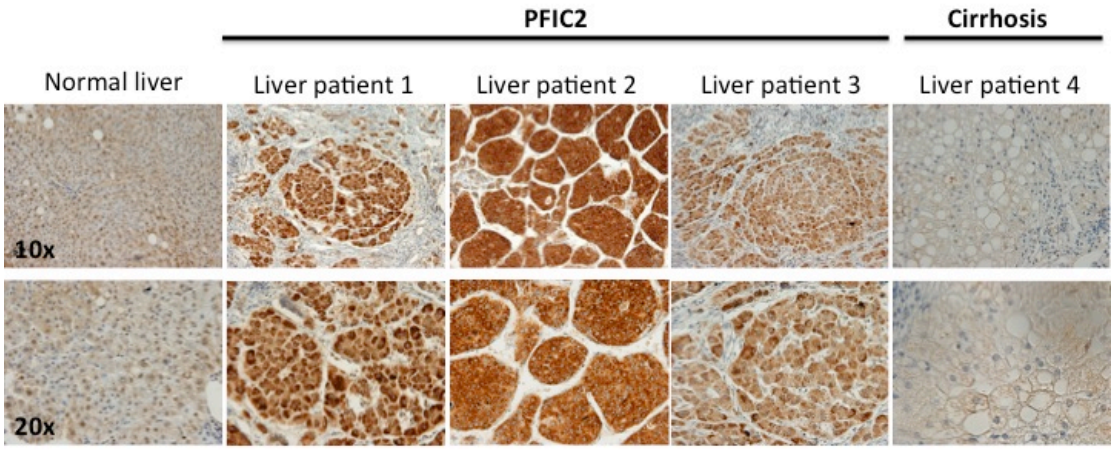

Figure 3.8: Patients with PFIC2 express ST18 in the liver. IHC analysis of ST18 in normal liver and in three different PFIC2 patient liver biopsies and in cirrhotic liver samples. Livers from patients with PFIC2 were highly positive comparing the low signal in normal liver tissue and in cirrhotic tissue. 10x & 20x magnification images.

3.4 Ectopic expression of ST18 is toxic to hepatoblasts in vitro

To uncover the effect of the ectopic expression of ST18, we performed *in vitro* GFP competition assay using either E14.5 hepatoblasts (previously transformed with c-myc/shp53/H-Ras^{V12} (see section 3.1) or NIH/3T3 fibroblasts. Both cell types were transduced at low *multiplicity of infection* (MOI) with a GFP-tagged retroviral vector expressing human ST18 (MSCV-ST18-FLAG-IRES-GFP) in order to obtain an infection efficiency of ~35%. Expression of the tagged ST18 protein was confirmed by immunoblotting, with similar levels in both cell types achieved 24h after infection (Fig. 3.9). Monitoring the levels of GFP-positive cells showed a progressive reduction in ST18-expressing cells over the initial passages, which did not occur in cells infected with the corresponding empty vector (MSCV-IRES-GFP) (Figure 3.10 A, B). It is noteworthy that GFP expression levels obtained by the transduction of cells with the vector containing ST18 are lower than those with empty vector, albeit reproducibly above background fluorescence in uninfected cells. Moreover, the same effect is apparent in the immunoblots shown in Figure 3.9. In the case of the hepatoblasts, the counter-selection of ST18-expressing cells was confirmed in six independent experiments (Fig. 3.11). In populations infected with the ST18-expressing vector, GFP-positive cells showed clear morphological changes, in particular a large flat morphology reminiscent of the activation of a senescence program (Fig. 3.12-A, B). While the cellular and molecular mechanisms associated with this effect remain to be characterized in detail, our data show that ectopic expression of ST18 in either hepatoblast or fibroblast *in vitro* is toxic to the cells.

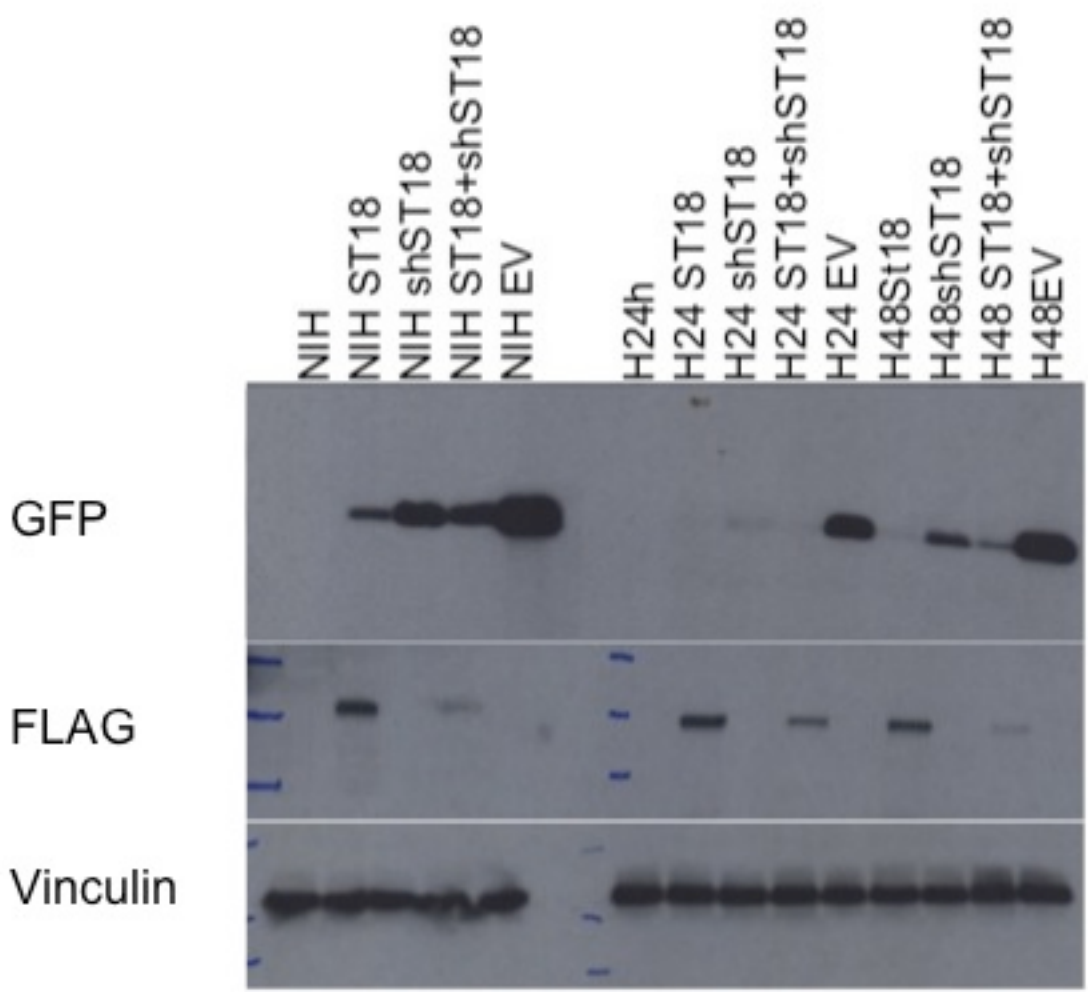

Figure 3.9: Immunoblot analysis in NIH/3T3 and hepatoblasts. Immunoblot analysis of FLAG-tagged ST18 in NIH/3T3 fibroblasts (48h after infection) and in transformed hepatoblasts (E14.5 c-myc/shp53/H-Ras^{V12}) at 24/48h. The efficiency of ST18 knockdown is also shown. ST18 knockdown is visible as a decrease of FLAG and GFP expression in cells coinfected with overexpression and silencing plasmids. The silencing of ST18 was used for further experiments (see below). Vinculin was used as a loading control.

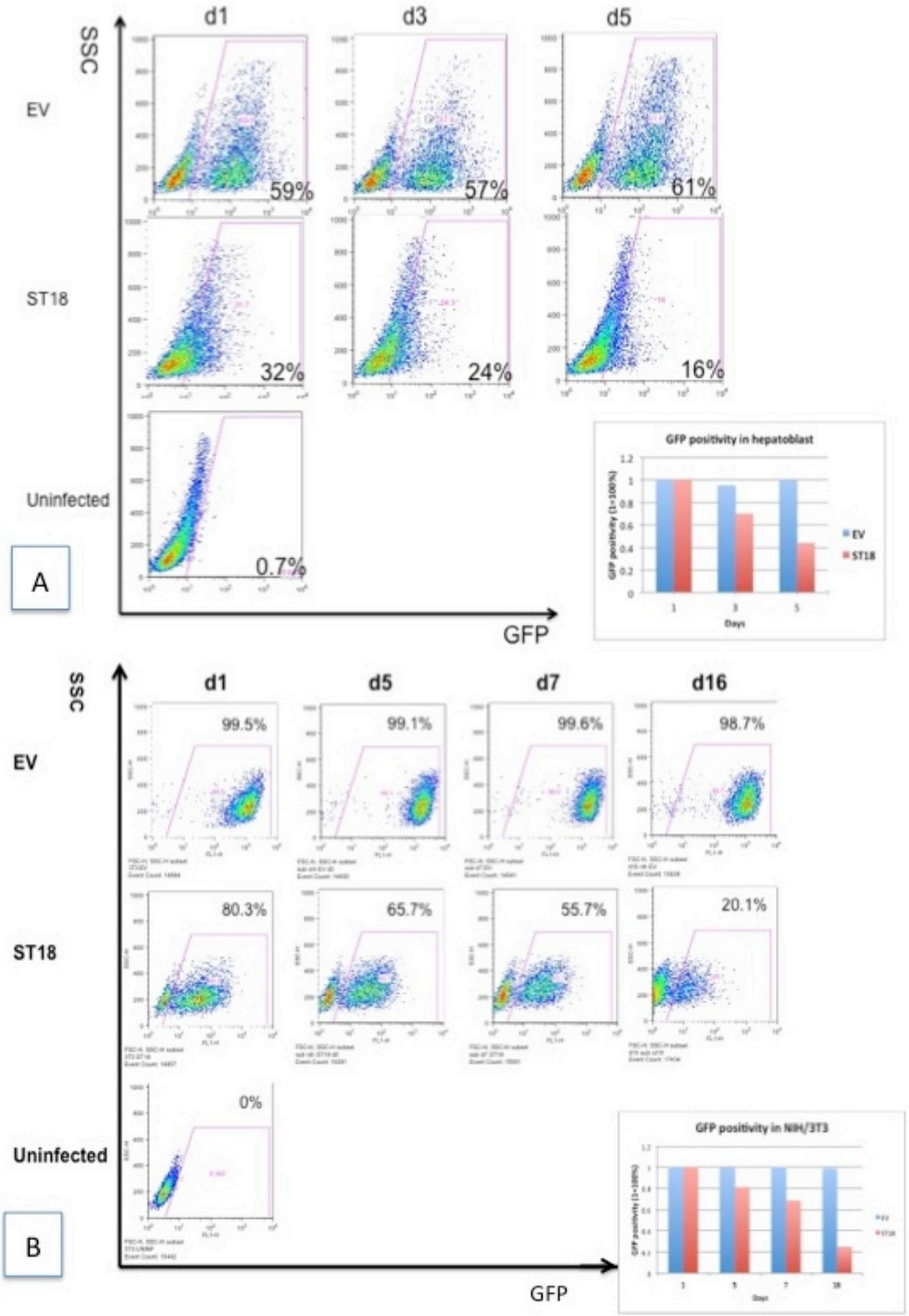

Figure 3.10: ST18/GFP^{+} expressing hepatoblasts and NIH/3T3 are counterselected. Flow cytometric analysis of single-cell suspensions prepared from transformed hepatoblasts (E14.5 c-myc/shp53/H-Ras^{V12}) (panel A) or NIH/3T3 (panel B) following infection with empty vector (EV, MSCV-IRES-GFP) or with MSCV-ST18-FLAG-IRES-GFP. Whilst, cells infected with EV maintained stable percentage of GFP+ cells over several passages, ST18-GFP expression in hepatoblasts or fibroblasts decreased over time. Insets give the percentages of GFP positivity normalized to the first day considered 100%. Blue columns (EV) remain constant and red columns (overexpression of ST18) decrease during the course of the experiment.

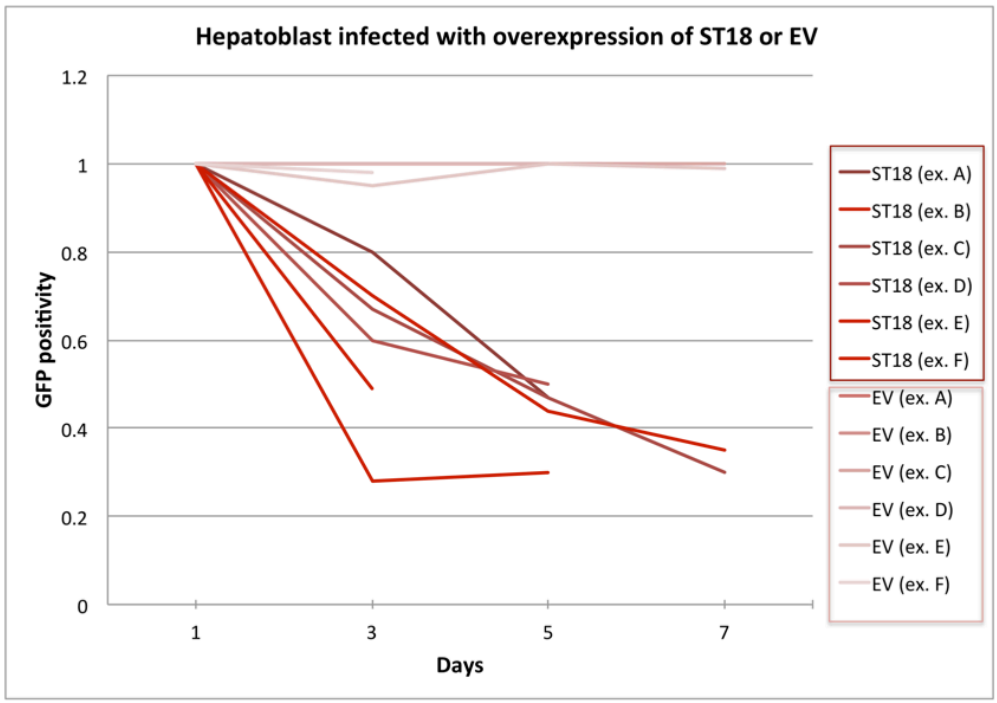

Figure 3.11: **The ectopic expression of ST18 in hepatoblasts is cytotoxic as GFP-positive cells are counterselected.** Chart summarizing flow cytometric analysis of GFP profiles seen in six independent experiments (A-F). Hepatoblasts infected with MSCV-ST18-FLAG-IRES-GFP lose GFP positivity over time whereas cells infected with EV (MSCV-IRES-GFP) remain GFP-positive. Analysis of variance (ANOVA) showed that the two groups are significantly different, P value of 1.4e-6 ***.

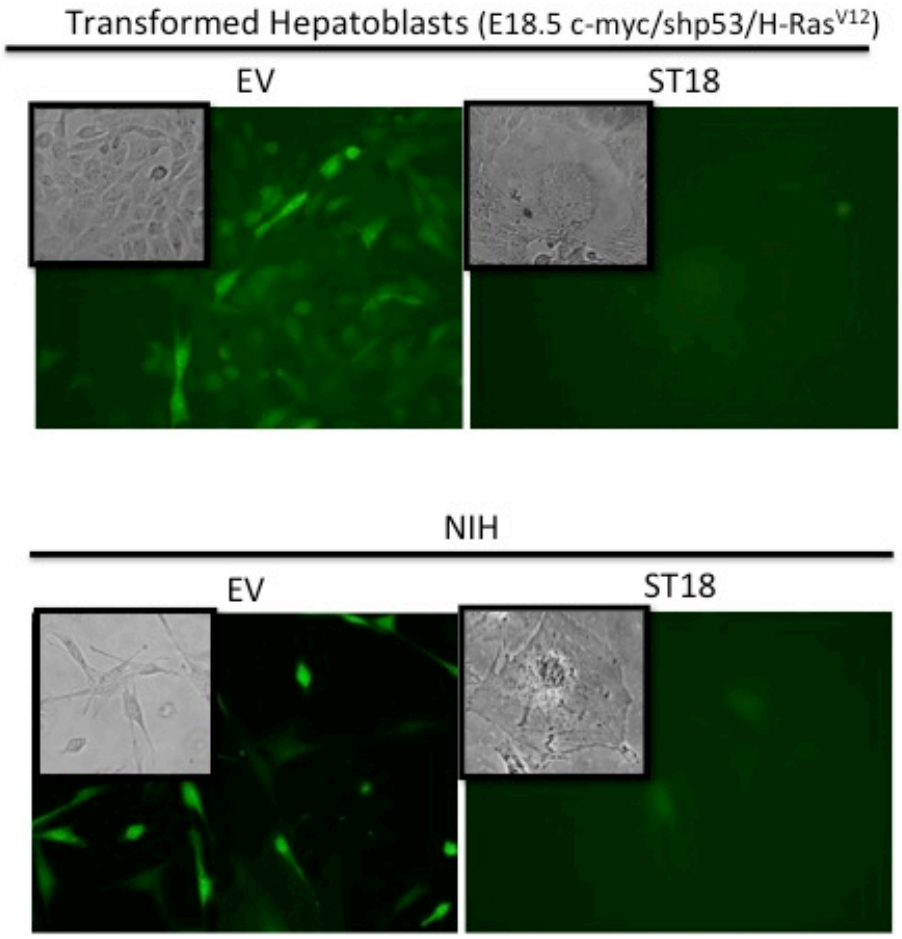

Figure 3.12: Morphological changes upon ST18 overexpression in hepatoblast and NIH. Overexpression of ST18 (here shown indirectly by observing GFP^+ cells) leads to *morphological* changes (large flat shape) both in transformed hepatoblasts and in fibroblasts. No morphological changes are apparent in the cells infected with EV.

3.5 Conditional expression of ST18 in CRE-ERT2 hepatoblasts

As ectopic expression of ST18 *in vitro* led to impaired hepatoblast proliferation, and as the *in vivo* model system used here requires initial transduction of hepatoblasts *ex vivo*, we decided to set up a conditional expression system that would allow us to induce expression of ST18 directly in tumors following transplantation. We thus derived E14.5 hepatoblasts from heterozygous CRE-ERT2 embryos, transduced these cells with the transforming constructs (c-myc/shp53/H-Ras^{V12}: see 3.1.) and subsequently with a vector allowing conditional expression of ST18 under the control of Cre recombinase (MSCV-LSL-ST18-FLAG). This vector included a dsRed expression cassette flanked by LoxP sites inserted upstream of the VENUS-ST18 coding sequence, thus blocking translation of ST18. The deletion of dsRed by Cre recombinase results in the rapid loss of the red marker accompanied by the activation of ST18 expression (Fig. 3.13).

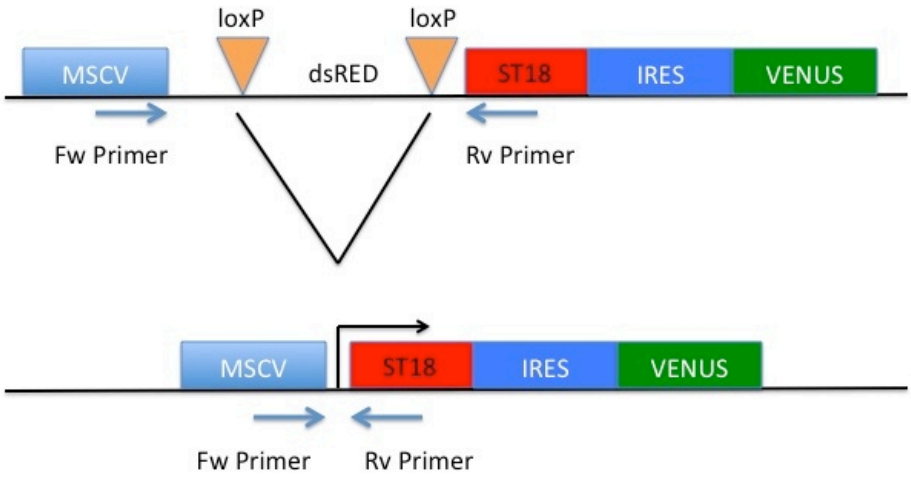

Figure 3.13: MSCV-LSL-ST18-FLAG map and primers. The conditional overexpression vector for ST18 includes a dsRED cassette flanked by LoxP sites that once deleted by Cre-recombination leads to the expression of ST18. The blue arrows show the positions of the primers used to determine a successful recombination that was seen as a disappearance of a 1000bp band replaced by a 250bp band following Cre-recombination.

As described above, constitutive ST18 overexpression led to clear morphological changes (see Fig. 3.12), in particular a large flat morphology. On the contrary, the treatment of cells infected with the conditional vector with 4-hyydroxy-tamoxifen (OHT) to activate CRE-ERT2, did not induce any morphological changes (Fig. 3.14). In a parallel experiment, a recombinant TAT-CRE protein was added instead of OHT into the culture medium (Fig. 3.14). This treatment let to a rapid increase in GFP expression in all hepatoblasts (Data not shown) followed at 48h by the appearance of cells displaying large flat morphology and induction of massive mortality similarly to the phenotype seen in hepatoblasts transduced with the constitutive ST18 (Fig. 3.14). These data indicate that the heterozygous CRE-ERT2 transgene was insufficient to induce efficient recombination of the integrated MSCV-LSL-ST18-FLAG provirus, while TAT-Cre was, inducing effective expression of ST18 and the concurrent cellular arrest. To verify this prediction, we designed two PCR primers, the forward on the MSCV plasmid, before the dsRed cassette flanked by LoxP sites, and the reverse in the ST18 coding sequence (Fig. 3.13). We performed a PCR reaction on transformed CRE-ERT2 hepatoblasts transduced with the MSCV-LSL-ST18-FLAG treated or not with OHT. In untreated hepatoblast a 1000bp band (corresponding to the un-recombined vector) was aplified, whereas after 72 and 120 hours of OHT treatment both 1000 and 250 bp bands were seen. We, thus, concluded that only a small percentage of cells was able to recombine RERT (Fig 3.15). Hepatoblasts transduced with EV with or without OHT show any PCR bands, as expected from the primers design (Fig.3.13 and 3.15).

We conclude that CRE-ER mediated deletion efficiency was not sufficient for further *in vivo* experiments and that TAT-Cre was much more efficient. We are currently deriving hepatoblasts from homozygous CreERT2 embryos in order to achieve

effective recombination, an essential condition to address the effects of ST18 activation on tumor progression *in vivo*.

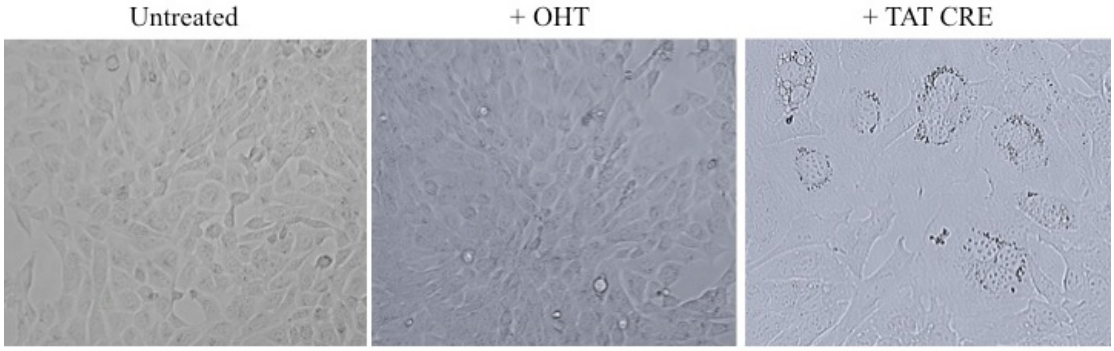

Figure 3.14: Conditional expression of ST18 in vitro. CRE-ER +/- transformed hepatoblasts infected with conditional expression of ST18, after activation with OHT or TAT CRE. OHT seems to be unable to activate the overexpression, instead cells upon activation with TAT CRE show morphological changes compared to untreated cells.

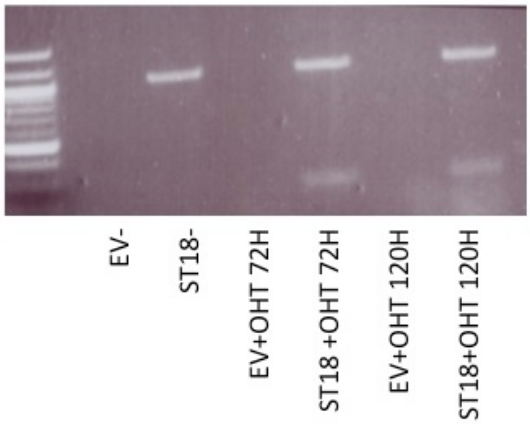

Figure 3.15: **PCR to verify the efficiency of Cre recombination.** PCR shows only a partial recombination of MSCV-LSL-ST18-FLAG conditional vector upon treatment with OHT at the indicated times. Upper band 1000bp show no recombination, lower band 250 bp show the recombined vector. Only partial recombination upon OHT treatment is visible after 72 and 120h, as the upper band does not completely disappear as expected.

3.6 ST18 overexpression does not substitute for RAS in oncogenic transformation of hepatoblasts

As outlined in section 3.1, we used liver hepatoblasts to assess the transforming activity of ST18. We wanted to determine whether ST18 could act as an oncogene by transforming *in vivo*-derived embryonic hepatoblasts. Simultaneous expression of c-Myc and shp53 in hepatoblasts isolated from fetal livers of embryonic day E18.5 leads to immortalization of cells that can be propagated *in vitro* (Zender et al., 2005). These cells provide a sensitized background where expressing additional oncogenes might trigger transformation and therefore tumorigenesis. As proof of concept, we have transduced E18.5 hepatoblasts, previously coinfected with c-myc and an shRNA targeting p53, with the oncogenic mutant form of Ras (H-Ras^{V12}). As expected, mice injected subcutaneously with E18.5 c-myc/shp53/H-Ras^{V12} liver progenitors developed tumors within two weeks, while E18.5 c-myc/shp53 cells did not give rise to any tumors (mice were monitored for six weeks). We also performed an *in vitro* colony formation assay, culturing E18.5 c-myc/shp53/H-Ras^{V12} cells in a semisolid methylcellulose-based medium: two weeks after plating, colonies were only visible in the E18.5 c-myc/shp53/H-Ras^{V12} transformed cells (data not shown). To determine whether ST18 could phenocopy the results observed with oncogenic Ras in this context, we transduced E18.5 c-myc/shp53 immortalized cells with a retroviral vector expressing ST18 (MSCV-ST18-FLAG). We injected a cohort of mice subcutaneously with E18.5 c-myc/shp53/ST18 cells as well as with E18.5 c-myc/shp53 control cells. Neither control, nor ST18 expressing cells gave rise to tumors *in vivo*, suggesting that over-expression of ST18 is not sufficient to cause HCC in cooperation with c-Myc and shp53. This conclusion, however, is hampered by the observation that ST18 overexpression was toxic to the *in vitro* cultured hepatoblasts, as described in the

following section. Conclusive assessment of ST18' s oncogenic potential awaits completion of the inducible expression system, as described in the previous section.

3.7 Expression of ST18 is required for tumor development and maintenance in vivo

Recently, *Shukla et al.* identified ST18 as a candidate oncogene activated by L1 retro-transposition in human HCC (Shukla et al., 2013). As described above, ST18 is not expressed in transformed hepatoblasts *in vitro*, but induced upon tumor development *in vivo* (Fig. 3.4-5): we thus sought to address the consequences of ST18 silencing on tumor development. Toward this aim, we first designed a series of shRNA hairpins targeting both human and mouse ST18 and initially tested their silencing efficacy by western blot in transiently transfected cells (Fig. 3.16). To this end, 293T cells were co-transfected with an expression vector containing human ST18 (MSCV-ST18-FLAG), and several silencing vectors containing single shRNA against ST18, cloned into the MLP vector. Among the several shRNAs tested, we selected three of them (No 1, 6 and 7, Fig 3.16) showing the highest efficiency of knockdown.

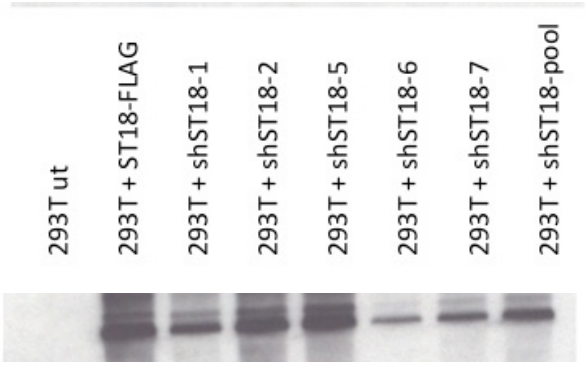

Figure 3.16: Immunoblot analysis to verify the efficiency of ST18 knockdown. Immunoblot analysis of exogenously expressed human ST18 in 293T cells co-transfected with MSCV-ST18-FLAG and several shST18 (single hairpins or as pool). After 48h of transfection the hairpin shST18-6 has the highest silencing efficiency.

To functionally investigate the consequences of ST18 silencing *in vivo*, we cloned the three functional shRNAs against ST18 (No 1, 6 and 7) into a tetracycline-inducible vector that also expresses VENUS (TtRMPVIR, Zuber et al. 2011). We isolated hepatoblasts from E18.5 $p53^{-/-}$ embryos, infected them with retroviruses encoding c-myc and $H\text{-}RAS^{V12}$, and further infected this stable population of transformed hepatoblast with the conditional shRNAs against ST18. For initial experiments, we used shRNA.6, which showed the highest knockdown efficiency. Cells infected with TET-on shST18.6 or the control shREN.713 were FACS-sorted to isolate VENUS positive cells, allowing us to obtain a population homogeneously transduced with the shRNAs vector (Fig 3.17).

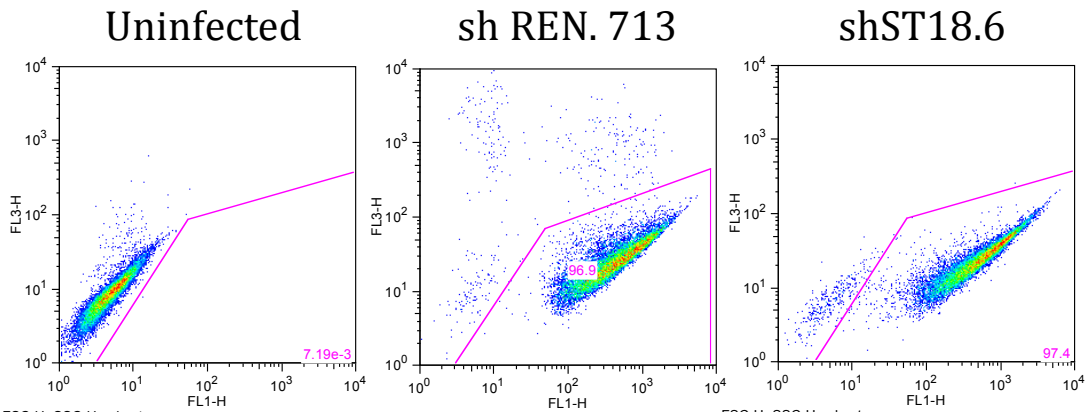

Figure 3.17: **FACS-sorted analysis for Venus tag.** Flow cytometric analysis of a single-cell suspension prepared from transformed hepatoblasts (E.18.5 $p53^{-/-}$/c-Myc/$H\text{-}RAS^{V12}$) infected with inducible shST18.6 or shREN.713 after cell-sorting for Venus tag.

Purified cells infected with either shST18 or shREN.713 were injected subcutaneously into CD-1 nude mice, and the animals were monitored daily for the appearance of tumors (Fig. 3.18). Once the tumors were palpable (day 15) we divided mice into two groups: one group was fed with doxycycline-containing food to induce the activation of the shRNA, while the control cohort was fed with regular food.

Another cohort of mice was fed on doxycycline-containing food from the day of seeding (day 0) and the results for this group of animals is shown first.

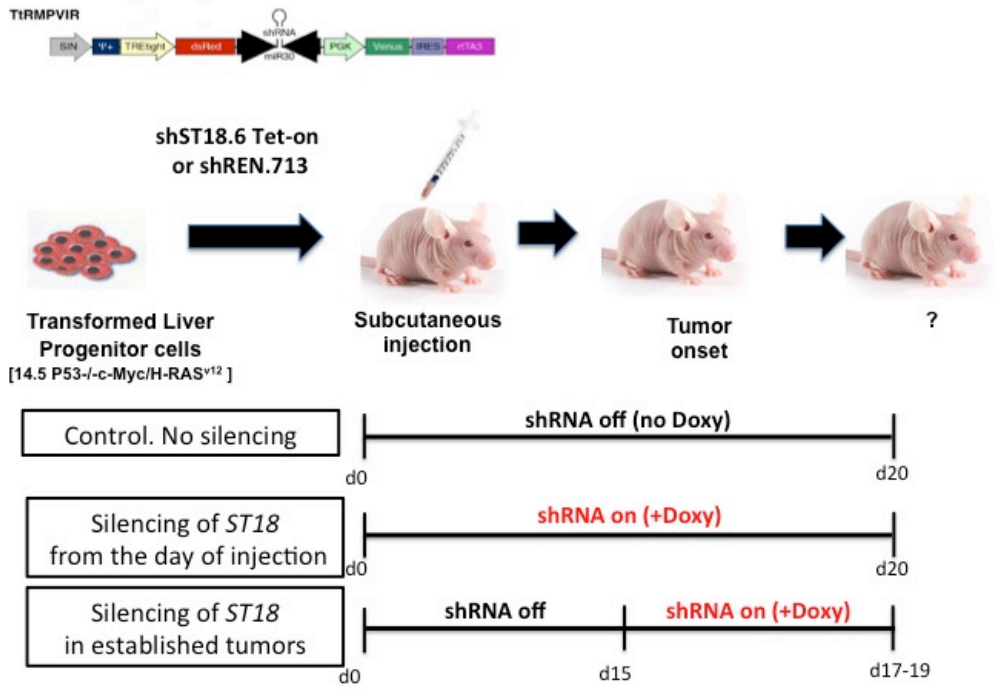

Figure 3.18: **Schematic representation of the general strategy for knockdown of ST18 *in vivo*.** Transformed hepatoblasts were infected with an inducible shST18.6 vector that expresses Venus-GFP constitutively. We injected these cells subcutaneously into CD-1 nude mice and provided them doxycycline-containing food, which activate the shRNA, at different time points from the day of injection (d0) or after tumor onset (d15).

Induction of ST18 knockdown on the day of cell injection caused a significant delay of two weeks in tumor development. Moreover, mice treated with doxycycline (active shST18) developed smaller tumors, as compared to either untreated mice (shST18 off) or mice infected with the control vector (shREN.713), with or without doxycycline treatment (Fig. 3.19 and 3.20). At the end of the experiment, tumors

expressing shST18 from day 0 were five times smaller than those not expressing it. Thus, the expression of ST18 is required for tumor development *in vivo*.

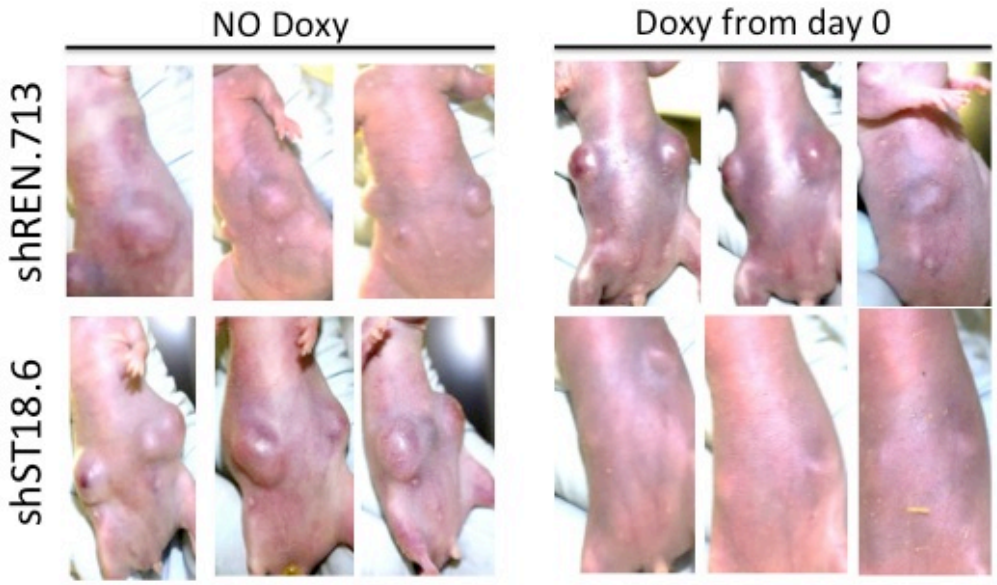

Figure 3.19: Visible differences in tumor formation after ST18 silencing from the day of injection. Photographs of three different mice per experimental condition. Top panel: uninduced (in the absence of doxycycline), , and – bottom panel – induced by doxycycline-containing food from the day of injection silencing with shREN.713 or shST18.6 from day 0. Mice with tumors arising from activated shST18 bear very small growths compared to the non-induced and induced shREN.713.

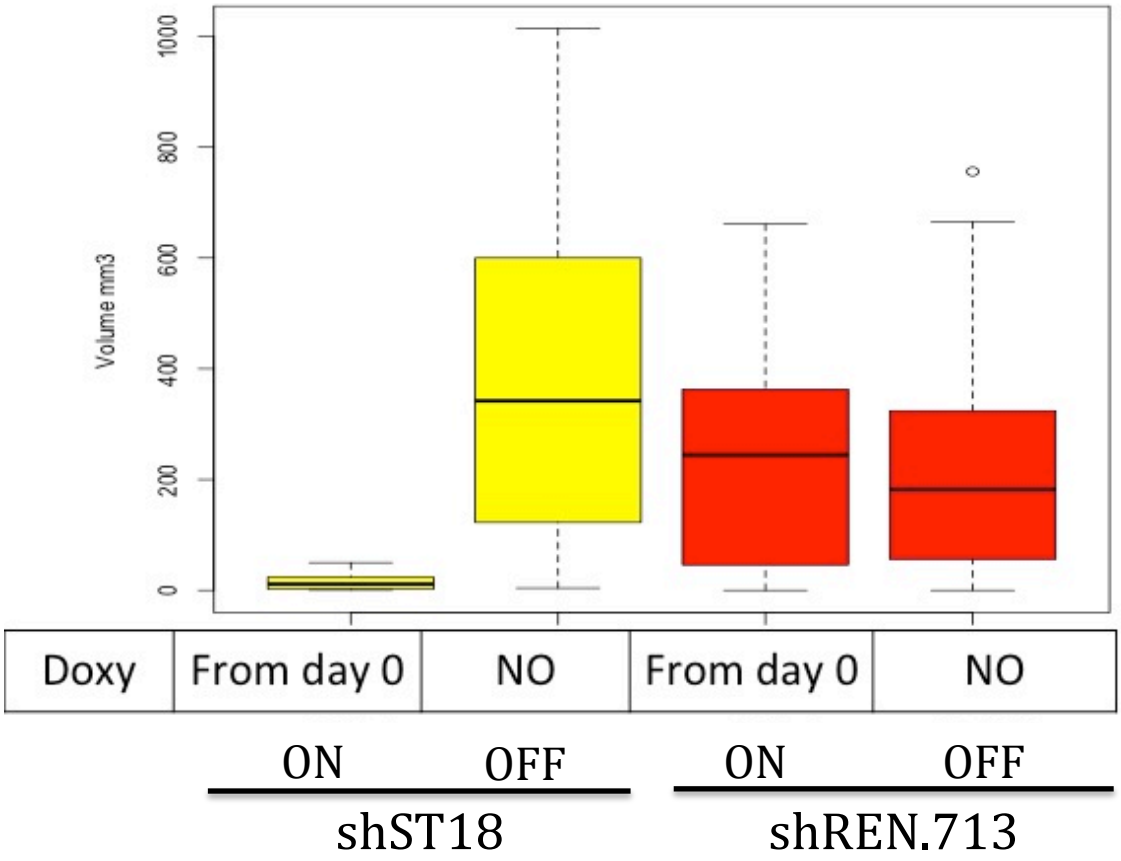

Figure 3.20: Differences in tumor volumes after ST18 silencing from the day of injection. Boxplots of subcutaneous tumor volumes derived from transformed hepatoblasts infected with shST18 or shREN.713 after three weeks from injection. Tumors arising from activated shST18 have very small tumor volumes compared to the non-induced tumors (shST18 off). The observations are not due to effects of doxycycline *per se* but due to induction of the shST18 because shREN.713 induction shows no phenotype.

The same experiment included a third cohort of mice in which KD of ST18 was induced in already established tumors. For this purpose, we let the tumors grow for two weeks before switching to doxycycline-containing food, thereby activating the shRNA. Two days after the exposure to doxycycline we observed a dramatic change in ST18 knockdown (KD) tumor morphology, with multiple edematous and hemorrhagic areas (Fig.3.21-A and B), while control tumors arising from shREN.713-infected hepatoblasts did not show any obvious alterations. To characterize the

phenotypic changes at the histological level, formalin-fixed paraffin-embedded sections were stained with hematoxilin/eosin and evaluated by a mouse pathologist. Widespread necrotic and hemorrhagic areas were observed in tumors with induced shST18, but absent in control shREN.713 tumors (Fig.3.22).

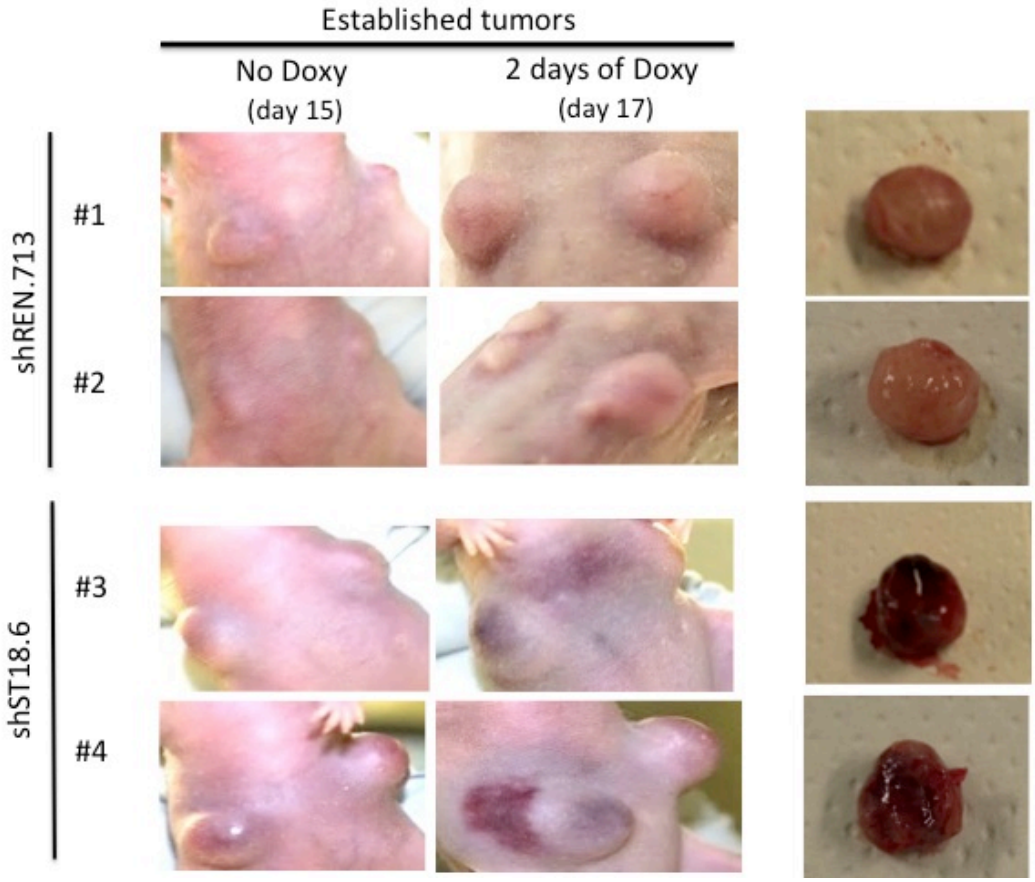

Figure 3.21: **Tumor alterations in tumors upon ST18 knockdown after two days from induction.** Photographs of mice after 15 days from injection of transformed hepatoblasts infected with shST18 or shREN.713. Tumor alterations, in the form of hemorrhagic areas, were visible after induction with doxycycline for 2 days and were seen only in tumors expressing shST18 whilst tumors expressing shREN.713 were solid and without blood infiltrations on the surface.

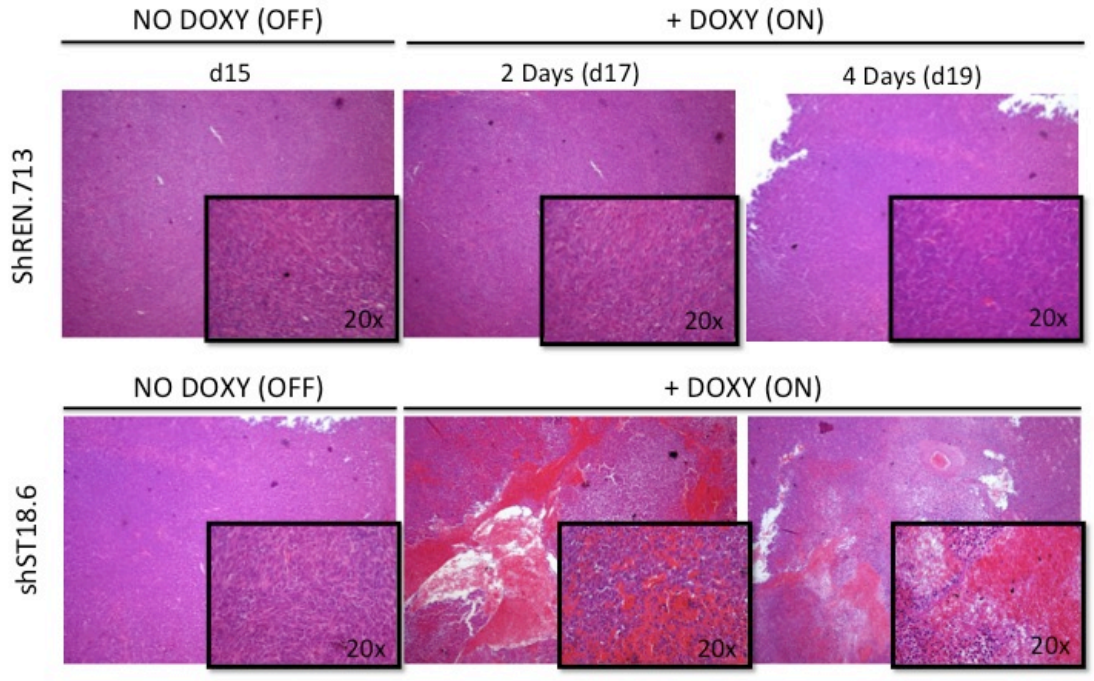

Figure 3.22: Hemorrhages and necrosis caused by silencing of ST18 in tumors. Hematoxilin/eosin staining of tumors after shRNA induction by doxycycline-treatment. Samples of shREN.713 expression tumors were comparable between induced and uninduced interference in tumors. Instead, shST18 induction in tumors led to high levels of hemorrhages and necrosis.

We then stained for markers of proliferation (Ki67) and apoptosis (Caspase3). Tumors with no induction of shST18 were positive for Ki67 and showed no caspase3 signal, whereas those with active shST18 progressively lost Ki67, accompanied by an increase in cleaved caspase 3 (Fig 3.23). Taken together these results indicate that knockdown of ST18 in established tumors leads to decreased cell proliferation, accompanied by increased apoptotis and visible hemorrhages.

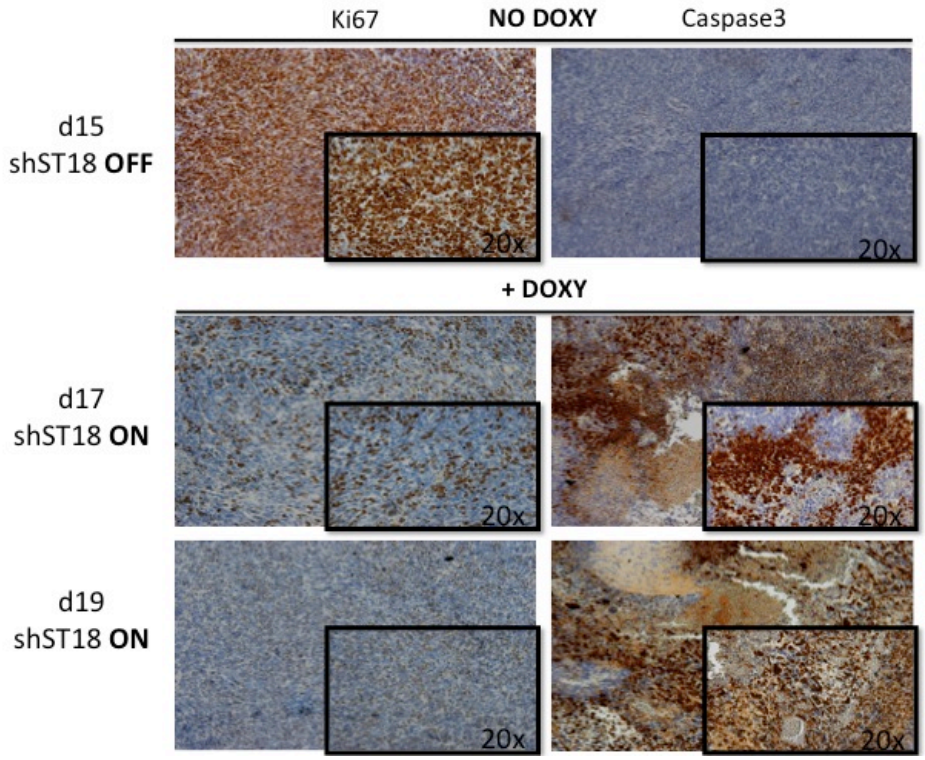

Figure 3.23: Increase in apoptosis and decrease in proliferation in tumors upon ST18 knockdown. IHC of subcutaneous tumors with activated/inactivated shST18 using antibodies against Ki67 (left panel) and caspase3 (right panel). Ki67 staining in shST18 tumors resulted in progressive decrease of signal since the day of induction, whereas the apoptotic signal increased over time. Insets denote the higher magnification view (20x versus 10x).

To confirm that the expression of ST18 is required for tumor maintenance *in vivo* and to exclude possible off-target effects we repeated the same experiment with three different shRNAs targeting ST18 (No 1, 6 and 7, Fig.3.16) and induced ST18 knockdown in established tumors for shorter time-periods (4, 8, 12 and 24h). Moreveor, to maximize the activation of shST18, doxycycline was administered by oral gavage. At 4 hours, hemorragic areas were already appearing nearby the tumors with induced shST18 and after 24h of treatment, the tumor had a clearly altered structure compare to the control (Fig. 3.24-A). A repeat of this experiment with

shST18.7 showed that hemorrhage occurred as rapidly as 2 hours following doxycycline treatment (Figure 3.24-B).

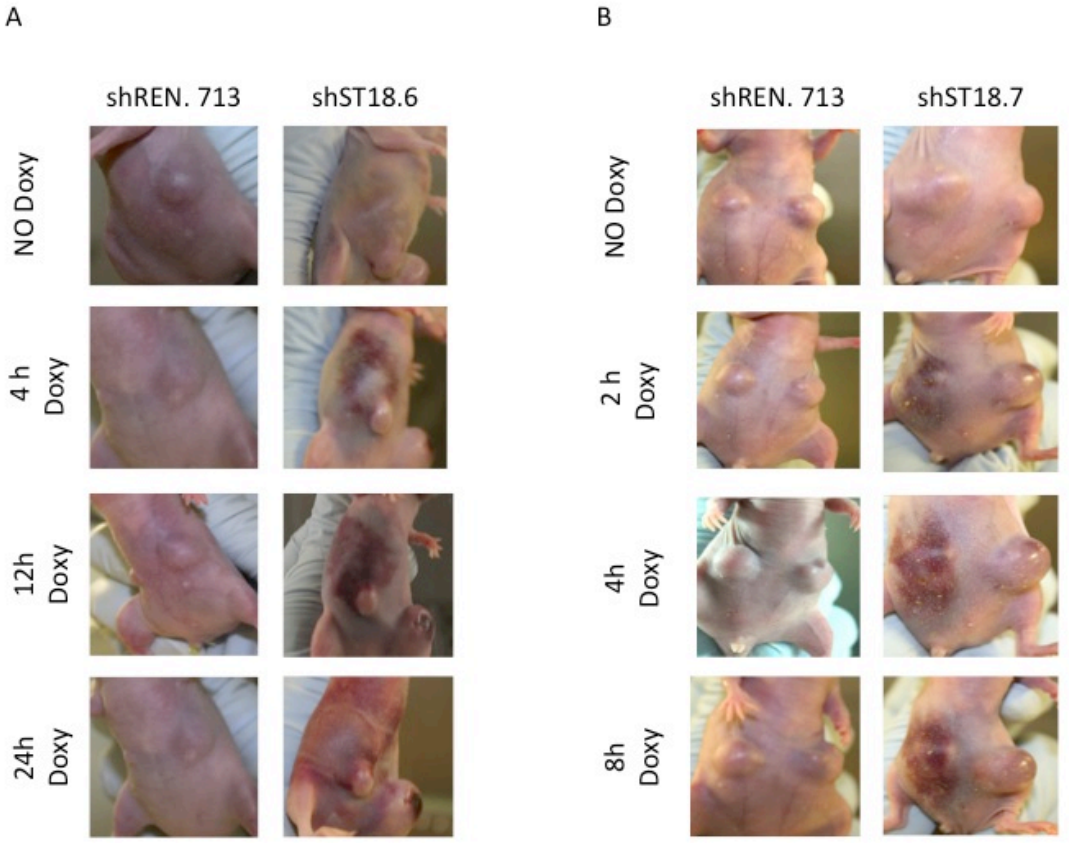

Figure 3.24: Tumor alterations are visible in mice upon ST18 silencing. Photographs of mice with subcutaneous tumors arisen from transformed hepatoblasts infected with shST18 or shREN.713. Panel A show mice before treatment with Doxycycline and after 4, 12, 24 hours of induction of the shST18.6 hairpin. Panel B show hemorrhages in shST18 mice after 2, 4, 8 hours of induction obtained by the induction of shST18.7 hairpin. Tumors derived from transformed hepatoblast infected with shREN.713, whether treated or not with doxycycline, show no macroscopical alterations.

To confirm that these rapid phenotypic changes could possibly be due to the depletion of ST18, we measured mRNA levels by RT-PCR, confirming the rapid and significant knockdown of the ST18 mRNA, already apparent after 4 and progressing further until 24 hours (Fig. 3.25). A similar picture emerged by immunohistochemical analysis with ST18-specific antibodies, demonstrating a general decrease in

expression of ST18 (Fig. 3.26). In particular, the expression of ST18 was seen in non-necrotic areas after 12 and 24 hours post induction. This piece of evidence let us hypothesize that ST18 silencing leads to cell death. (Fig. 3.26).

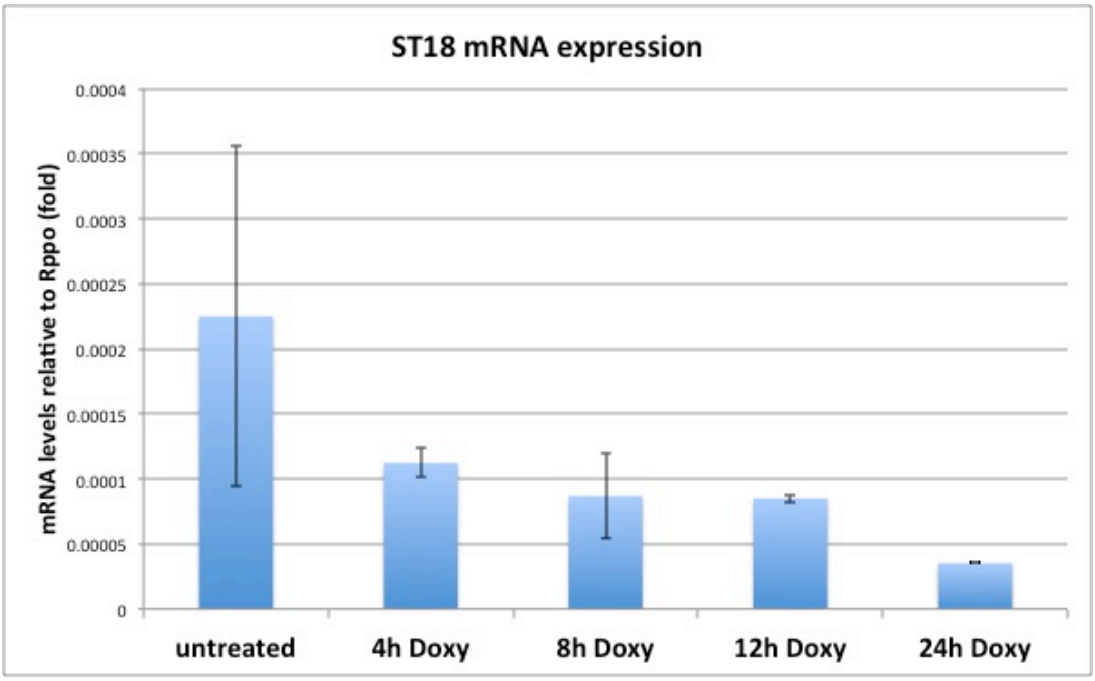

Figure 3.25: Efficiency of ST18 knockdown in tumors. Quantitative RT-PCR analysis of mRNA levels of ST18 in tumors arisen from transformed hepatoblast infected with shST18 N.6, kept untreated or treated with doxycycline after 4, 8, 12, 24 hours. The efficiency of knockdown in tumors already after 4hours was clear, and after 24 hours is almost complete.

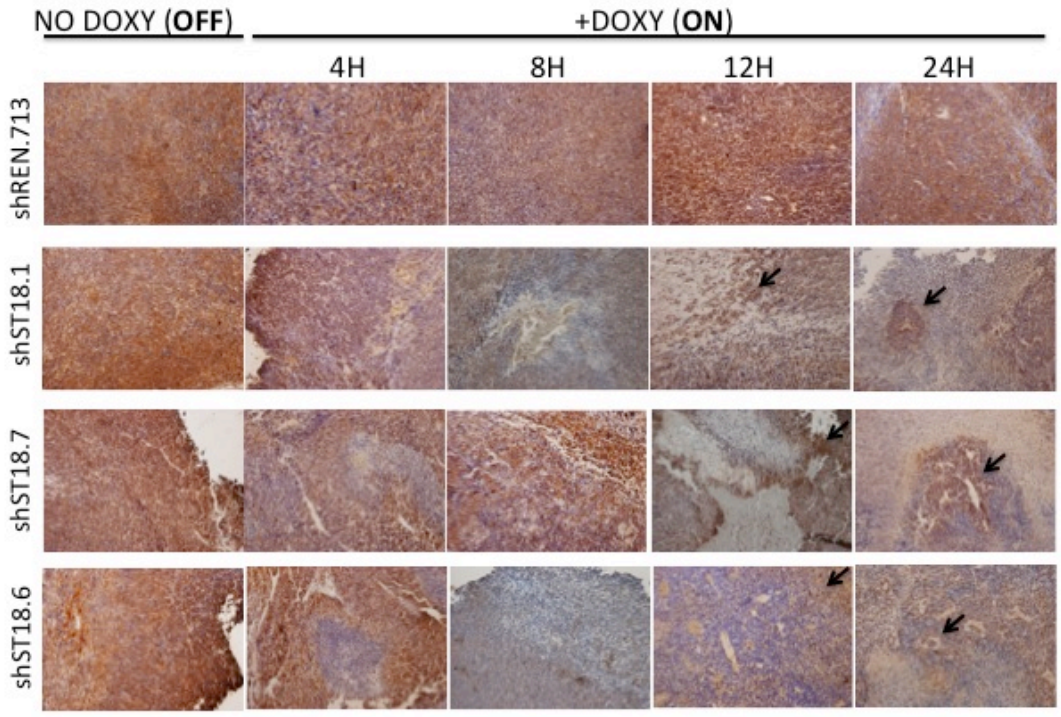

Figure 3.26: ST18 protein decrease in shST18 tumors after doxycycline treatment. IHC for ST18 expression of subcutaneous tumors untreated and after 4, 8, 12, 24 hours of induction with doxycycline. 10x images were taken to demonstrate the differences between tumors. The first column shows ST18 expression tumors before the induction of shRNAs. The first row includes tumors from transformed hepatoblasts infected with shREN.713, thus, ST18 is detectable at all time points. Instead, the staining for ST18 in shST18 activated tumors, progressively decreases post induction. The expression of ST18 at late time-points is present only in the non-necrotic areas (black arrows).

To describe the morphological changes induced upon ST18 knockdown, formalin-fixed paraffin-embedded sections were stained with hematoxylin/eosin (Fig 3.27) and evaluated by an experienced mouse pathologist (**Camilla Recordati**) with the following diagnosis: In untreated mice (NO Doxy), *the subcutaneous mass was composed of solid sheets of atypical cells. Atypical cells were polygonal to pleomorphic, 20-30 µm in diameter, with indistinct cell borders (highly cohesive). Cells had moderate nucleus to cytoplasm (N/C) ratios with moderate amount of eosinophilic granular cytoplasm and round vesicular nuclei with 1-3 distinct*

eosinophilic nucleoli per cell. Occasionally, and mainly located in the centre of the mass, few areas of necrosis and hemorrhages were found. Morphologically, the mass was consistent with a poorly differentiated tumor, most likely of epithelial origin. In shST18 expressing tumors (+ DOXY), *multifocal to coalescing moderate to severe intratumoral hemorrhages and necrotic areas appeared after doxycycline treatment, and increased over time (from 4h to 24h after treatment). The severity of hemorrhages and necrosis was variable depending on the shST18 hairpin (6 >> 7 > 1)*. Importantly, the histological description and the severity of bleeding and necrosis correlated with the knockdown efficiency assayed in 293T cells (Fig 3.16), but to sustain this relationship also in tumors ST18 RT-PCR data with all hairpins are still missing. *Over time, in ST18 KD tumors atypical cells were multifocally less cohesive, arranged in bundles, and spindle-shaped, suggesting an epithelial to mesenchymal transition (EMT). Overall, atypical cells were moderate, 30-40 micron in diameter, with lower N/C ratio, and more abundant eosinophilic granular cytoplasm compared to those in untreated mice*. Tumors arising from transformed hepatoblast infected with shREN.713 had the same morphology of shST18 untreated tumors, and after doxycycline treatment maintained solid phenotype with highly cohesive cells (Fig. 3.27).

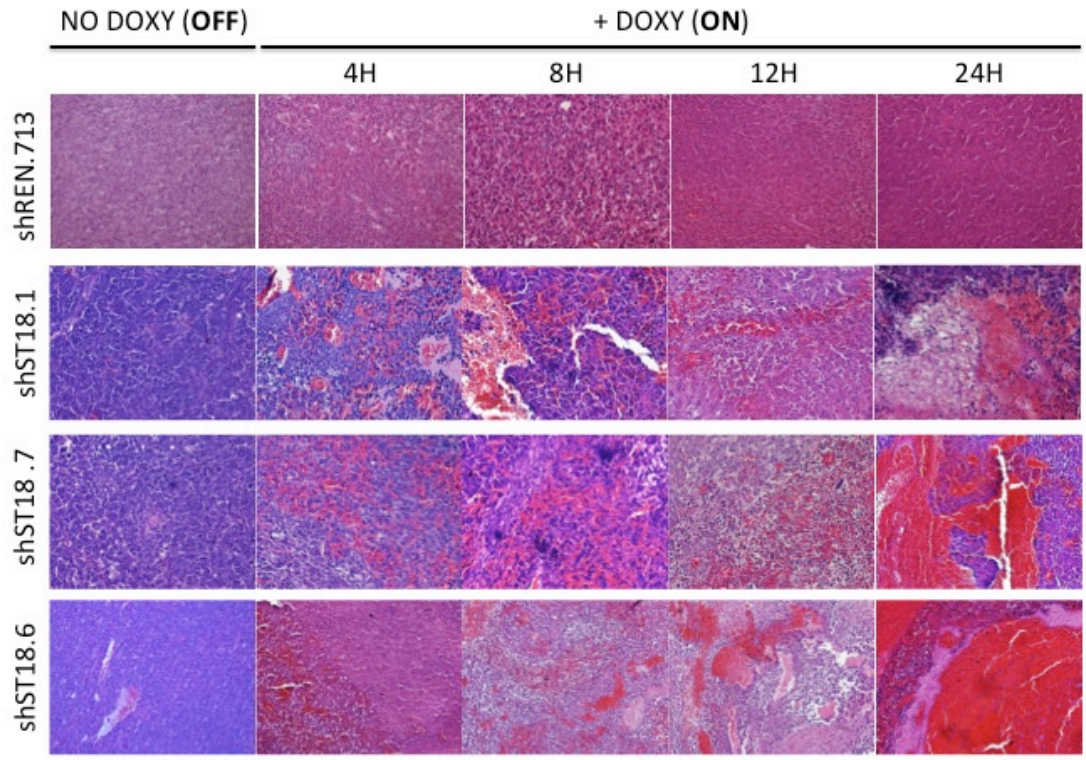

Figure 3.27: Hemorrhages and necrosis in tumors after few hours of ST18 KD. Hematoxilin/eosin staining of tumors with inactive (NO DOXY) or active (+ DOXY) shST18 or shREN.713 after 4, 8, 12, 24 hours. Hemorrhages and necrosis with progressively strong phenotypes were present in all three shRNAs against ST18 but not in the control shREN.713.

We hypothesized that the hemorrhages seen in tumors upon ST18 knockdown were linked to alterations in the tumor vasculature. Therefore, we stained these tumors for VE-cadherin, a marker of vascular endothelial cells (Giannotta 2013) (Fig. 3.28). The structure of the vessels appeared normal, but after 4 hours of doxycycline exposure intratumoral blood vessels in ST18 KD tumors were dilated and larger (ectasia) compared to untreated mice (Fig 3.28). At the moment, the mechanisms by which ST18 elimination leads to this vascular phenotype remain to be clarified, and several hypotheses appear plausible. One such theory is that this phenotype might be a direct consequence of a specific signaling pathway activated only upon loss of ST18 expression. Alternatively, tumor necrosis might indirectly lead to alteration of the tumor vasculature.

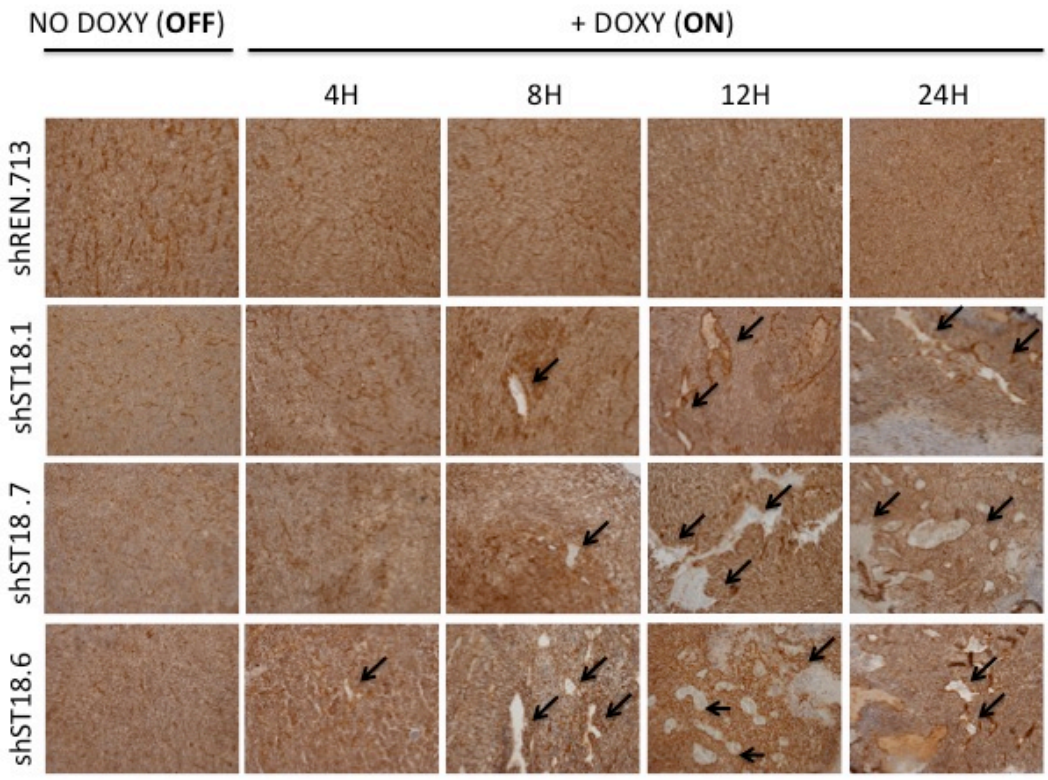

Figure 3.28: Vascular alterations are induced in tumors after ST18 silencing. IHC for VE-cadherin of shREN.713 and shST18 subcutaneous tumors uninduced (No doxy) or induced for 4, 8, 12, 24 hours (+ doxy). Blood vessels in shST18 induced tumors appear dilated (see arrows) after 8 hours of treatment.

In previous experiments (Fig. 3.24) we had observed a decrease in proliferation and the induction of apoptosis after longer periods of shST18 induction. To determine how quickly those changes occur, we stained for Ki67 and cleaved caspase3 at early time-points (Fig. 3.29 and 3.30). In untreated tumors arising from hepatoblasts infected with shST18 or with shREN.713 we detected a strong positivity for Ki67. Tumors derived from shREN.713-infected hepatoblasts maintained a high proliferative index during the time-course of doxycycline treatment. Instead tumors with activated shST18 showed a progressive decrease in Ki67 from 8 to 24 hours, indicative of a proliferative arrest (Fig 3.29).

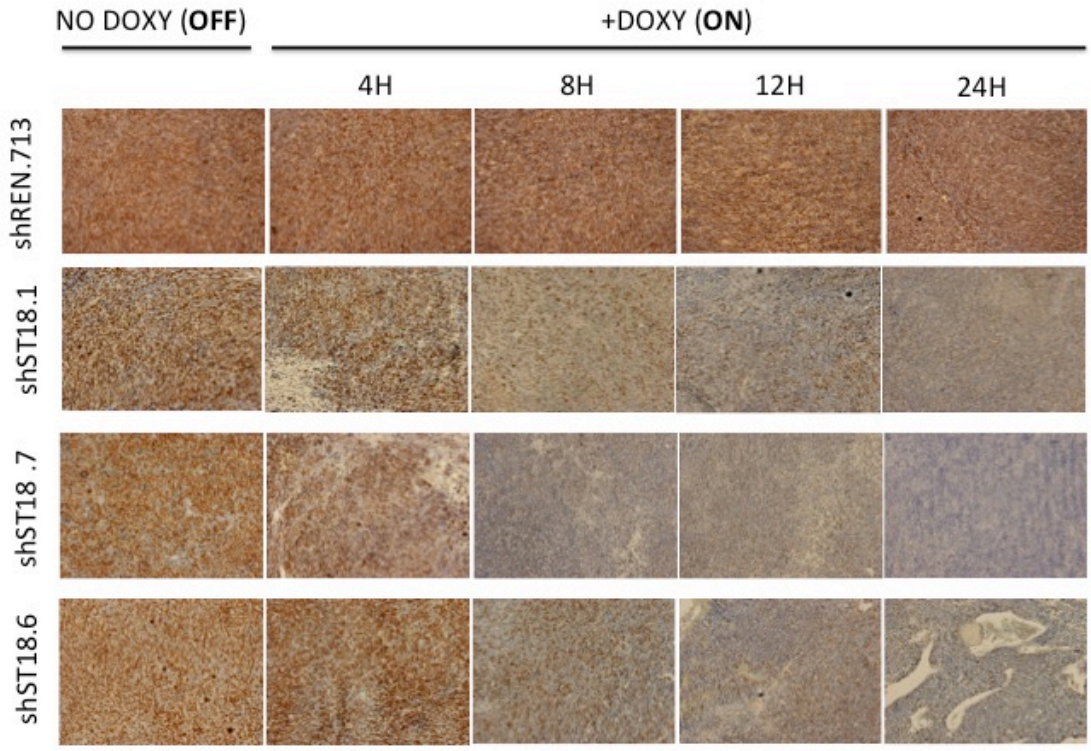

Figure 3.29: Silencing of ST18 in tumors leads to decrease in proliferation. IHC against Ki67 of shREN.713 and shST18 subcutaneous tumors uninduced (No doxy) or induced for 4, 8, 12, 24 hours (+ doxy). Images (10x magnification) show in the first column untreated samples with strong positivity for Ki67 underlying high proliferation. In the first row, tumors arising from transformed hepatoblasts infected with shREN.713 do not show any alteration in proliferation during treatment with doxycycline. Instead in tumors with shST18, a progressive decrease in Ki67 signal is visible over time.

Caspase3 staining increased in the samples with activated shST18, with variable kinetics (Fig. 3.30). Tumors derived from hepatoblast infected with shST18.6, which in 293T cells resulted in the highest knockdown efficiency (Fig. 3.16), displayed positive caspase3 staining already after 4 hours of treatment, whereas the tumors arising from the others two shRNAs against ST18 (No 1 and 7) showed high level of caspase3 staining after 24 hours and very low signal after 8 and 12 hours of activation. Control tumors arising from shREN.713-infected hepatoblasts were negative for caspase3 even after doxycycline treatment (Fig. 3.30). Altogether, we conclude that the silencing of ST18 leads to concomitant proliferative arrest and

induction of apoptosis: the relationship between these effects remains to be addressed in further detail.

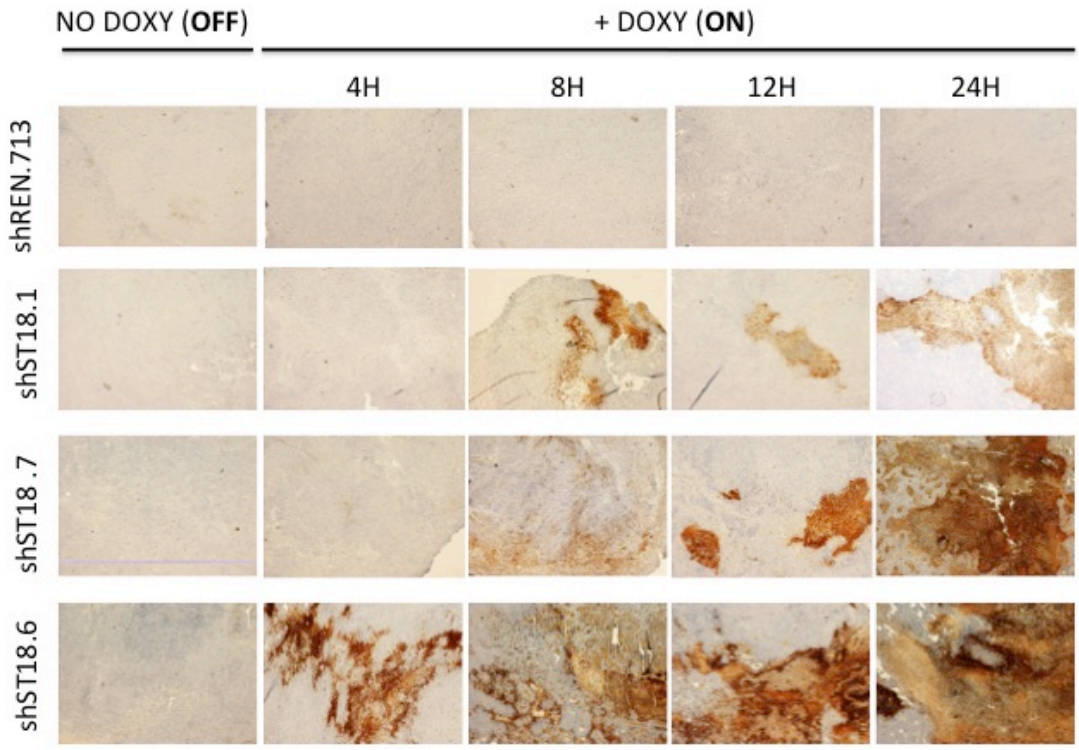

Figure 3.30: Silencing of ST18 in tumors leads to an increase in apoptosis. IHC against caspase3 of shREN.713 and shST18 subcutaneous tumors uninduced (No doxy) or induced for 4, 8, 12, 24 hours (+ doxy). Low magnification (4x) images were taken to demonstrate the difference between tumors. Untreated tumors (first column) and tumors derived from transformed hepatoblasts infected with shREN.713 (first row) are negative for caspase3. Instead in tumors with shST18, a progressive increase in caspase3 signal is visible during the hours of activation.

We further verified the morphological alterations within the tumors when upon induction of shST18 for longer periods. As observed previously, four hours after silencing *ST18*, intratumoral and peritumoral hemorrhages extending to the adjacent subcutis were readily noticeable. These hemorrhages became progressively more severe over time, causing extensive red discoloration of the whole ventral aspect of the mouse after 2 days (Fig. 3.31). At this point we dissected some mice to observe the changes in the tumor and to understand the origin of the hemorrhages. The masses

were hemorrhagic and friable, difficult to collect for histological examination and no gross lesions were found involving the internal organs, indicating that hemorrhages were restricted to the tumor and adjacent subcutis (Fig. 3.32). In animals maintained further on doxycycline-containing food, the ventral subcutaneous hemorrhages were almost completely resolved after 4 days and fluid filled masses were present. However, one week after ST18 silencing, some escapers start to proliferate again leading to new tumor formation (Fig.3.31). Pathological analyses are ongoing to verify the nature of the residual tissue after one week of treatment and additional staining will be necessary (first of all ST18) to understand the molecular changes occurring between the different time points.

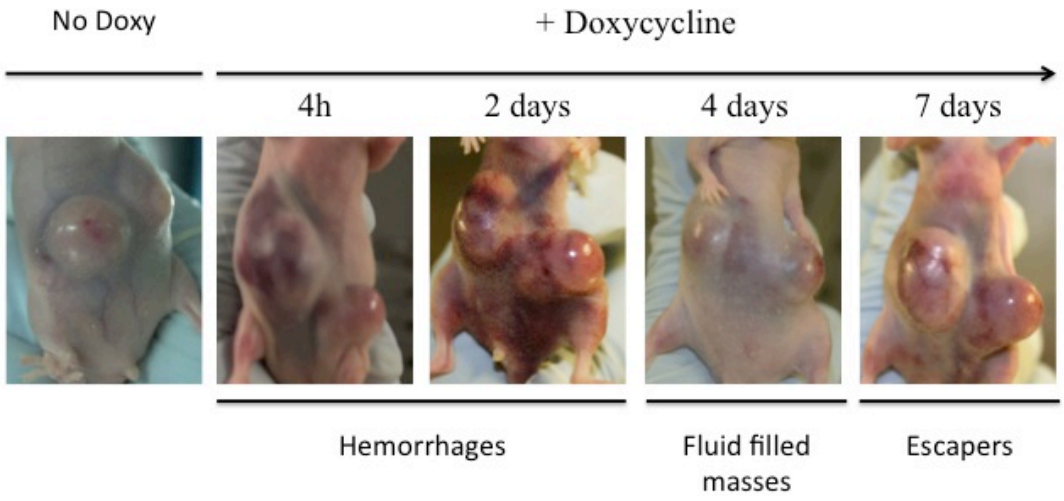

Figure 3.31: Long term analysis of tumors following *ST18* silencing. Photographs of mice with subcutaneous shST18 tumors untreated and treated with doxycycline for 4 hours and 2, 4, 7 days. Hemorrhages are visible after 4 hours of treatment and became detectable in the whole body of the mice after two days. Mice after four days of doxycycline absorbed the hemorrhages before start to proliferate again.

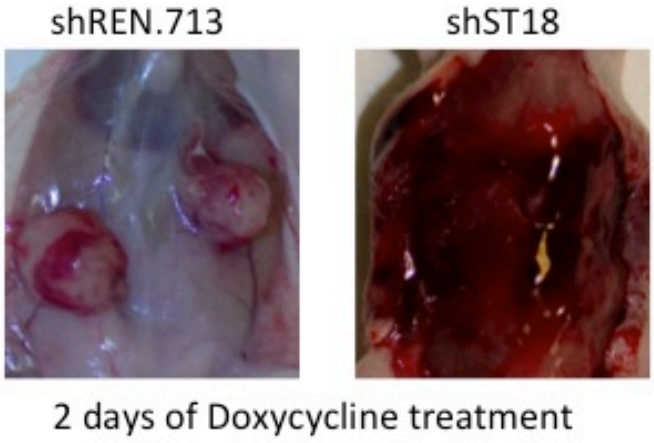

Figure 3.32: Severe hemorrhages in tumor upon ST18 knockdown.
High levels of hemorrhages were present and restricted to the tumor and adjacent subcutis in ST18 silenced tumors after 2 days of doxycycline compared to tumors arisen from shREN.713.

Taken together, our *in vivo* data clearly underline the requirement for ST18 during tumor development and progression of murine HCC. Pathological analysis revealed ST18 to be a gene that is necessary for the maintenance of the epithelial origin of the tumor. Additional stainings are ongoing to confirm the occurrence of epithelial-to-mesenchymal transition after doxycycline treatment.

3.8 ST18 inhibits genes involved in epithelial to mesenchymal transition

To understand what genes and pathways are involved and regulated by the inactivation of ST18 we performed RNA-seq analyses in control tumors and ST18 KD tumors treated for 4 hours with Doxycycline (three different tumors each, all derived from hepatoblasts infected with shST18.6). Expression values for the roughly 22.000 mouse genes were compared between the two conditions: using a significance value (p-value adjusted with Benjamini-Hochberg correction for multiple testing) of less then 0.05, we detected 1,690 differentially expressed genes (DEGs). Then we

divided them in UP and DOWN regulated genes using the log2 Fold Change (log2FC) of the expression ration between the control and the ST18KD samples. We identified 677 UP (Table S1) regulated genes as those ones that have a log2FC > 0.5, and 467 DOWN (Table S2) regulated genes with a log2FC < -0.5. To compare gene expression levels within and between replicates, Reads Per Kilobase per Million of mapped reads (RPKM) values for each gene were calculated. Hierarchical clustering analysis of gene expression based on RPKM values separated the tumor samples according to the two categories: control (noDox) and ST18KD (4hDox) (Fig. 3.33).

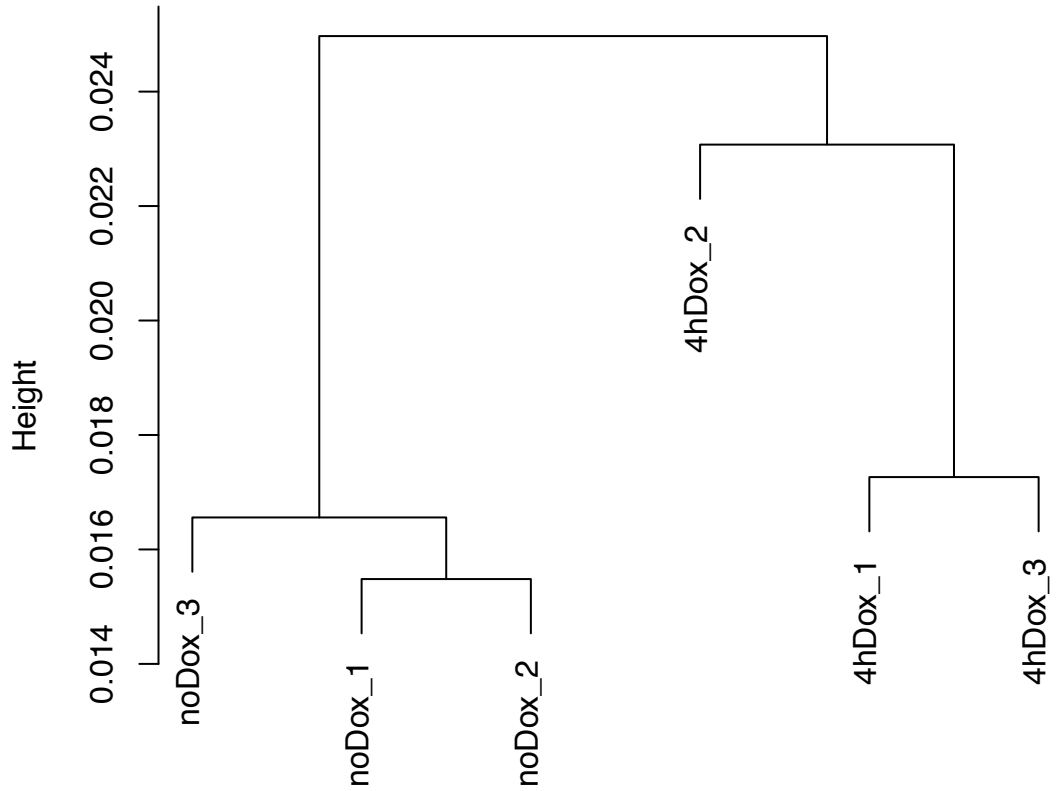

Figure 3.33: Hierarchical clustering analysis separated the tumors into untreated and treated. Clusters based on RPKM gene expression values denote a correlation between the six different biological samples by grouping them according to the two categories: control (noDox) and ST18 knockdown (4hDox) tumors.

To interpret the gene expression data and identify possible molecular mechanisms underlying tumor regression upon ST18 inactivation, we used the Gene Set Enrichment Analysis (GSEA) software based on the Molecular Signature Database (MSigDB), a collection of annotated gene sets. The MSigDB gene sets are divided into 7 major collections: c1 positional gene sets, c2 curated gene sets, c3 motif gene sets, c4 computational gene sets, c5 GO gene sets, c6 oncogenic signatures and c7 immunologic signatures. We concentrated our analysis on collection c2 (curated gene sets form already published databases in PubMed), yielding 1923/3262 gene sets up-regulated in control (noDox) samples versus ST18KD (4hDox), of these 1923 just 407 gene sets were significantly enriched (p value <0,01) showing a positive enriched score (+ES). We also detected 1339/3262 gene sets down-regulated in control samples versus ST18KD (meaning that these gene sets were up-regulated in ST18KD versus control samples), of these 1339 only 301 gene sets were significantly downregulated (-ES) in control versus ST18KD samples with p value <0,01.

In control samples we found several enriched gene sets correlating with inflammation; in particular we found a high correlation between genes enriched in control and genes up-regulated in hepatic stellar cells after stimulation with LPS (the Seki gene set) with an enrichment score (ES) of +0,62 (Fig. 3.34) (Seki et al., 2007). This gene set was very interesting, considering that we have previously shown that there is a correlation between LPS stimulation *in vivo* and *ST18* expression (Fig. 3.6).

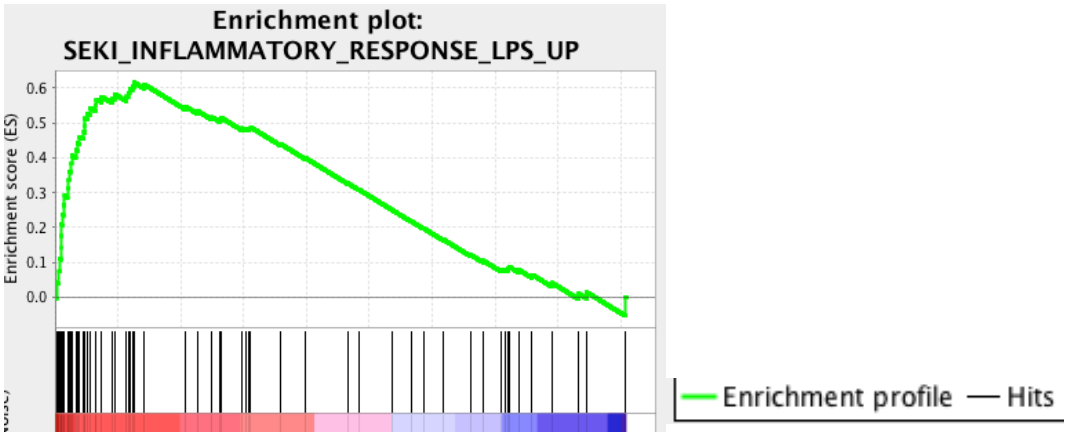

Figure 3.34 Enrichment plot of upregulated gene set in control tumors. The green line in the enrichment profile gives the enrichment score (+0,62 at its summit) for the gene set 'SEKI_INFLAMMATORY_RESPONSE_LPS_UP). The bottom portion of the plot shows where the members of the gene set appear in the ranked list of genes. The leading edge subset of a gene set is the subset of members that contribute most to the ES. In this case the hits (black lines) are in the red profile control samples (No Doxy) and the leading edge subset are the set of members that appear in the ranked list prior to the peak score.

Several gene sets strongly enriched (1339 / 3262 gene sets are downregulated in control versus 4hDox) upon ST18 silencing were highly correlated with genes up-regulated during epithelial to mesenchymal transition. In particular we found an ES for one EMT set (the Anastassiou gene set) of -0,79, this score is the degree to which this gene set is overrepresented at the ranked list of genes in the expression dataset (Fig 3.35) (Anastassiou et al., 2011). In detail, the following genes contribute to the leading-edge subset within this gene set: CRISPLD2, **COL1A2**, **THY1**, **TNFAIP6**, COL1A1, COL6A2, **ACTA2**, COMP, LRRC15, **COL5A2**, SULF1, **CDH11**, NOX4, OLFML2B, MFAP5, ADAM12, GLT8D2, LOX, ASPN, THBS2, COL11A1, **POSTN**, **PRRX1**, **DCN**, LUM, ITGBL1, C1QTNF3 (Fig 3.36). Highlighted in bold typeface are 9 known EMT-associated genes coming from the list of upregulated "EMT core signature" genes (Taube et al., 2010) and four additional genes

(underlined) have also been reported as EMT related (Huang et al., 2013; Jechlinger et al., 2003; Li et al., 2013a; Wu et al., 2014).

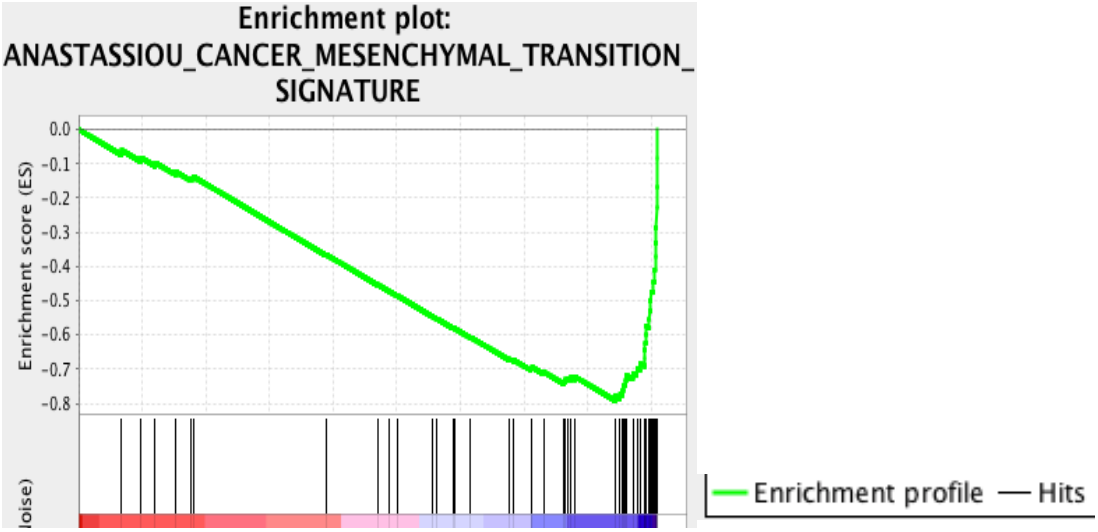

Figure 3.35 Enrichment plot of upregulated geneset in ST18 knockdown tumors. The top portion of the plot shows in green the enrichment profile and the enrichment score (ES) of -0,79 for this particular gene set. The bottom portion of the plot shows where the members of the gene set appear in the ranked list of genes. In this case the hits (black line) are in the blue profile (ST18KD - 4h Doxy treated) and the leading edge subset are the set of members that appear in the ranked list subsequent to the peak score.

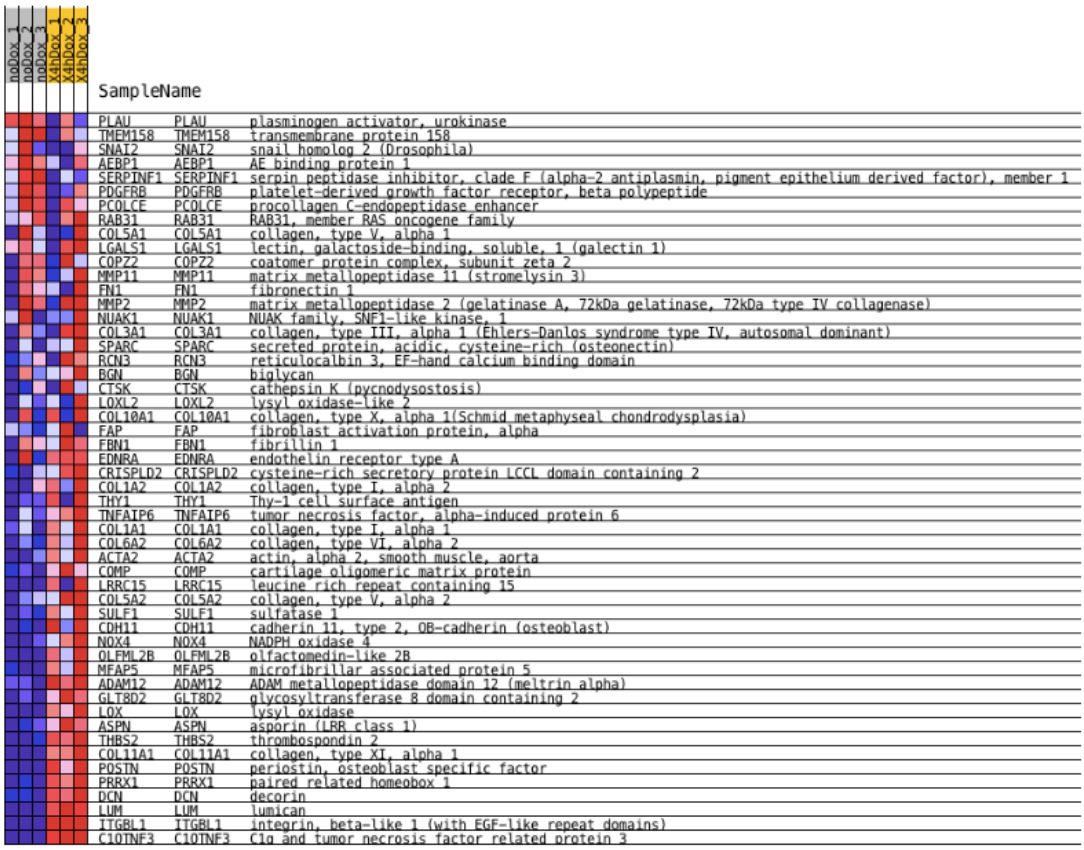

Figure 3.36: Heatmap of gene sets upregulated in ST18 knockdown tumors. Heatmap of genes in the gene set 'Anastassiou_cancer_mesenchymal_transition' ordered by their position in the ranked list of genes. Genes related with epithelial to mesenchymal transition were highly expressed in ST18KD (4h Doxy) tumors compared to control. The analysis includes only those genes in the gene set that are also in the expression dataset. In this representation, expression values are detected as colors, where the range of colors (red, pink, light blue, dark blue) shows the range of expression values (high, moderate, low, lowest).

We also analyzed our data with the ingenuity pathway analyzer software (IPA®) that correlate RNAseq data with 5 million published individual findings, most of which describing relationships between molecules, diseases or biological functions. IPA was used to analyze selected sets of genes after ST18 silencing to identify possible altered canonical pathways. The most significant one associated with the higher ratio, determining high overlap with the genes of our dataset, was the so-called hepatic fibrosis pathway; however, there was no evidence of how the genes are up- or down-regulated in association with this pathway. The overall activation/inhibition states of

canonical pathways are predicted based on a Z-score algorithm that is used to compare the uploaded dataset with the canonical pathway patterns. It is clear that there is a significant and positive association with inflammatory pathways (i.e. IL-8 and NF-kB) and VEGF signaling, instead Wnt/β-catenin signaling was negative associated (Table 3.1).

Ingenuity Canonical Pathways	-log(p-value)	Ratio	z-score
Hepatic Fibrosis / Hepatic Stellate Cell Activation	8.72E+00	2.13E-01	
Calcium Signaling	4.69E+00	1.74E-01	0.832
IL-8 Signaling	2.05E+00	1.31E-01	1.342
NF-kB Signaling	1.78E+00	1.27E-01	0.853
Cardiac β-adrenergic Signaling	1.51E+00	1.28E-01	1.265
Growth Hormone Signaling	1.38E+00	1.45E-01	1
TGF-β Signaling	1.11E+00	1.26E-01	0.378
VEGF Signaling	1.61E+00	1.43E-01	1.732
Wnt/β-catenin Signaling	1.15E+00	1.12E-01	-3.051

Table 3.1: Canonical pathways altered in ST18 knockdown tumors. IPA analysis identified many alterations in association between our defined data sets and the canonical pathways; in particular, the most significant one was the hepatic fibrosis pathway. The ratio indicates the strength of the association; whereas the p-value measures its statistical significance and the Z-score indicates the sign of the regulation.

ST18 is a zinc finger protein, but genome-wide chromatin profiling is still missing and therefore its target genes are not known. ST18 could function as transcriptional activator or repressor since we observed 677 upregulated and 467 downregulated genes (padj <0.05, Log2FC>0,5 or <-0,5) after ST18 silencing, albeit these responses might be at least partly indirect. This will require the mapping genomic target sites for

ST18 by ChIP-seq. As yet, however, ChIP analysis of ST18 has not been performed as it will require the characterization of available antibodies, and - if needed - the generation of new ones.

Gene regulation by ST18 may also be indirect, mediated by other transcription factors. In order to identify these factors we used the GSEA MSigDB collection C3, a collection of motif gene sets based on conserved cis-regulatory motifs from a comparative analysis of the mouse genomes. In ST18KD tumors we found up-regulated 464/797 gene sets within this category (116 with p <0.01). Snapshot of the top six enrichment results reveal an enrichment of the transcription factor myocyte enhancer factor 2 (MEF2), meaning that differentially expressed genes contain the MEFs consensus site within their promoter (Fig. 3.37).

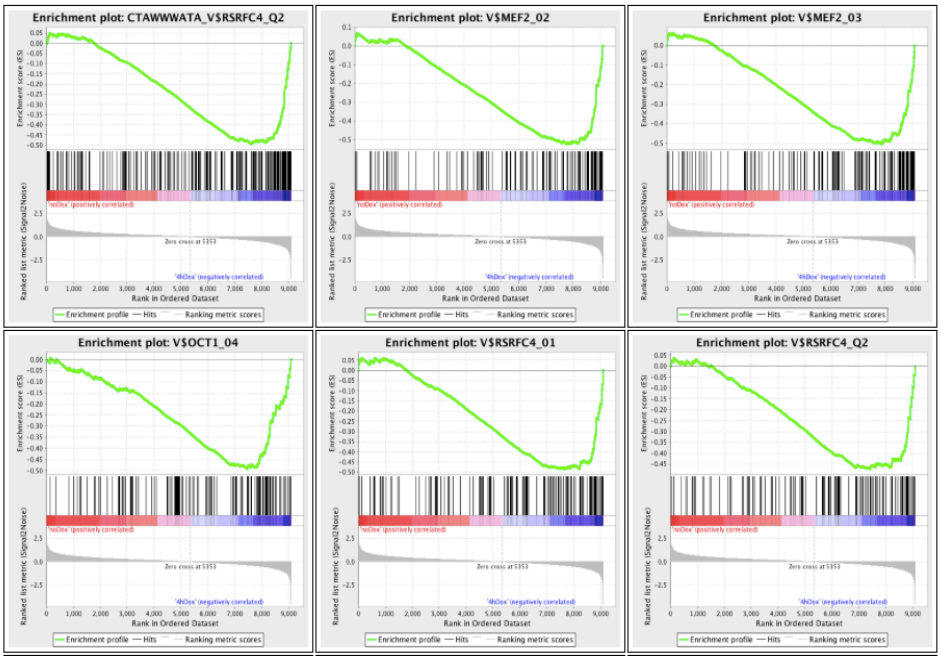

Figure 3.37: Snapshot of top results in GSEA motif gene set. Several enrichment plots for the gene sets with the highest absolute normalized enrichment scores were correlated with the myocyte enhancer factor 2 (MEF2) transcription factors.

In vertebrate, the MEF2 family of transcription factors consists of four members (a-d), and plays a central role in activating genetic programs that control cell differentiation, proliferation and morphogenesis (Potthoff and Olson, 2007). All the Mef2 family members were expressed in our experimental model, but only Mef2c was one of the genes differentially expressed in ST18KD tumors compared to control (padj <0.05, Log2FC +1.2). We conclude that upon ST18 silencing, MEF2 activity may increase and participate to the biological effects described above. We hypothesize that ST18 may repress genes by suppressing MEF2 and we will verify this hypothesis in the future experiments.

4. DISCUSSION

4.1 Hepatocellular carcinoma: genetic heterogeneity and therapeutic targets

Hepatocellular carcinoma (HCC) is the primary form of liver cancer and the third greatest cause of cancer-related death worldwide (Llovet et al., 2003). HCC is a complex disease, which can have different etiological origins, including infection by hepatitis B or C viruses (HBV, HCV), alcohol abuse, or aflatoxin exposure (Gomaa et al., 2008). HCC management is further complicated because it is diagnosed mostly at advanced stages, when limited therapeutic options are available. HCC is a chemoresistant cancer and the only treatments are surgical resection or liver transplantation (Llovet and Bruix, 2003). Until recently, patients with advanced HCC could only be proposed supportive therapy and care. The advent of Sorafenib, approved by the U.S. Food and Drug Administration in 2007, has offered hope to patients with advanced HCC (Llovet et al., 2008). Sorafenib is a multi-kinase inhibitor that blocks the MAPK pathway, which inhibits the ability of the cell to resist apoptosis and decreases angiogenesis, cell migration and proliferation (Llovet et al., 2008). Despite the successful use of Sorafenib in treatment of HCC, patients with advanced tumor still die and there is an urgent need for the development of novel targeted methodologies.

HCC is a heterogeneous tumor with several genetic alterations that can cause p53 inactivation, Myc over-expression, deregulated Wnt or TGFβ signaling. These genetic changes are just a part of the constellation of different types of alterations that lead to cancer development and progression: it is therefore clear that combination therapies would be critical to overcome the complexity of HCC. The increasing knowledge and

the identification of possible HCC driving pathways will provide new therapeutic targets.

4.2 The controversial role of ST18 in cancer

Recently Shukla et al. have shown that insertional mutagenesis mediated by the endogenous L1 retrotransposon occurs at the *ST18* locus (suppressor of tumorigenicity 18) in human HCC pointing to *ST18* as candidate oncogene in HCC (Shukla et al., 2013). In the same report, other observations support the putative oncogenic role of *ST18* in liver cancer: (i) clonal amplification of tumor cells with L1 insertion in *ST18*; (ii) *ST18* expression in tumors and liver cancer cell lines; (iii) *ST18* amplification and expression in inflammation-driven HCC nodules in Mdr2-/- mice (Shukla et al., 2013). However, further functional validation of *ST18* was achieved neither in this paper, nor in a previous report identifying *ST18* as a putative oncogene in Pediatric Acute Myeloid Leukemia (Steinbach et al., 2006). Other work, instead, depicted *ST18* as a tumor suppressor in breast cancer (hence the name "Suppressor of Tumorigenicity 18") (Jandrig et al., 2004). *ST18* was expressed at low levels in mammary epithelial cells and further downregulated in breast cancer cell lines and in breast tumors. Moreover, ectopic expression of *ST18* in breast cancer cells inhibited colony formation in soft agar and tumor formation in xenograft mouse model (Jandrig et al., 2004). The tumor suppressor role of *ST18* is consistent with its pro-apoptotic action, described in human fibroblast (Yang et al., 2008) and in pancreatic β-cells (Henry et al., 2014).

The *ST18* gene encodes a zinc-finger DNA-binding protein (Jandrig et al., 2004) with similarity to members of the *NZF/MyT* family of zinc-finger transcription factors involved in development and homeostasis of the nervous system (Yee and Yu, 1998).

In 1998 a third member of the *NZF/MyT* family was cloned, neural zinc finger factor 3 (NZF-3), renamed few years later as *ST18* (Yee and Yu, 1998) (Jandrig et al., 2004). The transient overexpression of *ST18* caused spontaneous neuronal induction and differentiation in mouse P19 embryonic carcinoma cells, suggesting a central role of *ST18* in neuronal differentiation (Kameyama et al., 2011). On the other hand, a pro-inflammatory role for *ST18* was suggested in human fibroblasts, in which *ST18* silencing with small interfering RNA (siRNA) led to the down-regulation of genes involved in several inflammatory pathway (including NF-kB, TNF, IL-6) . In the same report, overexpression of *ST18* significantly increased the expression of TNF-α, IL-1α and IL-6, suggesting that *ST18* regulates pro-inflammatory gene expression in human fibroblast (Yang et al., 2008). In summary, different roles for *ST18* have been described in several tissues, suggesting that its biological function may be context dependent.

4.3 The role of inflammation and micro-environmental signals in modulating *ST18* function

Following up from the controversial reports on the role of *ST18* in different contexts and the recent paper of Shukla et al (2013) that proposed *ST18* as a putative oncogene in liver cancer, we decided to investigate the role of *ST18* during liver tumor onset and progression. In accordance with published observations (Jandrig et al., 2004), we confirmed that ST18 was expressed at very low levels in normal liver, as well as in liver progenitor cells overexpressing a combination of oncogenes (c-Myc and H-Ras^{v12}) with knockdown of the tumor suppressor p53 (shp53). In matched tumor samples derived from subcutaneous injection of the same cells into CD-1 nude mice,

we observed an increase of *ST18* expression both at the mRNA and protein levels. Our results provide direct evidence that simple oncogene activation (or repression of tumor suppressors) is not sufficient to induce expression of *ST18*. Instead, *ST18* expression in vivo requires additional tumor-derived micro-environmental signals, likely including cell-cell interactions or soluble factors, such as inflammatory mediators or tumor metabolites.

The tumor environment is a complex mix of tumor cells, tumor-associated cells and extracellular matrix components, which creates a system of reciprocal signaling (Hernandez-Gea et al., 2013). The interaction between cancer, stromal and inflammatory cells creates a network at the basis of a permissive tumor environment that favors tumor growth and progression. Stromal cells can be divided into three general classes: (i) angiogenic vascular cells, which promote tumor vascularization; (ii) cancer-associated fibroblasts, which contribute several tumor-promoting functions; (iii) infiltrating immune cells such as macrophages or T lymphocytes, whose role in cancer progression is complex and probably depends on context-specific cues (Hanahan and Coussens, 2012). In this regard, inflammatory infiltrates are found in most solid tumors, and cytokines released by innate immune cells, such as TNF-a and IL-6, promote tumorigenesis through several mechanisms (Mantovani et al., 2008). As mentioned above, the overexpression of *ST18* in human fibroblasts significantly increased the expression of TNF-α, IL-1α and IL-6 suggesting a reciprocal link between *ST18* and inflammation (Yang et al., 2008).

To address a possible link between *ST18* expression and inflammation in the liver, we induced an acute inflammatory response in C57/B6 mice by intra-peritoneal injection of Bacterial lipopolysaccharide (LPS) (Zhong et al., 2006). LPS causes accumulation of macrophages and to the release of many inflammatory cytokines including IL1β,

TNF-α, TGFβ and IL-6 in the liver, leading to an acute inflammatory response (Zhong et al., 2006). Immunohistochemical analyses on livers upon LPS treatment showed that *ST18* was induced in the inflamed livers suggesting that the gene responds acute inflammatory conditions, and thus probably to one or more of the cytokines released in these circumstances.

In accordance with the notion that inflammation and liver tumorigenesis are highly interconnected, our RNA-seq analyses on subcutaneous tumors from transformed hepatoblasts pointed out an inflammatory gene expression signature. Moreover, based on our RNA sequencing data, genes up-regulated in hepatic stellar cells after stimulation with LPS (Seki et al., 2007) were expressed in subcutaneous tumors, and down regulated after ST18 knockdown. These observations suggest that *ST18* expression in HCC may be induced by inflammatory signals, and that ST18 itself regulates part of the transcriptional response induced by those signals. These findings may also explain why *ST18* is expressed at higher levels in subcutaneous tumors than in cell culture, where no inflammatory mediators are present. Different experiments are ongoing to mimic this condition of cytokine release *in vitro* with the aim of identifying the factor(s) that lead to induction of *ST18.*

In accordance with available data on the expression of *ST18* in *Mdr2*$^{-/-}$ mouse model of inflammation-driven HCC (Shukla et al., 2013) we decided to verify if *ST18* was expressed also in a condition of chronic inflammation. *Mdr2*$^{-/-}$ mice lack a P-glycoprotein on the bile canalicular membrane of hepatocytes, causing defective lipid secretion. The high concentration of monomeric bile salts causes persistent damage of the biliary epithelium, with a consequent inflammatory response, followed by development of HCC with a characteristic age-dependent progression from pre-neoplastic lesions to liver adenoma and finally carcinoma by the age of 12 months

(Katzenellenbogen et al., 2007). We demonstrated by immunohistochemistry on *Mdr2*$^{-/-}$ pre-tumoral inflamed livers that *ST18* was highly expressed in comparison with wt livers, consistent with a possible role of chronic inflammation in modulating *ST18* expression.

Mdr2-/- phenocopies a rare human liver disease called progressive familial intrahepatic cholestasis type 2 (PFIC2), caused by mutation of the *ABCB11* gene encoding for a bile salt export pump (Jacquemin, 2012). Mutations in this gene lead to bile duct hyper-proliferation and portal fibrosis, and patients often develop hepatocellular carcinoma or cholangiocarcinoma (Chan and Vandeberg, 2012). Immunohistochemical analysis showed elevated *ST18* expression in PFIC2 liver tumor biopsies compared to normal human liver, reminiscent of what observed in *Mdr2-/-* mice. It is noteworthy that *ST18* was not expressed in the surrounding cirrhotic tissue: this is probably due to the nature of cirrhosis, in which liver tissue is replaced by non-functioning scar tissue. Thus, *Mdr2-/-* mice and PFIC2 patients share a very similar tumorigenic process derived from a chronic inflammatory setting, which could be the reason for *ST18* activation. Altogether, the data indicate an important role of acute or chronic inflammatory signals in the induction of *ST18* expression in mouse and human livers.

One of our next experiments will be to test the expression of *ST18* in tissue derived from patients with two PFIC related diseases, PFIC1 and 3. Unlike PFIC2 these liver disorders, stemming from mutation on different hepatocellular transport system genes, do not degenerate into hepatocellular carcinoma (Jacquemin, 2012). PFIC3 patients carry a mutation in the ortholog of mouse *Mdr2* the ABCB4 gene (also called *MDR3*), which encodes for a phospholipid floppase involved in biliary phosphatidylcoholine secretion, similarly to *Mdr2* (Chan and Vandeberg, 2012). However, unlike *Mdr2*

deletion in mice, this mutation does not lead to cancer development in humans: the biological basis for this difference is currently unclear.

We have demonstrated that *ST18* is expressed in subcutaneous tumors and in liver under acute and chronic inflammation, however we have not investigated possible gene amplifications in these conditions. *ST18* amplification was observed in HCC nodules in *Mdr2-/-* mice (Shukla et al., 2013) as well as in tumors from 6/7 patients with PFIC2 mutations (Iannelli et al., 2014). Thus, amplification of *ST18* - or a closely linked gene - was positively selected during tumor development in chronically inflamed liver. Considering the correlation between *ST18* expression and amplification in *Mdr2-/-* HCC nodules and in PFIC2 liver patient, it remains to be addressed whether gene amplification also occurred in the ST18-expressing subcutaneous tumors derived from transformed hepatoblasts. Altogether, the above observations suggest that inflammatory conditions induce expression of ST18 and that further increases in expression, whether occurring through gene amplification, L1 insertion or other mechanisms, may be positively selected during tumor progression.

4.4 Possible roles of ST18 in liver tumorigenesis

The expression of *ST18* in inflamed livers and HCC in human and mouse samples has been extensively discussed in our report. However, the oncogenic potential of *ST18* in liver proposed by Shukla et al (2014) is still unclear and we tried to determine whether *ST18* could act as an oncogene by transforming *in vivo*-derived embryonic hepatoblasts. Liver progenitor cells isolated from E18.5 $p53^{-/-}$ embryonic mouse livers and infected with retrovirus expressing c-Myc are only immortalized but not transformed (Zender et al., 2005). These cells provide a sensitized background where expression of additional oncogenes might trigger transformation and therefore

tumorigenesis. *ST18*, unlike H-Ras^{v12}, did not cooperate with c-myc and shp53 to induce transformation of immortalized fetal hepatoblasts. Additional experiments with different combination of oncogenes and tumor suppressors are needed to verify whether *ST18* may have oncogenic properties. In addition, pro- or antitumoral properties of *ST18* may depend on its expression levels. Ectopic expression of *ST18* induced cell death in both hepatoblasts and NIH/3T3, but it remains to be addressed whether this was due to over-expression of exogenous ST18 above physiological levels (such as those observed for the endogenous protein in inflamed liver or HCC) or to a context-dependent effects of ST18.

Following from the above observations, we studied the role of *ST18* in tumor development and maintenance *in vivo.* In particular, we infected a stable population of transformed hepatoblasts with conditional shRNAs against *ST18* and FACS-sorted the cells to obtain a homogeneously transduced population that was then injected subcutaneously into CD-1 nude mice. When *ST18* knockdown was induced immediately upon injection, mice developed smaller tumors compared to control mice, as scored two weeks after injection. When *ST18* KD was induced in established tumors, instead, we observed a dramatic change in tumor morphology, with multiple edematous and hemorrhagic areas. Silencing of *ST18* in tumor cells led to changes in tissue consistence, increase in apoptosis, decrease in proliferation and blood vessel alterations. We conclude that *ST18* is involved in both tumor development and maintenance in liver cancer.

Pathological analysis of tumor samples after *ST18* KD revealed an increased number of less cohesive spindle-shaped cells, suggesting that tumor cells had undergone epithelial to mesenchymal transition (EMT). EMT is a very complex process in which epithelial cells acquire mesenchymal features including loss of cell-cell adhesion,

altered polarity and cytoskeletal reorganization (Ogunwobi and Liu, 2012). A hallmark of EMT is the loss of epithelial characteristic (e.g., a decrease in E-cadherin) and acquisition of mesenchymal markers (such as Vimentin and Twist) (Li et al., 2013b). For this reason we are planning to perform immunohistochemical stainings to verify the expression of EMT-related genes in *ST18* KD tumors.

The aforementioned pathological observations were in agreement with our RNAseq analysis on *ST18* KD tumors, where several enriched gene sets included EMT-associated genes. The mesenchymal transition is an established process in embryonic development and plays an important role in liver fibrosis (Lee et al., 2014). We furthermore observed using the IPA software that many pathways resulted altered after *ST18* KD; in particular the pathway that was most significant and at the same time had highest overlap with the genes in our dataset was the hepatic fibrosis pathway, suggesting a change in the nature of ST18 KD tumor cells and confirming a possible epithelial to mesenchymal transition (Lee et al., 2014). In summary, *ST18* KD in established tumors leads to morphological changes, whereby epithelial cells seem to acquire mesenchymal features as revealed by both pathological and RNAseq analysis.

Mesenchymal cells show enhanced flexibility and motility, at the basis of their migratory and metastatic potential (Ogunwobi and Liu, 2012). However the evidence that silencing *ST18* leads to metastasis was still not addressed in our system. To study the metastatic capacity of *ST18* KD hepatoblasts, it will probably be necessary to change the experimental procedure and to inject the cells orthotopically instead of subcutaneously.

4.5 Possible ST18 mediators preventing the epithelial to mesenchymal transition

As we previously described, inflammation has a critical role in tumorigenesis and in modulating *ST18* expression. Moreover inflammation is a key inducer of EMT, and EMT has been linked to both inflammation and cancer (Zhou et al., 2012). As described above *ST18* seems to prevent the onset of EMT in our tumor model: while the mediators of ST18 implicated in this biological effect are still unknown, our RNAseq analysis allows us to hypothesize a role for TGFβ signaling and/or for the transcription factor MEF2 (myocyte enhancer factor 2).

TGFβ is an important element in the maintenance of normal tissue homeostasis, in which it can either suppress cell proliferation or induce apoptosis, while in cancer tissue it can promote tumor progression by inducing EMT and rendering tumors more invasive (Giannelli et al., 2014). TGFβ has been shown to induce apoptosis in a fraction of cells and to simultaneously induce EMT in other cells within the same tumor mass, meaning that cells can respond differentially to the same factor (Song, 2007). There is also evidence that the cell cycle state and changes in the cellular microenvironment are important determinants of whether TGFβ can induce EMT or apoptosis (Leight et al., 2012; Song, 2007). Dysregulation of apoptosis and EMT are implicated in several pathological events, such as fibrosis of the liver (Song, 2007). Moreover TGFβ has a central role in all stages of liver disease from initial injury through inflammation, fibrosis and progression to HCC (Giannelli et al., 2014).

In our RNAseq data, the TGFβ pathway was upregulated after *ST18* KD in tumors, even though not significantly enriched. While additional experiments are needed to dissect the role of TGFβ in *ST18* KD, we surmise that the possible inhibition of TGFβ by *ST18* could have an important clinical relevance (Fig. 4.1). Recent results of phase

II clinical trials of TGFβ inhibitors show clinical benefits and reduction of EMT in HCC patients (Giannelli et al., 2014).

To identify possible transcription factors affected by *ST18* KD, we analyzed our RNA-seq data with the Gene Set Enrichment Analysis (GSEA) software based on the Molecular Signature Database (MSigDB). This revealed an enrichment of the transcription factor myocyte enhancer factor 2 (MEF2) in the promoters of activated genes in *ST18* KD tumors samples. MEF2 is a transcription factors family that plays a central role in activating genetic programs that control cell differentiation, proliferation, morphogenesis, survival and apoptosis (Potthoff and Olson, 2007). Recently, MEF2 family members were found to increase during TGFβ1 stimulation, further promoting the expression of TGFβ1 in HCC cells (Yu et al., 2014). In the same report, the authors concluded that MEF2 promotes EMT and invasiveness through this TGFβ1 auto-regulation circuitry (Yu et al., 2014).

We therefore checked which MEF2 members were expressed in our experimental model and we found MEF2c as one of the genes differentially expressed and up-regulated in *ST18* KD tumor. MEF2c is known to be a central regulator of cell differentiation and organogenesis (Potthoff and Olson, 2007) and a recent paper provides evidence that MEF2c showed double-edged activities in HCC (Bai et al., 2014): MEF2c inhibited HCC cell proliferation *in vitro* and in xenograft models by impinging on Wnt/β-catenin pathway via blockade of nuclear translocation of β-catenin, and/or promoted tumor progression by stimulating VEGF. In our RNAseq data, the Wnt/β-catenin pathway was inhibited, while the VEGF pathway was upregulated after *ST18* KD. These data suggest a possible role of *ST18* in inhibiting MEF2c to prevent EMT and tumor progression (Fig.4.1). Future experiments of

conditional silencing of MEF2c in co-operation with silencing of *ST18* are needed to verify the hypothesis that *ST18* inhibits MEF2c.

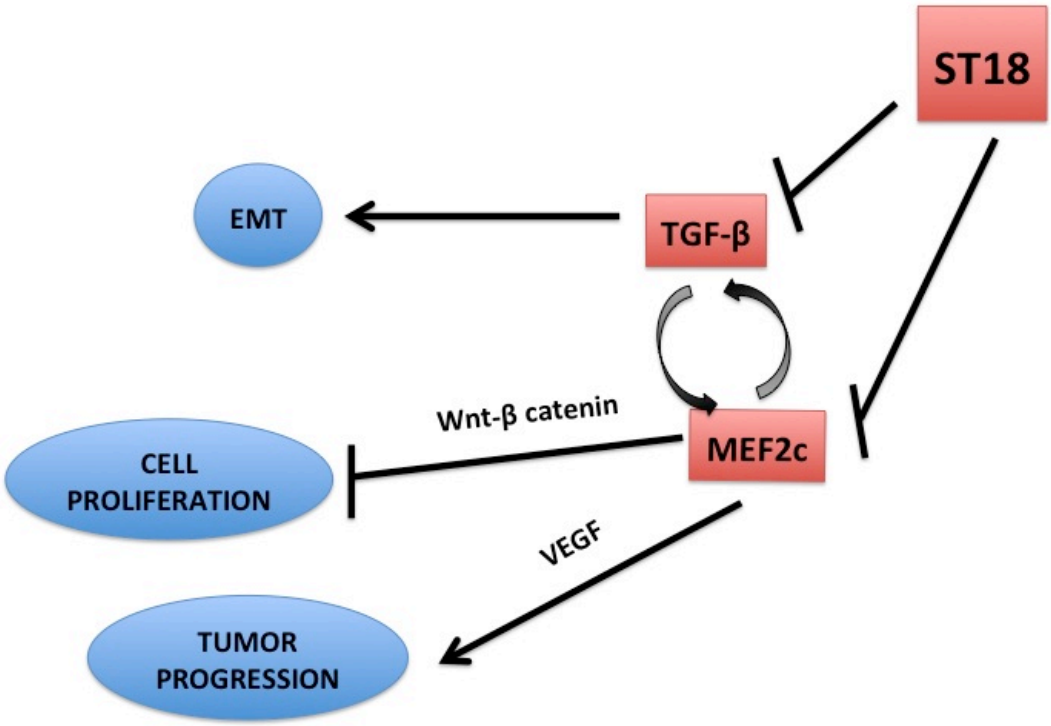

Figure 4.1: Schematic representation of *ST18* mediators in preventing EMT and tumor progression.

4.6 Vascular alterations in the tumors after ST18 silencing

Silencing *ST18* in established tumors leads to high level of hemorrhages and we demonstrated by immunohistochemistry on VE-cadherin, a marker of vascular endothelial cells, that intra-tumoral blood vessels were dilated as compared to vessels in untreated mice. The mechanisms by which *ST18* KD leads to this vascular ectasia remain to be clarified, but it might be a direct consequence of a specific signaling pathway activated only upon loss of *ST18* expression. TGFβ, as we previously mentioned, is a possible mediator after *ST18* KD, and regulates EMT but is also the principal regulator of the endothelial-mesenchymal transition (EndMT). EndMT is the

process by which endothelial cells acquire mesenchymal phenotype leading to vascular remodeling and cancer progression (Cooley et al., 2014). To investigate the phenotype of endothelial cells lining the vascular ectasia in the *ST18* KD tumors we are planning to perform immunohistochemistry against EndMT markers such as N-cadherin, SLUG and smooth muscle actin.

EndMT also contributes to the formation and progression of cerebral cavernous malformation (CCM) through increased TGFβ signaling (Maddaluno et al., 2013). CCM lesions are formed by enlarged blood vessels that result in cerebral hemorrhages reminiscent of the morphological alterations in tumor vessel after ST18 KD. Interestingly, *ST18* is a member of the *NZF/MyT* family of zinc-finger transcription factors involved in development and homeostasis of the nervous system (Yee and Yu, 1998): it could thus be interesting to investigate the expression of *ST18* during the onset and progression of CCM disease.

The vascular endothelial growth factor (VEGF) pathway is a critical pro-angiogenic factor and has an important role in increased vascular permeability and endothelial migration during angiogenesis (Esser et al., 1998). High concentrations of VEGF, as suggested by our RNAseq analysis after ST18 KD, have been associated to fusion of vessels, which results in abnormally large lumens (Drake and Little, 1995). Altogether, we hypothesize that the mechanisms by which *ST18* silencing leads to the vascular malformations present in subcutaneous tumors may be a consequence of VEGF and/or TGFβ and MEF2 signaling (Fig. 4.2). However, we cannot discard the possibility that tumor necrosis induced after ST18 KD might indirectly lead to alteration of the tumor vasculature.

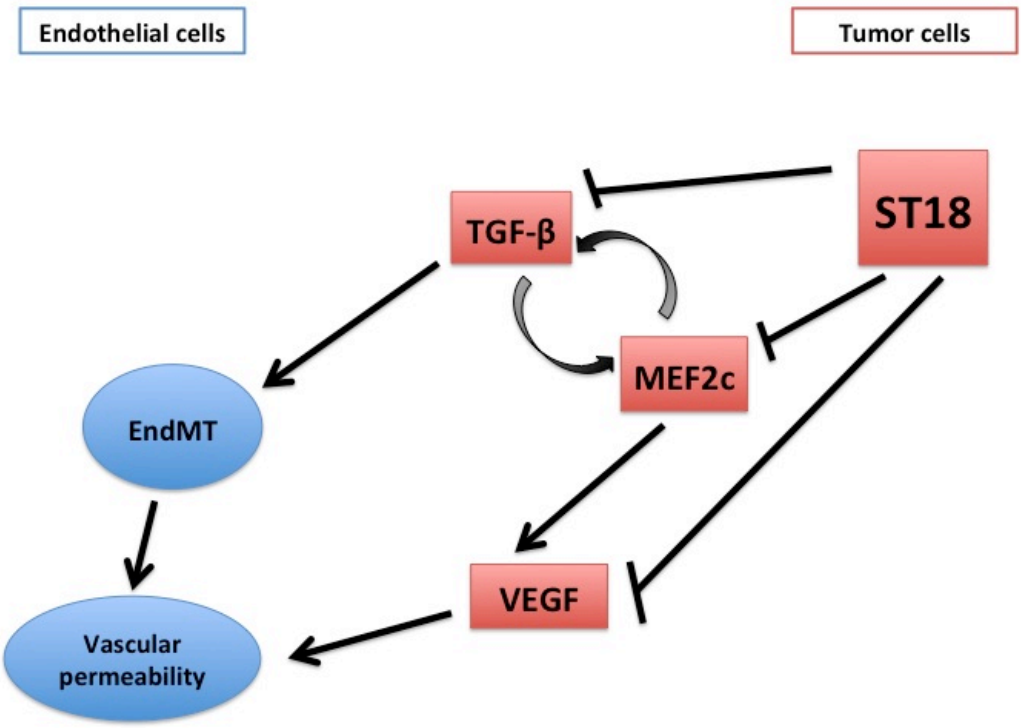

Figure 4.2: Schematic representation of ST18 mediators in preventing blood vessels alteration.

4.7 Conclusions

Our study suggests that *ST18* is induced by different inflammatory signals, providing a possible explanation for *ST18* expression in subcutaneous tumors and not in cell culture where inflammatory mediators are not present. The role of inflammation in driving tumorigenesis and subsequently EMT has been widely studied. In this setting, our work suggests that inflammation-induced *ST18* constitutes a negative regulatory loop that prevents EMT in conditions that would otherwise support it: abrupt knockdown of ST18 would thus lead to a rapid and concerted induction of EMT, as achieved in our tumor model (Fig. 4.3). We hypothesize that *ST18* may have a dual role in controlling cancer onset and progression: on one hand, as documented in this report, *ST18* plays a crucial role in tumor development and maintenance; on the other

it may also acts as tumor suppressor by inhibiting EMT through different mediators such as TGFβ and MEF2 signaling (Fig. 4.3). This context- or stage-dependent action of *ST18* may help rationalizing the apparently contradictory reports that dubbed it either as a tumor suppressor or an oncogene in different types of tumors. Based on the results presented here, impinging on *ST18* signaling responses could represent a relevant therapeutic strategy in liver cancer.

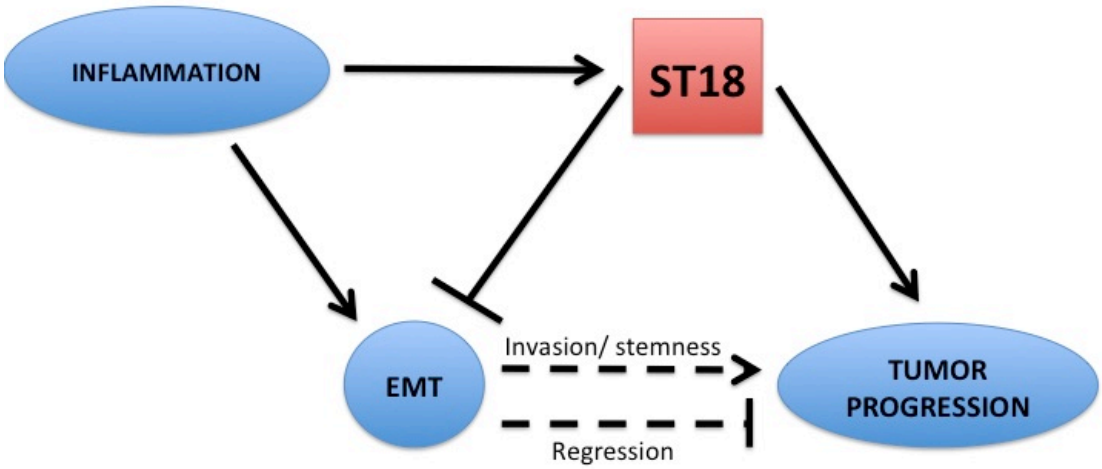

Figure 4.3: Schematic representation of the dual role of ST18 in liver cancer.

5. SUPPLEMENTARY TABLES

Table S1: Differentially expressed genes (DEGs) UP in ST18 KD tumors.
We identified 677 DEGs UP regulated genes in ST18 KD tumors as those ones that have a log2FC > 0.5 and p-value < 0.05.

gene name	log2FC	gene name	log2FC	gene name	log2FC
Ildr2	1.48	Ak1	0.91	Col8a1	3.21
Gm3893	1.69	Aldh1a1	1.66	Col1a1	0.64
Tigit	0.99	Aldh3a1	2.20	Cplx2	0.50
Lrrc19	0.76	Prelp	1.30	Cryab	2.39
Mir1895	1.49	Alpk3	1.59	Csf1r	0.61
Fam46b	1.26	Aox1	0.86	Vcan	1.29
3425401B1	1.99	Cd5l	2.67	Csrp3	2.87
Slco2b1	1.10	Apobec1	0.65	Ctsh	0.89
Cyp4v3	1.16	Synpo2	1.56	Ctss	0.60
Myzap	1.44	Arnt2	1.39	Cybb	0.59
Dnm3	1.33	Atp2a1	1.74	Cyp1b1	2.65
Cyp27a1	1.23	Slc7a2	0.87	Cd55	2.27
Pld4	0.59	Bach2	0.50	Dclk1	1.72
Akr1c14	1.76	Bicd1	0.82	Dcn	2.14
Csdc2	2.03	Smyd1	1.95	Dmd	2.31
Ankrd12	0.60	Serping1	1.24	Dok2	0.72
Kazald1	0.93	C3	1.29	Dpep1	2.52
Mylk	0.69	Cacna1g	0.51	Dpp4	2.09
Sema3d	1.92	Cacna1s	2.22	Ebf1	1.06
Galnt16	2.28	Cacna2d1	0.78	S1pr1	0.60
Als2cr12	1.53	Car3	2.33	Eef1a2	2.91
Ms4a7	1.46	Casp12	0.96	Emr1	0.79
Mybpc1	2.54	Casp6	0.52	Eno3	0.52
Itga1	0.96	Casq1	2.03	Epas1	0.77
Art4	1.94	Casq2	1.47	Epb4.1l3	1.73
Manba	0.76	Cav1	0.50	Epha3	3.79
Pp2d1	0.94	Cbr2	1.19	Ptprv	1.26
Scn2a1	1.31	Cd1d1	0.76	Celf2	0.80
Scn4a	1.85	Cd34	0.68	Mecom	0.65
Slc8a3	1.17	Cd36	0.95	Ppp1r3a	2.45
Abca1	0.75	Cd59a	1.22	F8	0.77
Lyve1	2.10	Cdh11	1.09	Sesn1	0.72
Acta1	1.76	Cdh3	1.10	Fcna	1.11
Brdt	0.82	Cfh	1.78	Fgf1	0.77
Hsd17b11	0.72	Chl1	2.66	Fgf7	1.67
Actn2	2.63	Ckm	2.19	Fhl1	2.46
Actn3	2.23	Clca1	1.14	Figf	1.33
Acta2	0.64	Ccr2	1.17	Fkbp7	0.58
Cygb	0.78	Col11a1	3.27	Fli1	1.01
Adam12	0.87	Col12a1	2.33	Fmn1	0.95
Adam22	1.13	Col14a1	1.49	Fmo1	1.42
Add2	0.81	Col15a1	1.09	Fmod	2.76
Adssl1	0.88	Col4a5	1.01	Aff2	1.28
Acan	2.60	Col5a2	0.88	Asb14	1.74
Angpt1	1.82	Col6a2	0.56	Folr2	1.27

gene name	log2FC	gene name	log2FC	gene name	log2FC
Frk	1.42	Maf	0.99	Ptpn22	1.33
Fst	1.98	Il17rd	0.65	Ptprb	0.72
Gas6	0.96	Masp1	0.67	Ptprd	1.80
Gas7	1.33	Mb	1.69	Ptprk	0.76
Ggh	0.76	Mcf2l	0.69	Fam211b	1.64
Ghr	0.77	Mcpt4	2.45	Ptrf	0.62
Gjb3	1.57	Cma1	1.52	Pvalb	3.53
Gnal	1.11	Tpsb2	1.59	Pygm	0.99
Gnb4	0.64	Mef2c	1.19	Reps2	0.92
Gpc3	2.57	Meg3	1.68	Robo1	1.03
Gpr65	1.26	Mme	2.54	Rpgr	0.56
Gpm6b	1.32	Mrc1	0.92	Ryr1	1.65
Gpx3	1.19	Myh11	1.00	S100a4	0.78
Gsta4	1.18	Myh2	2.97	Scn7a	3.05
Gstm2	0.62	Myh3	2.52	Ccl11	2.38
H2-Ab1	0.80	Myh4	4.95	Ccl8	1.65
H2-Eb1	0.76	Myh8	2.46	Ccl9	0.84
Mr1	0.69	Myl4	1.38	Cxcl12	0.79
Hmgcs2	1.60	Myl1	2.47	Sdpr	0.98
Hrc	2.11	Mylpf	2.65	Sema3a	0.92
Sdc2	0.71	Myo6	0.53	Sema3c	1.97
Slc6a4	1.35	Myog	2.22	Sema5a	0.63
Igf1	2.64	Myom1	1.09	Sepp1	1.03
Itga4	0.61	Myom2	2.78	Sfrp1	2.67
Itih2	1.29	Naip2	0.76	Sfrp4	1.73
Itm2a	1.75	Ncf1	0.77	Sgce	0.51
Sspn	0.51	Neb	2.41	Sorbs3	1.15
Lama2	1.58	Nov	1.65	St6gal1	0.70
Anpep	0.52	Nrap	2.77	Sla	1.26
Lepr	0.78	Ntrk2	1.31	Slc8a1	1.02
Lifr	0.53	Ocln	1.11	Slit2	1.78
Lox	3.03	Ogn	1.14	Slit3	2.62
Loxl1	1.31	P2rx6	1.71	Sod3	3.23
Loxl3	0.70	Pappa	1.91	Sox5	0.75
Ltbp2	2.10	Pbx1	0.59	Sox6	1.50
Lum	2.20	Pcsk5	3.15	Serpinb6b	1.85
Lxn	0.58	Pde1a	0.60	Serpinb9	0.82
BC002163	0.90	Per2	0.85	Pknox2	1.18
Ly6c1	0.90	Phex	1.34	Aph1b	0.72
Papln	0.90	Prkcb	0.54	Btla	1.64
Tlr7	1.35	Pkia	1.93	Fam180a	1.93
Tlr8	1.93	Plcb4	0.74	Phldb2	0.72
Eltd1	0.73	Pltp	1.23	Etl4	1.47
Asic3	0.77	Prrx1	1.72	Itih5	0.51
Havcr2	1.54	Inpp5k	0.52	Dock10	1.17

gene name	log2FC	gene name	log2FC	gene name	log2FC
Pamr1	1.83	Tnnt2	1.55	Neil3	0.52
Efhb	1.40	Tnnt3	1.60	Inpp4b	1.38
Tifa	0.62	Tpd52l1	1.06	Zfp810	0.70
Chpt1	0.75	Ttn	2.36	Adamts15	1.77
Fam46a	1.33	Unc5c	1.58	Zbtb16	1.09
Itga10	1.43	Itgbl1	3.77	Plscr4	1.08
Ankrd35	2.26	Vcam1	0.61	Acpl2	0.75
Il20rb	0.89	Abra	2.65	Ppp2r3a	0.57
Rassf4	0.90	Wisp2	1.52	Arhgef9	0.80
Tagln	0.91	Tmem44	0.56	Stard8	1.33
Lgi3	1.54	Xirp1	3.81	Klhl4	1.04
Xist	0.91	Xk	0.81	Tceal1	1.54
Tcap	2.68	Zfp758	0.56	Col23a1	1.44
Tcea3	1.36	Ankrd29	1.52	Adam23	2.29
Cilp	3.60	Fhod3	1.65	Adamts5	1.08
She	0.88	Alpk2	2.17	Aplnr	1.51
Aldh5a1	0.86	Pla2g16	1.18	Sdk2	1.27
Zmat1	0.91	Myrf	1.15	Akap6	1.01
Pik3ip1	0.78	Slc6a20b	1.06	Macc1	0.96
Ccdc85a	1.59	Tmem252	1.20	Pde4d	0.84
Efemp1	3.10	Pgm5	1.95	Gpr34	0.83
Adamts2	1.18	Siae	0.67	Grem2	2.04
Wnt9a	1.84	Ablim1	0.64	Kctd12	0.75
Tef	0.75	Igfn1	1.93	Lamc3	1.11
Tek	1.25	C130074G1	1.08	Lynx1	1.83
Adap2	1.01	Zfp2	0.61	Tspyl5	1.60
Abca9	1.35	Dnah7b	1.10	Mid2	0.87
Pqlc3	0.82	Zfp90	0.54	Gpr156	1.49
Ankmy2	0.53	Gsn	0.63	Sulf1	1.48
Stxbp6	1.48	Klhl41	1.81	Xirp2	3.82
Tfpi2	2.33	Mylk2	1.66	Pde5a	1.34
Rapgef5	0.68	Ctso	0.81	D630039A0	1.09
Tgfb2	1.15	Slc16a4	0.71	Myom3	2.27
Thbs2	1.21	5730409E0	1.00	Gpr133	2.94
Thbs3	0.59	Cyp26b1	1.51	A430033K0	0.60
Thbs4	2.94	Frmd4b	0.91	Gimap8	0.60
Thy1	1.25	Gxylt2	0.92	Zfp791	1.53
Pde8b	0.88	A2m	2.51	Abcc12	1.68
Gcnt4	1.08	Clec12a	0.95	Nxpe4	0.63
Scara3	0.80	Ccdc136	0.50	Layn	1.00
Tnnc2	3.01	B3gnt8	0.68	Klhl31	1.99
Tnfrsf11a	0.85	Mybpc2	2.58	Col6a6	1.69
Tnni1	1.46	Ano5	2.06	Zfp300	0.62
Tnni2	2.51	Synm	0.75	Zc4h2	0.67
Tnnt1	1.37	Spon1	1.93	Mum1l1	0.98

gene name	log2FC	gene name	log2FC	gene name	log2FC
Tbc1d8b	0.65	Mcc	0.63	Hmcn1	1.18
Olfr920	1.98	Ankrd44	1.03	Ccdc141	1.16
Srgap3	1.69	Accs	0.58	Pdgfc	1.48
Ceacam1	0.91	Fat4	1.43	Plxnc1	0.81
Prnd	1.63	AI464131	0.70	Cpxm2	2.13
Ror1	1.64	Frem1	1.02	Fmo2	2.01
Gm1564	1.72	Col8a2	3.20	Dgke	0.53
Abcd2	1.24	9530026P0	0.67	Plac1	1.52
Abat	0.83	Rnf150	1.01	Dpt	0.70
Dysf	0.54	Dixdc1	0.95	Cyp2d22	0.78
Kif26b	0.83	Cntln	0.74	Ctsf	0.79
Islr	1.76	Txlnb	1.01	Vmn2r1	1.32
Clec4a1	1.11	Obscn	2.34	Ankrd2	2.52
Pon3	0.80	Fam189a2	1.51	Serinc4	0.97
Maml2	0.72	Atp2b4	0.64	Usp29	1.92
Amica1	1.17	Nxpe5	1.89	Slc43a3	1.08
Pdk4	2.61	Zfp667	0.60	Rnase4	1.09
Nrep	0.69	Ecm2	0.85	Myot	3.44
Timd4	1.54	Mettl21c	1.18	Fxyd6	0.94
Vsig4	2.17	Trim63	1.85	Tmem8	1.45
Spin2c	1.33	Trim72	1.83	Gucy1a3	0.96
Tlr13	1.00	Nox4	1.23	Trp53inp1	1.18
Rabgap1l	0.61	Mfap5	3.35	A230073K1	0.80
Ndrg2	0.67	Postn	2.73	Zfp963	0.67
Hspb7	2.45	Dkk3	1.84	Nrgn	0.66
Pde7b	0.97	Hmgn5	0.97	Smoc2	1.08
Angptl3	0.70	C1s	2.05	Gpr88	1.86
Zfp354c	0.75	Srpx	2.15	Ms4a8a	1.95
Pik3cg	0.87	Ccdc39	1.12	Lpin3	0.96
Pcmtd1	0.66	D7Ertd715e	0.90	Slc9a3r2	0.55
Cxxc4	0.87	Ldlrad4	0.53	Smpx	2.22
Zfp182	0.65	Cd300lg	0.69	Fbxo36	0.93
Zfp944	0.63	Lurap1l	1.42	Mustn1	1.61
Fsd1l	0.50	Dlg3	0.64	Fam134b	0.68
Dsel	0.69	Pdlim3	2.98	Mgst3	1.14
Apba1	1.55	Hif3a	0.85	Rwdd3	1.02
Olfml2b	1.55	Gria3	2.79	Dcbld1	0.51
Fbxl13	1.30	Tlr5	1.58	Aspn	1.27
4930412C1	1.47	Pcdh7	1.02	Tab3	0.51
Scai	0.61	Ctnnal1	0.95	Ptplad2	0.84
Glt28d2	1.44	Cpq	0.73	Gm9079	1.15
P4ha3	2.36	Mtmr7	0.79	Snord123	0.76
Abi3bp	2.15	Slc4a4	1.82	Cir1	0.56
Zhx3	0.55	Hpgds	0.64	2310030G0	1.26
Lrrn4	1.31	Kalrn	0.94	Fam210b	0.87

gene name	log2FC
Gpx7	1.56
Zfp606	0.53
3632451O0	2.23
Adck3	1.03
Plxdc2	0.89
Tbc1d23	0.51
Fibin	1.46
Zfp788	0.54
4930523C0	1.54
Rnf125	0.98
Fbxo32	0.71
S100a16	1.02
Rgs10	0.81
Tmem100	2.92
Ccdc80	0.96
Spata6	0.61
Murc	0.96
Cep70	0.69
5031426D1	0.88
Gstm7	0.96
Cthrc1	4.04
Fndc1	2.87
Fam198b	0.81
Lrrc16a	1.10
Synpo2l	1.64
Srpx2	3.23
Pdgfrl	2.29
Mypn	2.20
Nexn	0.79
Smim1	1.14
Cd209f	2.80
Cmbl	0.82
Pir	0.81
Ms4a6b	0.84
Wnk4	0.92
2810403D2	0.99
Ogfrl1	0.61
Gcc2	0.52
Ica1l	0.84
Filip1	0.97
Gulp1	1.01
Medag	2.08
Tspan2	1.84
Klhl30	1.60
P2ry12	1.47
Myl9	0.69
Cercam	1.13

gene name	log2FC
Pgm2l1	0.55
4931406C0	0.57
Scara5	1.43
Arhgap42	0.59
Gdpd2	2.07
Zfp949	0.51
4930506M0	0.92
Rarres2	1.57
Rbm43	0.52
Armcx3	0.82
Lrrcc1	0.76
Osbpl3	0.75
Ccdc19	0.69
Epn3	0.96
Klhl40	1.67
Palld	0.72
Zc2hc1c	0.64
2210408I21	0.56
Ttc30b	0.69
Usp13	1.70
Angptl1	0.98
Pard3b	1.27
Mblac2	0.62
March1	1.21
3110007F17	0.71
Clec4a3	1.07
Bmper	1.65
Arhgef6	0.66
1700049G1	0.63
Vgll3	2.34
Ms4a6c	0.60
Zbtb8a	0.57
Rftn2	0.97
Nphp3	0.65
Plce1	0.86
Ifltd1	1.71
Npl	0.98
F13a1	1.27
Lrguk	1.08
Myo18b	2.85
Cep72	0.64
Lrrc15	2.16
Lrrc17	0.85
Zfp943	0.54
Hhatl	1.61

gene name	log2FC
Glt8d2	1.06
Purg	0.75
Cep128	0.56
Zfp820	0.63
Calml4	1.05
Rian	1.33
4930578C1	1.32
Mfap4	1.27
Asb5	1.62
Tbx18	0.86
Cep112	0.70
Daam2	1.09
Prss23	1.00
Cmya5	2.56
Ckmt2	1.58
Trdn	3.94
Rab36	0.70
Il33	0.87
Anks1b	1.22
Adamtsl1	2.47
Adamtsl2	1.33
Ypel2	0.57
2810055G2	0.80
Zfp449	0.64
Hdac9	0.66
Wbscr27	0.68
Trim2	0.52
C1qtnf3	3.90
Tnxb	1.01
Trem2	1.40
Tktl1	1.51
Sytl2	1.98
Bicc1	0.54
Crispld1	2.31
Cd163	0.66
Lmod2	2.92
Smarca1	1.85
Peli2	0.59
Trim7	0.89
Trim9	1.84
Ophn1	1.42
Col4a6	1.14
Prg4	1.21
Pid1	0.81
Atp1a2	1.12

Table S2: Differentially expressed genes (DEGs) DOWN in ST18 KD tumors.
We identified 467 DEGs DOWN regulated genes in ST18 KD tumors as those ones that have a log2FC < -0.5and p-value < 0.05.

gene name	log2FC	gene name	log2FC	gene name	log2FC
Fam129c	-0.76	Hrk	-1.77	Hspa1b	-1.05
Isg15	-0.89	Bop1	-0.50	Ier3	-0.81
1110002L01	-0.81	Bsn	-0.73	Ier5	-0.55
Kti12	-0.55	Hyou1	-0.63	Cxcl10	-1.69
Akna	-0.68	Car6	-1.85	Ifit1	-0.76
Snord93	-0.57	Cbs	-0.80	Ifrd2	-0.76
Epg5	-0.70	Entpd6	-0.59	Il11	-2.41
Dos	-0.76	Cdkn1a	-0.65	Il1b	-1.48
Noc4l	-0.55	Cebpb	-0.91	Isl1	-1.13
Psph	-0.72	Cish	-0.71	Itgal	-1.08
Chchd10	-1.47	Plk3	-0.76	Jag2	-0.81
E130012A1	-1.07	Atf6b	-0.67	Jak3	-0.52
Tubg1	-0.57	Crmp1	-0.84	Jun	-0.78
Pcnxl3	-0.52	Csf3	-1.73	Junb	-0.52
Tecpr2	-0.73	Csf3r	-1.46	Kit	-0.62
Cdk20	-0.65	Csn3	-1.06	Arhgef2	-0.56
Gpsm3	-0.56	Cxadr	-0.93	Lck	-1.23
Wdr90	-0.50	Ddit3	-1.02	Lcn2	-1.27
LOC106740	-0.54	Dll1	-0.71	Lif	-1.11
Slc39a3	-0.62	Eif2b4	-0.59	Rtn4ip1	-0.74
Rrp12	-0.98	Eno1	-0.55	Bbc3	-0.68
Yars	-0.50	Epha2	-0.71	Hook2	-0.61
Guca1b	-1.47	Etv2	-2.12	Acot2	-0.76
Atf5	-1.05	Fanca	-0.53	Mef2b	-1.62
Cth	-0.89	Fhl3	-0.50	Mknk1	-0.62
Shmt2	-0.65	Foxc2	-1.40	Mthfd2	-0.64
Gpt2	-0.63	Fosl1	-1.08	Mybl2	-0.52
Atad3a	-0.51	Fosl2	-0.84	Ppp1r15a	-0.91
Nabp1	-0.88	Ncs1	-0.55	Ndrg1	-0.72
Pwp2	-0.50	Fut1	-1.67	Nfil3	-0.95
Dxo	-0.56	G0s2	-1.55	Nfkb2	-0.64
Aatk	-0.55	Gaa	-0.54	Nnmt	-1.07
Chrnd	-1.24	B4galnt2	-0.77	Slc11a2	-0.53
Impa2	-0.53	Gbp2	-0.63	Sigmar1	-0.52
Adam15	-0.53	Glp1r	-0.82	P2ry2	-0.99
Adora1	-1.16	Glrp1	-1.14	P4ha2	-1.00
Avil	-1.91	Slc6a9	-0.93	Pcx	-0.73
Alpl	-0.68	Got1	-0.61	Pdgfa	-0.61
Aqp3	-0.99	Gpaa1	-0.64	Pfkl	-0.52
Klf16	-0.73	Cxcl1	-1.13	Pim1	-0.52
Atf3	-1.23	Gys1	-0.78	Pitpnm1	-0.55
Slc7a1	-0.74	Hap1	-1.14	Por	-0.50
Bcat1	-0.77	Hdc	-1.48	Ppard	-0.72
Bcl6	-0.66	Hbegf	-0.56	Scand1	-0.83
Mrps6	-0.52	Hoxb9	-1.97	Prodh	-0.54

gene name	log2FC	gene name	log2FC	gene name	log2FC
Prss12	-0.94	Tmem194	-0.74	Rnd1	-1.30
Ptgir	-0.85	Nomo1	-0.52	Soat2	-1.39
Hps4	-0.61	Wwc1	-0.80	Wfs1	-0.71
Ptprn	-0.56	Mars2	-0.57	Uhrf1bp1	-0.60
Nacad	-1.25	Gm17296	-0.64	Ppp2r5b	-0.64
Rad9a	-0.55	Slc39a14	-0.62	Rin1	-0.66
Hspa1a	-1.14	Taf1c	-0.67	Tmem185b	-0.71
Rapsn	-1.05	Fbxo42	-0.53	Qsox2	-0.53
Rasal1	-0.87	Zfp598	-0.70	Oct4	-0.64
Relb	-0.79	Disp2	-1.11	Coq4	-0.52
Rfng	-0.57	Tcof1	-0.83	Slc25a25	-0.51
Polr1b	-0.51	Arid5a	-0.82	P2rx3	-1.32
Rps6ka2	-0.59	Csrnp1	-0.58	Rhov	-1.58
S100a8	-1.33	Lrrc20	-0.52	Mavs	-0.53
S100a9	-1.15	Polrmt	-0.59	Trib3	-1.36
Ccl2	-0.76	Sbno2	-0.61	Ppp1r16b	-0.75
Ccl20	-2.30	Aldh1l2	-0.87	Fitm2	-0.56
Ccl3	-1.84	Phlda1	-0.63	Slc35c2	-0.66
Ccl7	-0.82	Gemin5	-0.56	Helz2	-0.66
Cxcl2	-1.26	Kdm6b	-0.58	Ciart	-1.08
Sell	-1.22	Wrap53	-0.58	6330416G1	-0.55
Sema4d	-0.72	Neurl4	-0.57	Sesn2	-1.45
Sema6b	-0.80	BC030867	-0.51	Zbtb40	-1.04
Siah2	-0.90	Rhbdf2	-0.74	Cox18	-0.53
Clpb	-1.00	Engase	-0.78	Paqr3	-0.83
Slc1a5	-0.59	Terc	-0.99	Agpat9	-1.01
Slc20a1	-0.54	Tgfa	-0.65	Oasl1	-1.02
Slc2a1	-0.79	Lhfpl2	-0.59	Gcn1l1	-0.51
Slc2a3	-0.68	Mrps27	-0.65	Aimp2	-0.51
Slc7a5	-0.75	Tll1	-0.84	Lmtk2	-0.50
Slfn4	-1.54	Cd40	-0.56	H2afj	-0.88
Slpi	-1.79	Cmpk2	-1.37	Zfp428	-0.59
Smarcb1	-0.51	Ung	-0.53	Zfp574	-0.63
Sorl1	-0.95	Upp1	-0.51	Kctd13	-0.52
Urb1	-0.73	Vars	-0.55	Piezo1	-0.50
Srm	-0.61	Vegfa	-0.71	Igsf9b	-1.15
Dhx37	-0.78	Vldlr	-0.56	Lingo3	-1.75
Star	-0.63	Them6	-1.08	Gadd45g	-0.65
Stat1	-0.53	C030006K1	-0.86	Gdf15	-2.42
Stc2	-1.46	Arhgap39	-0.61	Cacna1i	-1.03
Alg3	-0.62	Ankrd54	-0.57	Oasl2	-0.89
Slc25a38	-0.66	Ttll12	-0.51	Sigirr	-0.68
Stra6	-1.16	Wars	-0.62	Dusp5	-0.84
Pycr1	-1.03	Pim3	-0.63	Map2k3os	-0.68
Tbc1d25	-0.63	Adm2	-1.88	Usp18	-1.06

gene name	log2FC
Dhrs9	-0.86
Fam171b	-1.46
Slc1a7	-1.71
Trim30b	-1.24
Retnlg	-1.36
Spata2	-0.51
Map2k2	-0.53
Slc7a11	-1.04
Stfa2l1	-1.42
Cln8	-0.57
Gcat	-0.61
Zfp346	-0.59
Slc4a11	-0.97
Ecsit	-0.51
Map1s	-0.60
Rab6b	-0.94
Cars	-0.52
Tbl2	-0.53
Rrp9	-0.51
Desi1	-0.60
Znhit2	-0.73
Pmm1	-0.71
Fbxl6	-0.52
Zbtb18	-0.78
Tor2a	-0.78
Ptpn7	-0.54
Maats1	-1.37
Cass4	-1.61
Tmem154	-1.14
Trmt61a	-0.59
Apol11b	-2.05
Ptrh1	-1.00
Lcmt2	-0.56
Slc5a6	-0.56
Trim66	-1.23
Hapln4	-1.34
Ppp1r13l	-1.03
Trim46	-1.34
Nckap5l	-0.50
Dnph1	-0.60
Ap5b1	-0.78
5830416P1(	-0.87
Vgf	-2.54
Kctd16	-1.69
Cdsn	-1.53

gene name	log2FC
Ndufa4l2	-0.91
Itprip	-1.16
4930404N1	-0.58
Prr7	-0.97
Gm5483	-1.68
Heatr2	-0.54
Slc28a1	-1.93
Fbxl8	-0.73
Capn15	-0.59
Cdk2ap2	-0.62
Coq5	-0.55
Pvr	-0.51
Agpat5	-0.54
Stbd1	-0.98
Slc52a2	-1.06
Cntnap1	-0.72
Banp	-0.66
Tomm40	-0.50
Bysl	-0.83
Irf7	-0.90
Nup210	-1.31
Slc1a4	-0.96
Agpat1	-0.57
Gtpbp2	-0.53
Rabggta	-0.54
Scamp4	-0.65
Extl1	-2.02
Adar	-0.65
Pard6a	-0.94
Txn2	-0.62
Sphk2	-0.56
Fgf21	-1.98
Pigo	-0.62
Pdxp	-0.70
Dolpp1	-0.61
Apba3	-0.68
Rsad2	-1.27
Nelfb	-0.61
Rrs1	-0.60
Pnkp	-0.56
Fetub	-0.97
Nrip2	-1.24
Fads3	-0.87
Fam43b	-1.67
Fam129a	-0.75

gene name	log2FC
Sdf2l1	-0.85
Ptges	-0.55
Fndc4	-0.67
D330041H0	-0.82
Rgcc	-0.59
Lyrm9	-0.64
Dus2	-0.71
Dhrs7	-0.50
Sac3d1	-0.55
Tmem238	-0.95
Timm50	-0.62
Acp6	-0.54
Ctu2	-0.65
Cdt1	-0.56
Dedd2	-0.75
Ankrd33b	-0.69
Eepd1	-0.57
Dph2	-0.71
Prpsap1	-0.71
Jagn1	-0.54
Rtp4	-0.75
Rab39b	-0.68
Dgat2	-0.99
Asprv1	-1.57
Pdf	-1.19
Mid1ip1	-0.69
Fam173b	-0.51
Otub2	-1.16
Coa4	-0.82
Leprotl1	-0.52
Slc25a22	-0.78
Ccdc163	-0.51
Ints1	-0.56
Tmem109	-0.51
Chac1	-1.55
Ydjc	-0.52
Comtd1	-0.69
Mocs3	-0.68
Bst2	-0.59
Ap5s1	-0.83
2310061I04	-0.52
Cad	-0.53
Eif1ad	-0.56
Ufsp1	-0.87
Rnf126	-0.61

gene name	log2FC
Cactin	-0.51
Cd3eap	-0.53
Reep6	-1.44
Steap1	-0.67
Dhrs13	-0.58
Slc25a33	-0.95
Angptl6	-1.54
Spef1	-0.55
Mus81	-0.50
Ulk3	-0.66
Tysnd1	-0.61
Osgin1	-0.92
Cyb5r1	-0.91
Usp36	-0.84
Faim2	-1.07
Tspyl4	-0.95
Ier5l	-0.89
Tdrkh	-1.00
Sppl2b	-0.61
1110008P1	-0.57
Whrn	-0.84
Mfsd12	-0.72
Abcb6	-0.64
Rbm19	-0.62
Pi16	-0.81
Syvn1	-0.62
Cluh	-0.58
Stk40	-0.84
1700017B0	-0.59
Klrg2	-0.97
Lonrf3	-0.90
Pgs1	-0.57
Scpep1	-0.60
Ddit4	-0.78
Mei4	-1.09
Dusp9	-0.68
Cdyl2	-0.81
Grhpr	-0.92
Ccdc134	-0.62
Mfsd2a	-1.14
Mib2	-0.50
2410131K1	-0.55
Rhbdd1	-0.76
Prdm8	-1.14
Enthd2	-0.53

gene name	log2FC
Aacs	-0.51
Ern1	-0.71
Recql4	-0.85
Slc16a3	-1.00
Slc12a9	-0.65
Dnaja3	-0.72
Pcdhgb2	-0.57
Pcdhga1	-0.63
Pcdhga2	-0.84
Pcdhga4	-0.64
Nkd1	-0.99
Cnnm4	-0.79
Wbscr16	-0.57
D930048N1	-0.91
Nat10	-0.51
Abtb2	-0.58
Ifi44	-1.14

6. REFERENCES

Anastassiou, D., Rumjantseva, V., Cheng, W., Huang, J., Canoll, P.D., Yamashiro, D.J., and Kandel, J.J. (2011). Human cancer cells express Slug-based epithelial-mesenchymal transition gene expression signature obtained in vivo. BMC cancer *11*, 529.

Arbuthnot, P., Capovilla, A., and Kew, M. (2000). Putative role of hepatitis B virus X protein in hepatocarcinogenesis: effects on apoptosis, DNA repair, mitogen-activated protein kinase and JAK/STAT pathways. Journal of gastroenterology and hepatology *15*, 357-368.

Bai, X.L., Zhang, Q., Ye, L.Y., Liang, F., Sun, X., Chen, Y., Hu, Q.D., Fu, Q.H., Su, W., Chen, Z*., et al.* (2014). Myocyte enhancer factor 2C regulation of hepatocellular carcinoma via vascular endothelial growth factor and Wnt/beta-catenin signaling. Oncogene.

Balkwill, F., and Mantovani, A. (2001). Inflammation and cancer: back to Virchow? Lancet *357*, 539-545.

Bishayee, A. (2014). The role of inflammation and liver cancer. Advances in experimental medicine and biology *816*, 401-435.

Bressac, B., Kew, M., Wands, J., and Ozturk, M. (1991). Selective G to T mutations of p53 gene in hepatocellular carcinoma from southern Africa. Nature *350*, 429-431.

Brouha, B., Schustak, J., Badge, R.M., Lutz-Prigge, S., Farley, A.H., Moran, J.V., and Kazazian, H.H., Jr. (2003). Hot L1s account for the bulk of retrotransposition in the human population. Proceedings of the National Academy of Sciences of the United States of America *100*, 5280-5285.

Burns, K.H., and Boeke, J.D. (2012). Human transposon tectonics. Cell *149*, 740-752.

Cairo, S., and Buendia, M.A. (2012). How transient becomes stable: an epigenetic switch linking liver inflammation and tumorigenesis. Journal of hepatology *57*, 910-912.

Chan, J., and Vandeberg, J.L. (2012). Hepatobiliary transport in health and disease. Clinical lipidology *7*, 189-202.

Chan, K.L., Guan, X.Y., and Ng, I.O. (2004). High-throughput tissue microarray analysis of c-myc activation in chronic liver diseases and hepatocellular carcinoma. Human pathology *35*, 1324-1331.

Clayton, R.J., Iber, F.L., Ruebner, B.H., and McKusick, V.A. (1969). Byler disease. Fatal familial intrahepatic cholestasis in an Amish kindred. American journal of diseases of children *117*, 112-124.

Cooley, B.C., Nevado, J., Mellad, J., Yang, D., St Hilaire, C., Negro, A., Fang, F., Chen, G., San, H., Walts, A.D*., et al.* (2014). TGF-beta signaling mediates endothelial-to-mesenchymal transition (EndMT) during vein graft remodeling. Science translational medicine *6*, 227ra234.

Davit-Spraul, A., Gonzales, E., Baussan, C., and Jacquemin, E. (2009). Progressive familial intrahepatic cholestasis. Orphanet journal of rare diseases *4*, 1.

Drake, C.J., and Little, C.D. (1995). Exogenous vascular endothelial growth factor induces malformed and hyperfused vessels during embryonic neovascularization. Proceedings of the National Academy of Sciences of the United States of America *92*, 7657-7661.

El-Serag, H.B. (2011). Hepatocellular carcinoma. The New England journal of medicine *365*, 1118-1127.

Esser, S., Lampugnani, M.G., Corada, M., Dejana, E., and Risau, W. (1998). Vascular endothelial growth factor induces VE-cadherin tyrosine phosphorylation in endothelial cells. Journal of cell science *111 (Pt 13)*, 1853-1865.

Faulkner, G.J. (2011). Retrotransposons: mobile and mutagenic from conception to death. FEBS letters *585*, 1589-1594.

Fickert, P., Fuchsbichler, A., Wagner, M., Zollner, G., Kaser, A., Tilg, H., Krause, R., Lammert, F., Langner, C., Zatloukal, K*., et al.* (2004). Regurgitation of bile acids from leaky bile ducts causes sclerosing cholangitis in Mdr2 (Abcb4) knockout mice. Gastroenterology *127*, 261-274.

Giannelli, G., Villa, E., and Lahn, M. (2014). Transforming growth factor-beta as a therapeutic target in hepatocellular carcinoma. Cancer research *74*, 1890-1894.

Gomaa, A.I., Khan, S.A., Toledano, M.B., Waked, I., and Taylor-Robinson, S.D. (2008). Hepatocellular carcinoma: epidemiology, risk factors and pathogenesis. World journal of gastroenterology : WJG *14*, 4300-4308.

Hanahan, D., and Coussens, L.M. (2012). Accessories to the crime: functions of cells recruited to the tumor microenvironment. Cancer cell *21*, 309-322.

Hanahan, D., and Weinberg, R.A. (2011). Hallmarks of cancer: the next generation. Cell *144*, 646-674.

Hancks, D.C., and Kazazian, H.H., Jr. (2012). Active human retrotransposons: variation and disease. Current opinion in genetics & development *22*, 191-203.

He, G., and Karin, M. (2011). NF-kappaB and STAT3 - key players in liver inflammation and cancer. Cell research *21*, 159-168.

Henry, C., Close, A.F., and Buteau, J. (2014). A critical role for the neural zinc factor ST18 in pancreatic beta-cell apoptosis. The Journal of biological chemistry *289*, 8413-8419.

Hernandez-Gea, V., Toffanin, S., Friedman, S.L., and Llovet, J.M. (2013). Role of the microenvironment in the pathogenesis and treatment of hepatocellular carcinoma. Gastroenterology *144*, 512-527.

Huang, C.H., Lujambio, A., Zuber, J., Tschaharganeh, D.F., Doran, M.G., Evans, M.J., Kitzing, T., Zhu, N., de Stanchina, E., Sawyers, C.L.*, et al.* (2014). CDK9-mediated transcription elongation is required for MYC addiction in hepatocellular carcinoma. Genes & development *28*, 1800-1814.

Huang, H.Y., Chen, S.Z., Zhang, W.T., Wang, S.S., Liu, Y., Li, X., Sun, X., Li, Y.M., Wen, B., Lei, Q.Y.*, et al.* (2013). Induction of EMT-like response by BMP4 via up-regulation of lysyl oxidase is required for adipocyte lineage commitment. Stem cell research *10*, 278-287.

Iannelli, F., Collino, A., Sinha, S., Radaelli, E., Nicoli, P., D'Antiga, L., Sonzogni, A., Faivre, J., Buendia, M.A., Sturm, E.*, et al.* (2014). Massive gene amplification drives paediatric hepatocellular carcinoma caused by bile salt export pump deficiency. Nature communications *5*, 3850.

Jacquemin, E. (2012). Progressive familial intrahepatic cholestasis. Clinics and research in hepatology and gastroenterology *36 Suppl 1*, S26-35.

Jandrig, B., Seitz, S., Hinzmann, B., Arnold, W., Micheel, B., Koelble, K., Siebert, R., Schwartz, A., Ruecker, K., Schlag, P.M.*, et al.* (2004). ST18 is a breast cancer tumor suppressor gene at human chromosome 8q11.2. Oncogene *23*, 9295-9302.

Jechlinger, M., Grunert, S., Tamir, I.H., Janda, E., Ludemann, S., Waerner, T., Seither, P., Weith, A., Beug, H., and Kraut, N. (2003). Expression profiling of epithelial plasticity in tumor progression. Oncogene *22*, 7155-7169.

Jemal, A., Bray, F., Center, M.M., Ferlay, J., Ward, E., and Forman, D. (2011). Global cancer statistics. CA: a cancer journal for clinicians *61*, 69-90.

Kameyama, T., Matsushita, F., Kadokawa, Y., and Marunouchi, T. (2011). Myt/NZF family transcription factors regulate neuronal differentiation of P19 cells. Neuroscience letters *497*, 74-79.

Katzenellenbogen, M., Mizrahi, L., Pappo, O., Klopstock, N., Olam, D., Jacob-Hirsch, J., Amariglio, N., Rechavi, G., Domany, E., Galun, E.*, et al.* (2007). Molecular mechanisms of liver carcinogenesis in the mdr2-knockout mice. Molecular cancer research : MCR *5*, 1159-1170.

Knisely, A.S., Strautnieks, S.S., Meier, Y., Stieger, B., Byrne, J.A., Portmann, B.C., Bull, L.N., Pawlikowska, L., Bilezikci, B., Ozcay, F.*, et al.* (2006). Hepatocellular carcinoma in ten children under five years of age with bile salt export pump deficiency. Hepatology *44*, 478-486.

Kortylewski, M., Kujawski, M., Wang, T., Wei, S., Zhang, S., Pilon-Thomas, S., Niu, G., Kay, H., Mule, J., Kerr, W.G.*, et al.* (2005). Inhibiting Stat3 signaling in the hematopoietic system elicits multicomponent antitumor immunity. Nature medicine *11*, 1314-1321.

Kubitz, R., Droge, C., Stindt, J., Weissenberger, K., and Haussinger, D. (2012). The bile salt export pump (BSEP) in health and disease. Clinics and research in hepatology and gastroenterology *36*, 536-553.

Lam, P., Wang, R., and Ling, V. (2005). Bile acid transport in sister of P-glycoprotein (ABCB11) knockout mice. Biochemistry *44*, 12598-12605.

Lee, S.J., Kim, K.H., and Park, K.K. (2014). Mechanisms of fibrogenesis in liver cirrhosis: The molecular aspects of epithelial-mesenchymal transition. World journal of hepatology *6*, 207-216.

Lee, S.J., and Michel, S.L. (2014). Structural metal sites in nonclassical zinc finger proteins involved in transcriptional and translational regulation. Accounts of chemical research *47*, 2643-2650.

Leight, J.L., Wozniak, M.A., Chen, S., Lynch, M.L., and Chen, C.S. (2012). Matrix rigidity regulates a switch between TGF-beta1-induced apoptosis and epithelial-mesenchymal transition. Molecular biology of the cell *23*, 781-791.

Li, H., Duhachek-Muggy, S., Dubnicka, S., and Zolkiewska, A. (2013a). Metalloproteinase-disintegrin ADAM12 is associated with a breast tumor-initiating cell phenotype. Breast cancer research and treatment *139*, 691-703.

Li, Y.M., Xu, S.C., Li, J., Han, K.Q., Pi, H.F., Zheng, L., Zuo, G.H., Huang, X.B., Li, H.Y., Zhao, H.Z.*, et al.* (2013b). Epithelial-mesenchymal transition markers

expressed in circulating tumor cells in hepatocellular carcinoma patients with different stages of disease. Cell death & disease *4*, e831.

Liu, P., Kimmoun, E., Legrand, A., Sauvanet, A., Degott, C., Lardeux, B., and Bernuau, D. (2002). Activation of NF-kappa B, AP-1 and STAT transcription factors is a frequent and early event in human hepatocellular carcinomas. Journal of hepatology *37*, 63-71.

Llovet, J.M., and Bruix, J. (2003). Systematic review of randomized trials for unresectable hepatocellular carcinoma: Chemoembolization improves survival. Hepatology *37*, 429-442.

Llovet, J.M., Burroughs, A., and Bruix, J. (2003). Hepatocellular carcinoma. Lancet *362*, 1907-1917.

Llovet, J.M., Ricci, S., Mazzaferro, V., Hilgard, P., Gane, E., Blanc, J.F., de Oliveira, A.C., Santoro, A., Raoul, J.L., Forner, A.*, et al.* (2008). Sorafenib in advanced hepatocellular carcinoma. The New England journal of medicine *359*, 378-390.
Maddaluno, L., Rudini, N., Cuttano, R., Bravi, L., Giampietro, C., Corada, M., Ferrarini, L., Orsenigo, F., Papa, E., Boulday, G.*, et al.* (2013). EndMT contributes to the onset and progression of cerebral cavernous malformations. Nature *498*, 492-496.

Mantovani, A., Allavena, P., Sica, A., and Balkwill, F. (2008). Cancer-related inflammation. Nature *454*, 436-444.

Mauad, T.H., van Nieuwkerk, C.M., Dingemans, K.P., Smit, J.J., Schinkel, A.H., Notenboom, R.G., van den Bergh Weerman, M.A., Verkruisen, R.P., Groen, A.K., Oude Elferink, R.P.*, et al.* (1994). Mice with homozygous disruption of the mdr2 P-glycoprotein gene. A novel animal model for studies of nonsuppurative inflammatory cholangitis and hepatocarcinogenesis. The American journal of pathology *145*, 1237-1245.

Miki, Y., Nishisho, I., Horii, A., Miyoshi, Y., Utsunomiya, J., Kinzler, K.W., Vogelstein, B., and Nakamura, Y. (1992). Disruption of the APC gene by a retrotransposal insertion of L1 sequence in a colon cancer. Cancer research *52*, 643-645.

Nesseler, N., Launey, Y., Aninat, C., Morel, F., Malledant, Y., and Seguin, P. (2012). Clinical review: The liver in sepsis. Critical care *16*, 235.

Nicolaou, M., Andress, E.J., Zolnerciks, J.K., Dixon, P.H., Williamson, C., and Linton, K.J. (2012). Canalicular ABC transporters and liver disease. The Journal of pathology *226*, 300-315.

Nitou, M., Sugiyama, Y., Ishikawa, K., and Shiojiri, N. (2002). Purification of fetal mouse hepatoblasts by magnetic beads coated with monoclonal anti-e-cadherin antibodies and their in vitro culture. Experimental cell research *279*, 330-343.

Oberhammer, F.A., Pavelka, M., Sharma, S., Tiefenbacher, R., Purchio, A.F., Bursch, W., and Schulte-Hermann, R. (1992). Induction of apoptosis in cultured hepatocytes and in regressing liver by transforming growth factor beta 1. Proceedings of the National Academy of Sciences of the United States of America *89*, 5408-5412.

Ogunwobi, O.O., and Liu, C. (2012). Therapeutic and prognostic importance of epithelial-mesenchymal transition in liver cancers: insights from experimental models. Critical reviews in oncology/hematology *83*, 319-328.

Paradis, V. (2013). Histopathology of hepatocellular carcinoma. Recent results in cancer research Fortschritte der Krebsforschung Progres dans les recherches sur le cancer *190*, 21-32.

Parkin, D.M., Bray, F., Ferlay, J., and Pisani, P. (2001). Estimating the world cancer burden: Globocan 2000. International journal of cancer Journal international du cancer *94*, 153-156.

Pikarsky, E., Porat, R.M., Stein, I., Abramovitch, R., Amit, S., Kasem, S., Gutkovich-Pyest, E., Urieli-Shoval, S., Galun, E., and Ben-Neriah, Y. (2004). NF-kappaB functions as a tumour promoter in inflammation-associated cancer. Nature *431*, 461-466.

Potthoff, M.J., and Olson, E.N. (2007). MEF2: a central regulator of diverse developmental programs. Development *134*, 4131-4140.

Ramakrishna, G., Rastogi, A., Trehanpati, N., Sen, B., Khosla, R., and Sarin, S.K. (2013). From cirrhosis to hepatocellular carcinoma: new molecular insights on inflammation and cellular senescence. Liver cancer *2*, 367-383.

Roncalli, M., Park, Y.N., and Di Tommaso, L. (2010). Histopathological classification of hepatocellular carcinoma. Digestive and liver disease : official journal of the Italian Society of Gastroenterology and the Italian Association for the Study of the Liver *42 Suppl 3*, S228-234.

Rudalska, R., Dauch, D., Longerich, T., McJunkin, K., Wuestefeld, T., Kang, T.W., Hohmeyer, A., Pesic, M., Leibold, J., von Thun, A.*, et al.* (2014). In vivo RNAi screening identifies a mechanism of sorafenib resistance in liver cancer. Nature medicine *20*, 1138-1146.

Sansone, P., and Bromberg, J. (2011). Environment, inflammation, and cancer. Current opinion in genetics & development *21*, 80-85.

Seki, E., De Minicis, S., Osterreicher, C.H., Kluwe, J., Osawa, Y., Brenner, D.A., and Schwabe, R.F. (2007). TLR4 enhances TGF-beta signaling and hepatic fibrosis. Nature medicine *13*, 1324-1332.

Severi, T., van Malenstein, H., Verslype, C., and van Pelt, J.F. (2010). Tumor initiation and progression in hepatocellular carcinoma: risk factors, classification, and therapeutic targets. Acta pharmacologica Sinica *31*, 1409-1420.

Shachaf, C.M., Kopelman, A.M., Arvanitis, C., Karlsson, A., Beer, S., Mandl, S., Bachmann, M.H., Borowsky, A.D., Ruebner, B., Cardiff, R.D.*, et al.* (2004). MYC inactivation uncovers pluripotent differentiation and tumour dormancy in hepatocellular cancer. Nature *431*, 1112-1117.

Shiraha, H., Yamamoto, K., and Namba, M. (2013). Human hepatocyte carcinogenesis (review). International journal of oncology *42*, 1133-1138.

Shukla, R., Upton, K.R., Munoz-Lopez, M., Gerhardt, D.J., Fisher, M.E., Nguyen, T., Brennan, P.M., Baillie, J.K., Collino, A., Ghisletti, S.*, et al.* (2013). Endogenous retrotransposition activates oncogenic pathways in hepatocellular carcinoma. Cell *153*, 101-111.

Smit, J.J., Schinkel, A.H., Oude Elferink, R.P., Groen, A.K., Wagenaar, E., van Deemter, L., Mol, C.A., Ottenhoff, R., van der Lugt, N.M., van Roon, M.A.*, et al.* (1993). Homozygous disruption of the murine mdr2 P-glycoprotein gene leads to a complete absence of phospholipid from bile and to liver disease. Cell *75*, 451-462.

Song, J. (2007). EMT or apoptosis: a decision for TGF-beta. Cell research *17*, 289-290.

Steinbach, D., Schramm, A., Eggert, A., Onda, M., Dawczynski, K., Rump, A., Pastan, I., Wittig, S., Pfaffendorf, N., Voigt, A.*, et al.* (2006). Identification of a set of seven genes for the monitoring of minimal residual disease in pediatric acute myeloid leukemia. Clinical cancer research : an official journal of the American Association for Cancer Research *12*, 2434-2441.

Taube, J.H., Herschkowitz, J.I., Komurov, K., Zhou, A.Y., Gupta, S., Yang, J., Hartwell, K., Onder, T.T., Gupta, P.B., Evans, K.W.*, et al.* (2010). Core epithelial-to-mesenchymal transition interactome gene-expression signature is associated with claudin-low and metaplastic breast cancer subtypes. Proceedings of the National Academy of Sciences of the United States of America *107*, 15449-15454.

Teramoto, T., Satonaka, K., Kitazawa, S., Fujimori, T., Hayashi, K., and Maeda, S. (1994). p53 gene abnormalities are closely related to hepatoviral infections and occur at a late stage of hepatocarcinogenesis. Cancer research *54*, 231-235.

Teufel, A., Staib, F., Kanzler, S., Weinmann, A., Schulze-Bergkamen, H., and Galle, P.R. (2007). Genetics of hepatocellular carcinoma. World journal of gastroenterology : WJG *13*, 2271-2282.

Vousden, K.H., and Lane, D.P. (2007). p53 in health and disease. Nature reviews Molecular cell biology *8*, 275-283.

Wang, D., and DuBois, R.N. (2013). The role of anti-inflammatory drugs in colorectal cancer. Annual review of medicine *64*, 131-144.

Wang, X.W., Forrester, K., Yeh, H., Feitelson, M.A., Gu, J.R., and Harris, C.C. (1994). Hepatitis B virus X protein inhibits p53 sequence-specific DNA binding, transcriptional activity, and association with transcription factor ERCC3. Proceedings of the National Academy of Sciences of the United States of America *91*, 2230-2234.

Wong, C.M., Fan, S.T., and Ng, I.O. (2001). beta-Catenin mutation and overexpression in hepatocellular carcinoma: clinicopathologic and prognostic significance. Cancer *92*, 136-145.

Wu, Y.H., Chang, T.H., Huang, Y.F., Huang, H.D., and Chou, C.Y. (2014). COL11A1 promotes tumor progression and predicts poor clinical outcome in ovarian cancer. Oncogene *33*, 3432-3440.

Wuestefeld, T., Pesic, M., Rudalska, R., Dauch, D., Longerich, T., Kang, T.W., Yevsa, T., Heinzmann, F., Hoenicke, L., Hohmeyer, A.*, et al.* (2013). A Direct in vivo RNAi screen identifies MKK4 as a key regulator of liver regeneration. Cell *153*, 389-401.

Yang, J., Siqueira, M.F., Behl, Y., Alikhani, M., and Graves, D.T. (2008). The transcription factor ST18 regulates proapoptotic and proinflammatory gene expression in fibroblasts. FASEB journal : official publication of the Federation of American Societies for Experimental Biology *22*, 3956-3967.

Yee, K.S., and Yu, V.C. (1998). Isolation and characterization of a novel member of the neural zinc finger factor/myelin transcription factor family with transcriptional repression activity. The Journal of biological chemistry *273*, 5366-5374.

Yu, W., Huang, C., Wang, Q., Huang, T., Ding, Y., Ma, C., Ma, H., and Chen, W. (2014). MEF2 transcription factors promotes EMT and invasiveness of hepatocellular

carcinoma through TGF-beta1 autoregulation circuitry. Tumour biology : the journal of the International Society for Oncodevelopmental Biology and Medicine.

Zender, L., Spector, M.S., Xue, W., Flemming, P., Cordon-Cardo, C., Silke, J., Fan, S.T., Luk, J.M., Wigler, M., Hannon, G.J*., et al.* (2006). Identification and validation of oncogenes in liver cancer using an integrative oncogenomic approach. Cell *125*, 1253-1267.

Zender, L., Xue, W., Cordon-Cardo, C., Hannon, G.J., Lucito, R., Powers, S., Flemming, P., Spector, M.S., and Lowe, S.W. (2005). Generation and analysis of genetically defined liver carcinomas derived from bipotential liver progenitors. Cold Spring Harbor symposia on quantitative biology *70*, 251-261.

Zender, L., Xue, W., Zuber, J., Semighini, C.P., Krasnitz, A., Ma, B., Zender, P., Kubicka, S., Luk, J.M., Schirmacher, P*., et al.* (2008). An oncogenomics-based in vivo RNAi screen identifies tumor suppressors in liver cancer. Cell *135*, 852-864.

Zhong, J., Deaciuc, I.V., Burikhanov, R., and de Villiers, W.J. (2006). Lipopolysaccharide-induced liver apoptosis is increased in interleukin-10 knockout mice. Biochimica et biophysica acta *1762*, 468-477.

Zhou, C., Liu, J., Tang, Y., and Liang, X. (2012). Inflammation linking EMT and cancer stem cells. Oral oncology *48*, 1068-1075.